Title

Convergently-evolved peptide-based cell-cell signaling system required for virulence of a eukaryotic pathogen

Author

Homer, Christina

Publication Date

2016

Peer reviewed|Thesis/dissertation

Convergently-evolved peptide-based cell-cell signaling system required for virulence of a eukaryotic pathogen

by

Christina M. Homer

DISSERTATION

Submitted in partial satisfaction of the requirements for the degree of

DOCTOR OF PHILOSOPHY

in

Biophysics

in the

GRADUATE DIVISION

of the

UNIVERSITY OF CALIFORNIA, SAN FRANCISCO

Acknowledgements

I could not have completed the work presented here without extensive help from a number of people.

I want to first thank my thesis advisor, Hiten Madhani, for his unending support throughout my thesis work. He was always a source of enthusiasm and confidence, even when experiments weren't working for me. I appreciate his openness to collaborations and new techniques, which allowed me to meet and work with a number of fantastic scientists throughout the course of this work. This work also benefited from the guidance and expertise of my committee members, Jeff Cox and Geeta Narlikar. I appreciate their thoughtful input on the project and the help their lab members provided for implementing the techniques they had suggested. I very much appreciate the kindness of Anita Sil and Suzanne Noble, who allowed me to attend and present at their joint lab meetings. Their input and ideas from their lab members provided an important fungal pathogenesis perspective in my work. Presentations from their lab meetings were an important part of my education. Both inside and outside of those lab meetings, Mark Voorhies taught me most of what I know about bioinformatics.

I'd like to thank the members of the Madhani Lab who provided crucial support and camaraderie during my time in the lab. Together, we had many lively and interesting discussions, both regarding science and other aspects of life. I'd like to especially thank Alexi Goranov, who mentored me extensively during our early morning conversations. Additionally, I was lucky to have the opportunity to collaborate with Phillip Dumesic, who taught me almost everything I know about heterochromatin. I'd like to thank Prashanthi Natarajan, my bench mate for the entire PhD, for her guidance and support, and for providing me with many crypto-related protocols over the years. Additionally, thank you to Jahan-Yar Parsa, Jordan Burke, Sandra

Catania, and Selim Boudoukha for always being game for discussions and questions, even when it was outside of their area of expertise.

I am very grateful for having great lab neighbors for the duration of my time in the Madhani Lab. Members of the Cox Lab were invaluable resources as I learned to work with mammalian cells for the first time. Robert Watson and Samantha Bell taught me how to perform cell culture and Trevor Parry showed me how to isolate bone-marrow derived macrophages. I am grateful to Bennett Penn and Oren Rosenberg for providing inspiration, career guidance, and examples of MD/PhDs further along in their training. I'd like to thank members of the Johnson and Guthrie laboratory for guidance, lively lunchtime discussions, and generously letting me use their lab's equipment and teaching me to use that same equipment.

While, I was lucky to meet many wonderful people during my time at UCSF, I am especially grateful to Veronica Pessino, Kelly Nissen, John Hawkins, Brian O'Donovan, and Kieran Mace for our fun lunches and coffees, support, and sharing my time at UCSF, both inside and outside of school. Outside of science, I am grateful to also have the support and friendship of Victoria, Joey, and Tess.

I cannot thank my family, Diane, Russ, and Michael, enough for their unceasing support and encouragement, even during the hardest times in graduate school. And finally, I want to thank my husband, Alex, who was there for me during every minute of my PhD. Not only did he pick me up from working late in lab on so many evenings, cook dinner for us, and take care of numerous household chores, he was a rock of emotional support for me during the ups and downs that science inevitably brings. I cannot thank him enough.

Abstract

Qsp1 is a peptide of unknown function secreted by the fungal meningitis pathogen *Cryptococcus neoformans*. We identified *QSP1* as a target of three transcription factors required for virulence. Indeed, mutants lacking Qsp1 are attenuated for infection and growth within macrophages. Qsp1 signaling modulates the activities of secreted proteases and promotes cell wall function at high cell densities. Production of the peptide requires its release from a secreted precursor by a cell-associated protease, while sensing of Qsp1 requires an oligopeptide importer. The effects of cytoplasmic expression of Qsp1 indicate that it can function intracellularly. These features closely mirror the quorum sensing systems of gram-positive bacteria in which peptide precursors are exported, processed and then imported to bind cytoplasmic receptors. Despite these remarkable similarities, the components of the respective systems are not ancestrally related, implying convergent evolution. Our studies reveal a bacterial-like signaling system that promotes the virulence of a eukaryotic pathogen.

Table of Contents

List of Tables

List of Figures

Chapter 1: Introduction

The encapsulated yeast *Cryptococcus neoformans* is an opportunistic pathogen that causes meningoencephalitis and is responsible for over half a million AIDS-related deaths annually, primarily in developing countries where highly-active antiretroviral therapy (HAART) is not readily available [1, 2]. Fungal infections are difficult to treat for several reasons: 1) Fungi are eukaryotes like humans. Therefore, many proteins that are potential drug targets cannot be targeted without the drug also cross-reacting with the human homolog and causing deleterious side-effects[3]. 2) Our understanding of fungal biology and the virulence factors that allow certain fungal species to become successful pathogens is quite limited compared to the sophisticated understanding of bacterial pathogens. Until this understanding is improved, many potential drug targets simply remain unknown. Due to both reasons described above, there are only three classes of antifungal drugs used routinely to treat cryptococcal infections [4]. 3) Finally, given the limited number of treatment options and the common practice of treating patients with lifelong antifungal therapy to prevent relapse, antifungal drug resistance can be problematic [5].

Epidemiology

C. neoformans is ubiquitous in the environment and most people test positive for antibodies against *C. neoformans*, indicating previous exposure, by age five [6]. However, this encapsulated yeast predominately causes symptomatic and disseminated infections in patients whose cell-based immunity is not properly functioning. Those most susceptible to disseminated cryptococcal infection include people with AIDS infections and people undergoing long-term immunosuppressant treatment, such as solid-organ transplant recipients [7, 8]. Less commonly,

cryptococcal infections occur in patients whose immune system may be weakened or compromised by underlying chronic diseases, such as cancer, diabetes mellitus, or inflammatory bowel disease [9]. While *Cryptococcus neoformans* is almost always found in an immunocompromised patient population, *Cryptococcus gattii* is a sister species that is thought to cause infections in people who are less immunocompromised or even immunocompetent [10].

A small number of patients diagnosed with disseminated cryptococcal infections have no apparent immune compromise [7, 11]. The reason they develop disseminated cryptococcal infection is not fully understand since the majority of the population is resistant. However, several researchers have proposed the theory that these apparently immunocompetent hosts have subclinical or unrecognized immune defects [7, 12]. Indeed, several more subtle immunodeficiencies were recently recognized as risk factors and explain some of the case reports of disseminated cryptococcal infection in immunocompetent patients [13-15]. As research continues in this area, we may eventually have the evidence to argue that disseminated cryptococcal infections almost always occur in the setting of some type of immune dysfunction. If this were the case, diagnosis with disseminated cryptococcal infection in a patient with no known risk factors could be a good screening method for identifying previously unknown forms of immune dysfunction.

Virulence Factors

Unlike most other fungal pathogens, which are ascomycetes and thermal dimorphs, *C. neoformans* is a basidiomycete and is almost always found in its yeast form in human tissues [16, 17]. Since its emergence as an important pathogen during the AIDS epidemic, research has focused on three characteristics of *C. neoformans* which impart the majority of its virulence: the

ability to grow at human body temperature, the production of melanin to protect against toxic insults, and the presence of a polysaccharide capsule. Additionally, the importance of an intact and properly-functioning cell wall for virulence and general fungal viability have been recently described and will be discussed below.

Thermotolerance

Since human body temperature is 37 degree Celsius, all successful systemic pathogens must be able to survive and replicate at this elevated temperature. Although there are many cryptococcal species, *Cryptococcus neoformans* and *Cryptococcus gattii* are the only two species that commonly cause disease and are also the only two species that can consistently grow at the elevated temperature found in the human host [18]. Studies of mutant *C. neoformans* strains that cannot grow at elevated temperatures have elucidated several pathways involved in regulating thermotolerance. Upon exposure to higher temperatures, *C. neoformans* increases its rate of trehalose production, a disaccharide that is thought to help proteins remain folded upon exposure to heat [19]. Mutants in the trehalose biosynthesis pathway, which have reduced cellular trehalose levels, are attenuated for growth at higher temperatures and demonstrate attenuated virulence in mice [19]. Cryptococcal growth at higher temperatures also appears to require an intact antioxidant defense system, perhaps due to increased mitochondrial respiration and increased accumulation of associated reactive oxygen species [20]. The transcription factor Mga2 is required for growth at higher temperatures and was found to control the expression of a number of lipid biosynthesis genes, likely regulating membrane remodeling to maintain membrane integrity [21]. Additionally, the Ras1-Cdc42 signal transduction pathway was found to be important for adapting to high temperature growth in *C. neoformans* as well as a number of

other fungal species [22]. As might be expected, all known temperature-sensitive mutants that have been tested were found to have decreased or loss of virulence in mammalian hosts [23].

Melanin Production

Melanin is a pigment produced by a number of microorganisms, where it has been found to protect those organisms against environmental insults and immune system attack [24]. Melanin is produced by *C. neoformans* in a regulated manner in response to stressors, including glucose starvation [25]. Laccase enzyme expression and melanin production is influenced by a number of factors, including other enzymes required for glycolysis, implying an interaction between melanin production and metabolic status [26]. Laccase is the enzyme that catalyzes the key chemical reaction in the melanin biosynthesis pathway [27]. The *C. neoformans* genome contains two genes *LAC1* and *LAC2* that encode laccases, although *LAC1* is the major transcript produced and encodes the dominant form of the enzyme [25]. Melanin is localized to the cell wall [28, 29] and thought to protect cryptococcal cells against oxidative insults and other stresses, partly due to the enzyme laccase's iron oxidative activity, melanin's ability to scavenge and neutralize oxidative species, and alteration of the cryptococcal cell surface charge due to the presence of melanin [25].

Soon after the discovery of the laccase gene and its role in promoting melanin production, investigators studied the impact of melanin on cryptococcal virulence. However, results varied depending on infection model, group performing the experiment, and cryptococcal strain background. In Serotype D, intravenous infection with melanin-deficient and melanin-producing strains showed that the melanin-deficient strains were significantly attenuated compared to their melanin-producing counterparts [30]. Additionally, the transcript encoding the

laccase enzyme was expressed in cryptococcal cells isolated from the cerebrospinal fluid of rabbits infected with the melanin-producing strain, lending some support to the idea that the appropriate signals and substrates might be present *in vivo* during an infection [30]. However, a later study using the same pair of cryptococcal strains found that, while the melanin-deficient strain was attenuated upon intratracheal infection and had fewer viable cryptococcal cells in extrapulmonary organs, that strain's virulence defect could be rescued by infecting through the intravenous route [31]. The authors postulated a role for melanin and the laccase enzyme in facilitating cryptococcal dissemination from the lungs, although it remains unclear from where the difference in their virulence results stem [31]. Infections done much later with the highly virulent serotype A clinical isolate, H99, and an H99 *lac1*Δ strain found that *LAC1* was required for pulmonary virulence as well as dissemination to extrapulmonary sites [32]. Additionally, the authors discovered that the murine host exhibited an altered pulmonary immune response to *lac1*Δ mutants [32].

In addition to its role in melanin biosynthesis, researchers have suggested that the laccase enzyme may play independent roles in cryptococcal biology. Namely, the production of the laccase enzyme protects cryptococcal cells from the antifungal activity of alveolar macrophages, the primary immune cells of the lung. Even in the absence of added L-DOPA, the substrate required for laccase to produce melanin, laccase mutants exhibit more sensitivity toward alveolar macrophages [33]. However, it remains difficult to definitively rule out that there is not another unknown phenolic substrate produced by either cell type or present in trace amounts in these types of experiments.

Cell Wall

As the outer layer of fungi, the fungal cell wall plays an important role in protection from and communication with the environment [34]. Discoveries regarding the cryptococcal biology involved in cell wall synthesis and maintenance were greatly aided by the virulence phenotypes described above: themotolerance and melanin. Screens for mutants with phenotypes such as melanin leakiness and sensitivity to growth at 37 degrees Celsius led to the discovery of a number of the cell wall mutants described below.

The majority of the biomass in cryptococcal cell walls is comprised of alpha and beta-glucans, chitin, chitosan, and mannoproteins. Of those, beta-glucans are the most abundant polymers and are postulated to be essential for cryptococcal viability. No *C. neoformans* mutants have been isolated that completely lack beta-glucan. Additionally, monoclonal antibodies that recognize beta-glucan polymers have been used to inhibit *C. neoformans'* growth *in vitro* and *in vivo* [35]. Echinochandins, a class of antifungal drugs that inhibits beta-glucan synthase [36, 37], have been used successfully to treat fungal infections due to *Candida albicans* and *Aspergillus niger*. However, *C. neoformans* is not sensitive to treatment with echinochandins, despite its glucan synthase being sensitive to these drugs when tested in an *in vitro* activity assay [38]. The factors behind this apparent contradiction between *in vitro* and *in vivo* phenotypes remain a mystery.

Alpha glucan, while not as abundant as beta glucan in the cell wall, plays a crucial wall in the integrity of the cell wall structure. A mutant lacking the enzyme responsible for alpha glucan synthesis, *ags1*Δ, completely lacked alpha glucan, but appeared to compensate for this loss by overproducing beta-glucan and chitin/chitosan [39]. This resulted in a hypertrophic cell wall structure that was phenotypically less effective at protecting cells from high temperature stress

and the cell wall probe SDS. Additionally, *ags1*Δ mutant cells appeared to have trouble dividing and formed unusually wide septa at the bud junction. In addition to these phenotypes, which might be expected from the loss of a major structural component of the cell wall, *ags1*Δ mutants displayed no cell surface polysaccharide capsule, an important cryptococcal virulence factor discussed further below, although these mutants were still able to secrete the macromolecule [39, 40]. While the capsule layer of cryptococcal cells was known to be outside of the cell wall layer, these findings implicate alpha-glucan as a candidate anchor, attaching the polysaccharide capsule to the cryptococcal cell wall.

While not as abundant as beta- and alpha-glucans, chitin and chitosan also play a crucial structural role in maintaining cryptococcal cell wall integrity. When the *C. neoformans* genome was sequenced, researchers found that it included eight genes encoding putative chitin synthases and three genes encoding putative chitin synthase regulators based on sequence homology to those enzymes already characterized in *Saccharomyces cerevisiae* [41]. No one chitin synthase in this expanded family is essential for cryptococcal viability; however, deletion mutants of some family members did show mild sensitivity to growth at higher temperature and growth in the presence of the cell wall stressors Congo Red, SDS, and caffeine. The *chs3*Δ and *csr2*Δ mutants' phenotypes were the most pronounced. Interestingly, these two mutants also shared an unusual phenotype: they were able to produce melanin but unable to keep it associated to their cell walls. Instead, these mutants leaked melanin into the media [41]. Upon further biochemical characterization, researchers associated this leaky melanin phenotype with a deficiency, but not complete lack, of chitosan production.

Subsequently, investigators identified four genes encoding putative chitin deacetylases. Only the triple mutant *cda1*Δ *cda2*Δ *cda3*Δ completely lacked chitosan and capitulated the same

leaky melanin phenotype described above, implying that these three enzymes (Cda1-3) were responsible for the production of all the chitosan in the cryptococcal cell wall [42]. The function of the fourth enzyme predicted to be a chitin deacetylase remains unknown. Surprisingly, chitosan does not appear to be required for growth at elevated temperature as the triple mutant was able to survive even when grown at 40 degrees Celsius [42]. However, the *cda1*Δ *cda2*Δ *cda3*Δ mutant was attenuated for virulence when used to infect mice [43], likely due to rapid clearance by host immune cells. No mutant cells were detected longer than 48 hours post-infection [43].

Given the importance of numerous cell wall components for cryptococcal cell integrity and virulence, the cell wall remains an active area of interest and an excellent antifungal drug target.

Polysaccharide Capsule

Until recently, the polysaccharide capsule was the only known mechanism by which *C. neoformans* avoided phagocytosis by macrophages, the first line of defense against cryptococcal infection [44]. Perhaps due to its sheer size (Figure 1), the polysaccharide capsule's properties have been studied extensively. These inquiries range from biochemical composition of the macromolecule to its immunomodulatory functions during mammalian infection. In particular, the capsule has been a key virulence factor studied because it contributes to *C. neoformans'* extreme resistance to phagocytosis in the absence of antibodies, such as the likely environment during early infection in the human lung [45].

C. neoformans sheds polysaccharide capsule into the media in which it is growing, in addition to maintaining a large amount of the capsule material attached to cells themselves [46].

Most biochemical studies of the polysaccharide capsule have been performed on the shed fraction, as the method to purify this material was developed first [47, 48]. Now, researchers have developed techniques for isolating both cell-attached and shed polysaccharide material, leading to the discovery that different capsule isolation techniques yield polysaccharide species which exhibit different biophysical properties [49]. Even when polysaccharide species are isolated only from shed material or only from the cell-associated fraction, variations exist depending on the isolation method employed. These findings could indicate that these biochemical purification protocols physically alter the polysaccharide through chemical reactions. Alternatively, *C. neoformans* might produce a wider range of capsular species than previously appreciated and the biochemical purifications enrich for different unique subpopulations.

Despite the minor variations observed, consensus remains that the cryptococcal polysaccharide capsule is largely composed of two polysaccharide species (glucoronoxylomannan and galactoxylomannan) and mannoproteins. Glucoronoxylomannan (GXM) is the major component of the capsule, comprising 90% of the cryptococcal capsule by mass [50]. Its structure has been determined to be a polysaccharide comprised of a mannan backbone from which branches containing glucoronic acid and xylose emanate. The minor component of the capsule is named galactoxylomannan (GalXM) or glucoronoxylomannogalactan (GXMGal) because its structure has been determined to be a galactan backbone from which branches containing mannose, xylose, and glucoronic acid emanate [50, 51].

Phenotypically, mutants that cannot produce GXM form “dry-appearing” colonies when grown on agar plates. Their lack of polysaccharide capsule is also easily determined by India ink

staining. This phenotype made it easier to identify mutants unable to produce GXM. Genes required for its synthesis were identified and found to be necessary for virulence in mammalian hosts [52-55]. Using these Cap mutants and purified GXM alone, a number of studies found that GXM plays a number of immunosuppressive roles [56], including suppression of the phagocytic activity of macrophages [57], interference with dendritic and T cell maturation [58, 59], induction of macrophage apoptosis [60], and regulation of neutrophil extracellular trap production [61].

Mutants unable to produce GalXM were not obtained until recently, perhaps due to the lack of a colony morphology phenotype. Prior to the discovery of any mutants lacking the minor component of the capsule, purified GalXM was used to determine the polysaccharide's immunomodulatory properties, which included inhibition of TNF-alpha production by peripheral blood mononuclear cells [62], inhibition of neutrophil migration [63], and induction of T cell apoptosis [64]. For the first time in 2007, investigators published two mutants, *uge1*Δ and *ugt1*Δ, that did not produce GalXM but still displayed GXM [65]. *uge1*Δ is a mutant that lacks a UDP-glucose epimerase and *ugt1*Δ is a mutant lacking a UDP-galactose transporter. Investigators were not able to detect galactose in whole cells of either mutant. Unlike the Cap mutants described above, these mutants had increased capsule size as measured by India Ink staining, likely indicating more production of GXM or a structural role for GalXM in organizing the capsule structure compactly. Despite still possessing a visible polysaccharide capsule, both mutant strains were attenuated in virulence using a tail vein model of infection [65]. Additionally, GalXM mutants had a defect in colonizing the lungs and brains of infected mice, although the number of cells throughout infected mice was significantly lower than wild type and decreased over time [65]. In addition to their capsule and virulence phenotypes, these two galactose

mutants have temperature sensitivity that can be rescued by growth with sorbitol, indicating a cell wall defect. This suggests the possibility that galactose could be involved in maintaining cell wall integrity as well as capsule biosynthesis, although further investigation is required.

Bacterial Quorum Sensing

Many virulence factors that have been well-characterized in bacterial pathogens have been discovered in eukaryotic pathogens as well, presumably due to fitness benefits that transcend kingdoms. One widespread virulence factor in bacteria is a type of signaling system known as quorum sensing [66]. While quorum sensing has been well-studied in bacteria, little is known about these types of signaling systems in eukaryotic organisms. As quorum sensing has been proposed to be a more general mechanism of decision-making in any decentralized system, including artificially-designed ones [67], it is logical to propose the hypothesis that quorum sensing is more widespread than we currently appreciate.

Bacterial quorum sensing was first discovered in the aquatic bacteria *Vibrio fischeri* and *Vibrio harveyi*. When found at high enough cell density, both bacterial species produce bioluminescence [68]. Although multiple mechanisms by which cells sensed their own density were proposed [69], researchers identified secreted signaling molecules that mediated this form of cooperation [70-72]. In this classic paradigm, *V. fischeri* produces a small molecule known as an acylhomoserine lactone (AHL). This chemical can freely diffuse across cell membranes; therefore, its intracellular and extracellular concentrations are the same and are proportional to the number of cells producing the signaling molecule. When cells in the bacterial culture reach a high enough concentration, or a "quorum," the concentration of AHL in the cytoplasm is above the threshold required to efficiently bind LuxR, the signal's receptor. This binding initiates a

signaling cascade, leading to the transcription of genes required to produce bioluminescence [66, 73-75]. Using quorum sensing, *V. fischeri* has evolved to only produce bioluminescence when enough cells of the species are present for their light to be visible.

Since its first discovery in *V. fischeri*, quorum sensing has been extensively studied in bacteria and two main signaling architectures have emerged. As described above, gram-negative bacteria signal with acylhomoserine lactones, which freely diffuse through cell membranes. They accumulate intracellularly in recipient cells and bind intracellular receptors. In most gram-positive organisms, the quorum sensing signals are small peptides and they bind a cell surface receptor upon reaching a threshold concentration [74]. However, in a small clade of *Bacillus spp.* gram-positive bacteria, an unusual signaling architecture exists: the signaling molecule is still a peptide, but it is imported into the cytoplasm of recipient cells, where it binds a cytoplasmic receptor [76-78]. These signaling architectures control a wide range of biological processes thought to involve community behavior: genetic transformation, bioluminescence, virulence factor expression, biofilm formation, and sporogenesis [79].

Evidence for Quorum Sensing in Eukaryotes

Several signaling-like phenomena have been identified in eukaryotes that are consistent with quorum-sensing systems. However, as described below, challenges have prevented investigators from examining these systems fully and determining whether they are quorum-sensing systems.

The dimorphic fungus *Histoplasma capsulatum* produces an unidentified factor in culture supernatants that regulates alpha-glucan content in the organism's cell wall in a cell-density-dependent manner [80]. However, since the factor was not identified, it is difficult to conclude

whether this density-dependent phenomenon is signaling or another phenomenon like coercion or response to cues.

Quorum sensing in eukaryotes is best known from work in *Candida albicans* [81]. *C. albicans* produces farnesol [82] and tyrosol [83], both side-products of metabolism [84]. When exogenous farnesol is added to cultures, it inhibits the yeast-to-hypha transition. On the other hand, when exogenous tyrosol is added to cultures, it promotes the yeast-to-hypha transition [84]. Consistent with quorum sensing, farnesol and tyrosol accumulate with culture density [85]. A *C. albicans* mutant lacking a phosphatase involved in farnesol production was isolated that produced 6-fold less farnesol than wild type [86]. This mutant was attenuated in a mouse model of infection. However, since the phosphatase deleted in this mutant is involved in the production of an entire class of lipids, investigators were not able to casually link this mutant's decrease in production of farnesol with its virulence defect. While farnesol certainly represents the best candidate eukaryotic quorum sensing factor, no mutants have been isolated that cannot produce the chemical. Additionally, the only currently-known mutant that has a decreased level of farnesol may have other alterations in its metabolism, making it difficult to link the phenotypes of that mutant directly to farnesol production.

Quorum Sensing and the Intracellular Lifestyle

As described above, quorum sensing is thought to be a method of communication facilitating community behavior and cooperation [87, 88]. However, thinking about quorum sensing in terms of a community of organisms can be misleading since quorum sensing is based on the concentration of the signaling molecule. Therefore, under certain conditions such as confinement or low diffusion environments, a community of just one cell could be sufficient to

induce quorum sensing behavior [89, 90]. Scientists have suggested that quorum sensing might be better termed "diffusion sensing" since it directly monitors the diffusion status of the quorum sensing signal [91, 92]. Thus, quorum sensing could be an ideal signaling system to facilitate the adaptation of intracellular pathogens upon internalization by host immune cells [93]. Quorum sensing systems have been found in some intracellular bacterial pathogens, including *Brucella melitensis* [94, 95]. Additionally, investigators have shown that confinement of single cells of *Staphylococcus aureus* [96] or 1-3 cells of *Pseudomonas aeruginosa* [97] in microfluidic compartments the size of phagosomes induced their quorum sensing systems. The quorum sensing system of *Brucella melitensis* regulates a secretion system required for intracellular replication [98]. Quorum sensing in *Staphylococcus aureus* is induced upon internalization by host cells and required for exit from their endosomes [99]. Thus, some quorum sensing systems in bacteria seem to be used to sense internalization, and genes regulated by quorum sensing are required for successful intracellular survival strategies.

Cryptococcal interactions with macrophages

Macrophages are a crucial cell-type in determining the outcome of cryptococcal infections. Alveolar macrophages are the first-line immune defense against pulmonary pathogens, including *C. neoformans*. Alveolar macrophages have been observed to quickly internalize *C. neoformans* cells after intratracheal infection and continue to interact with the fungal cells throughout the infection's course [100]. Hosts whose macrophages are resistant to *C. neoformans* were found to be more susceptible to cryptococcosis when their macrophages were depleted, consistent with a protective role [101]. However, hosts whose macrophages are more susceptible to cryptococcal infection gain a survival advantage when their macrophages are

depleted during cryptococcal infection [101], implying that *C. neoformans* benefits from the presence of macrophages in this context. Additionally, a cryptococcal mutant has been isolated that appears to depend upon macrophages for extrapulmonary dissemination. During infection with this mutant, mice gain a survival benefit from macrophage depletion [102]. Thus, the relationship between cryptococcal virulence and macrophages is complicated but appears to be a crucial determinant of the outcome of cryptococcosis.

The ability of *C. neoformans* to subvert the normal antifungal activity of macrophages is theorized to stem from natural selection in cryptococcal-amoeba interactions in the soil. *C. neoformans* naturally lives in the soil, where it has been found to interact extensively with amoebae. Mammals appear to be dead-end hosts for this fungal pathogen, raising the question as to how *C. neoformans* is so well-adapted to subvert the mammalian immune system [103]. Investigators have found that cryptococcal-amoeba interactions are similar to cryptococcal-macrophage interactions, including a phenomenon of exocytosis, in which *C. neoformans* escapes from these phagocytes [104-106]. Additionally, passaging *C. neoformans* strains through amoebae increases their ability to infect mammalian hosts, lending support to this theory [107]. Therefore, the likely possibility that remains is that *C. neoformans* has adapted to survive predation by amoebae.

Phagocytosis Inhibition

In the absence of opsonization, such as the likely environment in the lung during early infection, *C. neoformans* is incredibly resistant to phagocytosis [108]. Part of *C. neoformans*' ability to resist phagocytosis stems from the polysaccharide capsule [109, 110]. Capsule mutants that lack GXM have a moderately increased level of phagocytosis by macrophages compared to

wild type [111, 112]. Capsular material has been shown to bind CD14 and toll-like receptor 2, leading to macrophages that cannot activate in response to pathogens [113]. Additionally, the capsule is thought to act as a physical barrier, separating antibodies, complement, and macrophage receptors from the immunogenic epitopes in the fungal cell wall [114]. While the above studies have all been performed on isolated capsular material (the majority of which is GXM) or acapsular mutants that cannot produce GXM, to my knowledge, nothing is known about the role of GalXM in phagocytosis. Additionally, antibodies against GalXM have not yet proved to be opsonizing or protective [115].

Our laboratory recently discovered a mutant that is phagocytosed at a much higher rate than even acapsular mutants. This mutant lacks the transcription factor Gat201 [108]. This increased phagocytosis is due to one or more Gat201 transcriptional targets. Further work in the laboratory identified another transcription factor Gat204 as sharing part of Gat201's phenotype [116]. The authors also identified a target of Gat201 and Gat204, Blp1, as a candidate effector protein for the antiphagocytosis phenotype. Blp1 alone has a small, although significant, effect on phagocytosis [116]. In *C. neoformans*, Blp1 is part of a family of an eight-protein family whose members all contain the double-psi beta barrel structural domain and will be discussed further in Chapter 4 [116]. Redundancy between family members could explain the modest *blp1*Δ phenotype. Characterization of this protein family could lead to an increased understanding of how *C. neoformans* inhibits phagocytosis by macrophages.

Intracellular survival

During the course of an infection, *C. neoformans* is eventually opsonized by antibodies or complement and can become internalized by macrophages. While the phagolysosome is a harsh

environment for some microorganisms, *C. neoformans* survives and replicates in this niche [117]. While a common strategy for intracellular pathogens is to manipulate the host and thereby prevent phagolysosomal acidification, most reports show that *C. neoformans* replicates in the mature acidic phagolysosome [118]. In fact, *C. neoformans* has been found to replicate intracellularly more slowly in phagolysosomes that are artificially manipulated to prevent acidification [118], implying that perhaps this fungus is best adapted for a low pH environment. *In vitro* studies have shown three possible outcomes of this intracellular parasitism: 1) Division of *C. neoformans* until the macrophage lyses [57, 119]. 2) *C. neoformans* can be expelled from a macrophage with both cell types remaining viable through an unknown mechanism, a phenomenon that has been described recently [120, 121]. 3) Macrophage control or killing of *C. neoformans*. The variables that determine which of these outcomes occur after phagocytosis remain to be fully understood [114, 122].

This thesis describes multiple aspects of the interaction between *C. neoformans* and macrophages. In Chapter 2, I characterize a transcriptional network whose members regulate cryptococcal phagocytosis. We used the targets of this network to study aspects of cryptococcal-macrophage interactions. In Chapter 3, I describe a signaling system that impacts the ability of *C. neoformans* to survive inside macrophages. In Chapter 4, I characterize a family of cryptococcal proteins that contain Barwin domains and impact *C. neoformans*' phagocytosis and intracellular survival.

Figures

A

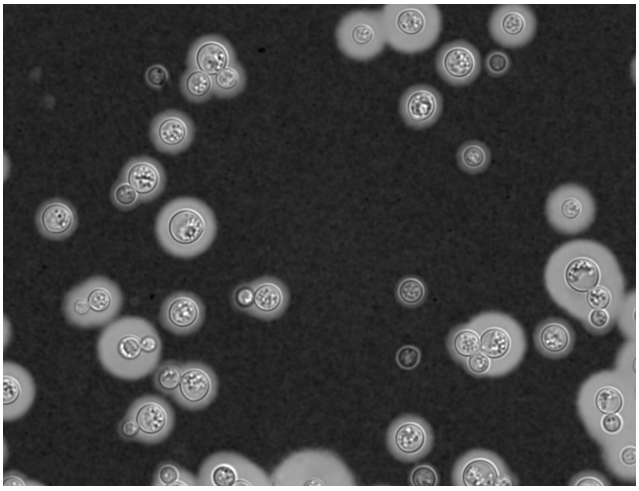

Figure 1

Figure 1: India Ink staining of the cryptococcal polysaccharide capsule

a) Capsule production was induced in wild type cells and visualized by India Ink staining.

Works Cited

1. Armstrong-James, D., G. Meintjes, and G.D. Brown, *A neglected epidemic: fungal infections in HIV/AIDS.* Trends Microbiol, 2014. **22**(3): p. 120-7.
2. Benjamin J Park, K.A.W., Barbara J Marston, Nelesh Govender, Peter G Pappas, Tom M Chiller, *Estimation of the current global burden of cryptococcal meningitis among persons living with HIV/AIDS.* AIDS, 2009. **23**(4): p. 525-530.
3. Liu, M., et al., *Conserved fungal genes as potential targets for broad-spectrum antifungal drug discovery.* Eukaryot Cell, 2006. **5**(4): p. 638-49.
4. John R. Perfect, W.E.D., Francoise Dromer, David L. Goldman, John R. Graybill, Richard J. Hamill, Thomas S. Harrison, Robert A. Larsen, Olivier Lortholary, Minh-Hong Nguyen, Peter G. Pappas, William G. Powderly, Nina Singh, Jack D. Sobel, and Tania C. Sorell., *Clinical Practice Guidelines for the Management of Cryptococcal Disease: 2010 Update by the Infectious Diseases Society of America.* Clinical Infectious Disease, 2010. **50**(3): p. 291-322.
5. Pfaller, M.A., *Antifungal drug resistance: mechanisms, epidemiology, and consequences for treatment.* Am J Med, 2012. **125**(1 Suppl): p. S3-13.
6. Goldman, D.L., et al., *Serologic evidence for Cryptococcus neoformans infection in early childhood.* Pediatrics, 2001. **107**(5): p. E66.
7. Perfect, J.R. and T. Bicanic, *Cryptococcosis diagnosis and treatment: What do we know now.* Fungal Genet Biol, 2015. **78**: p. 49-54.
8. Pyrgos, V., et al., *Epidemiology of cryptococcal meningitis in the US: 1997-2009.* PLoS One, 2013. **8**(2): p. e56269.

9. Pappas, P.G., *Cryptococcal infections in non-HIV-infected patients.* Trans Am Clin Climatol Assoc, 2013. **124**: p. 61-79.

10. Kwon-Chung, K.J., et al., *Cryptococcus neoformans and Cryptococcus gattii, the etiologic agents of cryptococcosis.* Cold Spring Harb Perspect Med, 2014. **4**(7): p. a019760.

11. Mitchell, D.H., et al., *Cryptococcal disease of the CNS in immunocompetent hosts: influence of cryptococcal variety on clinical manifestations and outcome.* Clin Infect Dis, 1995. **20**(3): p. 611-6.

12. Day, J.N., et al., *Most cases of cryptococcal meningitis in HIV-uninfected patients in Vietnam are due to a distinct amplified fragment length polymorphism-defined cluster of Cryptococcus neoformans var. grubii VN1.* J Clin Microbiol, 2011. **49**(2): p. 658-64.

13. Saijo, T., et al., *Anti-granulocyte-macrophage colony-stimulating factor autoantibodies are a risk factor for central nervous system infection by Cryptococcus gattii in otherwise immunocompetent patients.* MBio, 2014. **5**(2): p. e00912-14.

14. Rosen, L.B., et al., *Anti-GM-CSF autoantibodies in patients with cryptococcal meningitis.* J Immunol, 2013. **190**(8): p. 3959-66.

15. Netea, M.G., et al., *Two patients with cryptococcal meningitis and idiopathic CD4 lymphopenia: defective cytokine production and reversal by recombinant interferon-gamma therapy.* Clin Infect Dis, 2004. **39**(9): p. e83-7.

16. Feldmesser, M., Y. Kress, and A. Casadevall, *Dynamic changes in the morphology of Cryptococcus neoformans during murine pulmonary infection.* Microbiology, 2001. **147**(Pt 8): p. 2355-65.

17. Lin, X., *Cryptococcus neoformans: morphogenesis, infection, and evolution.* Infect Genet Evol, 2009. **9**(4): p. 401-16.

18. Casadevall, A. and J.R. Perfect, *Cryptococcus neoformans*. 1998, Washington, D.C.: ASM Press. viii, 541 p.

19. Petzold, E.W., et al., *Characterization and regulation of the trehalose synthesis pathway and its importance in the pathogenicity of Cryptococcus neoformans.* Infect Immun, 2006. **74**(10): p. 5877-87.

20. Giles, S.S., et al., *Cryptococcus neoformans mitochondrial superoxide dismutase: an essential link between antioxidant function and high-temperature growth.* Eukaryot Cell, 2005. **4**(1): p. 46-54.

21. Kraus, P.R., et al., *Identification of Cryptococcus neoformans temperature-regulated genes with a genomic-DNA microarray.* Eukaryot Cell, 2004. **3**(5): p. 1249-60.

22. Nichols, C.B., Z.H. Perfect, and J.A. Alspaugh, *A Ras1-Cdc24 signal transduction pathway mediates thermotolerance in the fungal pathogen Cryptococcus neoformans.* Mol Microbiol, 2007. **63**(4): p. 1118-30.

23. Perfect, J.R., *Cryptococcus neoformans: the yeast that likes it hot.* FEMS Yeast Res, 2006. **6**(4): p. 463-8.

24. Nosanchuk, J.D. and A. Casadevall, *The contribution of melanin to microbial pathogenesis.* Cell Microbiol, 2003. **5**(4): p. 203-23.

25. Zhu, X. and P.R. Williamson, *Role of laccase in the biology and virulence of Cryptococcus neoformans.* FEMS Yeast Res, 2004. **5**(1): p. 1-10.

26. Zhang, P., et al., *Cryptococcal phosphoglucose isomerase is required for virulence factor production, cell wall integrity and stress resistance.* FEMS Yeast Res, 2015. **15**(7).

27. Williamson, P.R., *Biochemical and molecular characterization of the diphenol oxidase of Cryptococcus neoformans: identification as a laccase.* J Bacteriol, 1994. **176**(3): p. 656-64.

28. Zhu, X., et al., *Laccase of Cryptococcus neoformans is a cell wall-associated virulence factor.* Infect Immun, 2001. **69**(9): p. 5589-96.

29. Mandal, P., et al., *Differences in the cell wall architecture of melanin lacking and melanin producing Cryptococcus neoformans clinical isolates from India: An electron microscopic study.* Brazilian Journal of Microbiology, 2007. **38**(4): p. 662-666.

30. Salas, S.D., et al., *Effect of the laccase gene CNLAC1, on virulence of Cryptococcus neoformans.* J Exp Med, 1996. **184**(2): p. 377-86.

31. Noverr, M.C., et al., *CNLAC1 is required for extrapulmonary dissemination of Cryptococcus neoformans but not pulmonary persistence.* Infect Immun, 2004. **72**(3): p. 1693-9.

32. Qiu, Y., et al., *Immune modulation mediated by cryptococcal laccase promotes pulmonary growth and brain dissemination of virulent Cryptococcus neoformans in mice.* PLoS One, 2012. **7**(10): p. e47853.

33. Liu, L., R.P. Tewari, and P.R. Williamson, *Laccase protects Cryptococcus neoformans from antifungal activity of alveolar macrophages.* Infect Immun, 1999. **67**(11): p. 6034-9.

34. M. Gonzalez, P.W.J.d.G., F.M. Klis, P.N. Lipke, *Glycoconjugate structure and function in fungal cell walls*, in *Microbial glycobiology: structures, relevance and applications*, A.P.M.O.H.P.J.B.M.v. Itzstein, Editor. 2009, Amsterdam: Academic Press. p. 169-183.

35. Rachini, A., et al., *An anti-beta-glucan monoclonal antibody inhibits growth and capsule formation of Cryptococcus neoformans in vitro and exerts therapeutic, anticryptococcal activity in vivo.* Infect Immun, 2007. **75**(11): p. 5085-94.

36. Denning, D.W., *Echinocandin antifungal drugs.* Lancet, 2003. **362**(9390): p. 1142-51.

37. Denning, D.W., *Echinocandins: a new class of antifungal.* J Antimicrob Chemother, 2002. **49**(6): p. 889-91.

38. Maligie, M.A. and C.P. Selitrennikoff, *Cryptococcus neoformans resistance to echinocandins: (1,3)beta-glucan synthase activity is sensitive to echinocandins.* Antimicrob Agents Chemother, 2005. **49**(7): p. 2851-6.

39. Reese, A.J., et al., *Loss of cell wall alpha(1-3) glucan affects Cryptococcus neoformans from ultrastructure to virulence.* Mol Microbiol, 2007. **63**(5): p. 1385-98.

40. Reese, A.J. and T.L. Doering, *Cell wall alpha-1,3-glucan is required to anchor the Cryptococcus neoformans capsule.* Mol Microbiol, 2003. **50**(4): p. 1401-9.

41. Banks, I.R., et al., *A chitin synthase and its regulator protein are critical for chitosan production and growth of the fungal pathogen Cryptococcus neoformans.* Eukaryot Cell, 2005. **4**(11): p. 1902-12.

42. Baker, L.G., et al., *Chitosan, the deacetylated form of chitin, is necessary for cell wall integrity in Cryptococcus neoformans.* Eukaryot Cell, 2007. **6**(5): p. 855-67.

43. Baker, L.G., C.A. Specht, and J.K. Lodge, *Cell wall chitosan is necessary for virulence in the opportunistic pathogen Cryptococcus neoformans.* Eukaryot Cell, 2011. **10**(9): p. 1264-8.

44. Jing, X., et al., *Overexpression of copper/zinc superoxide dismutase from mangrove Kandelia candel in tobacco enhances salinity tolerance by the reduction of reactive oxygen species in chloroplast.* Front Plant Sci, 2015. **6**: p. 23.

45. Claudia Monari, F.B.A.V., *Glucuronoxylomannan exhibits potent immunosuppressive properties.* FEMS Yeast Research, 2006. **6**: p. 537-542.

46. Bose, I., et al., *A yeast under cover: the capsule of Cryptococcus neoformans.* Eukaryot Cell, 2003. **2**(4): p. 655-63.

47. Cherniak, R., et al., *Facilitated isolation, purification, and analysis of glucuronoxylomannan of Cryptococcus neoformans.* Infect Immun, 1991. **59**(1): p. 59-64.

48. Turner, S.H., R. Cherniak, and E. Reiss, *Fractionation and characterization of galactoxylomannan from Cryptococcus neoformans.* Carbohydr Res, 1984. **125**(2): p. 343-9.

49. Frases, S., et al., *Cryptococcus neoformans capsular polysaccharide and exopolysaccharide fractions manifest physical, chemical, and antigenic differences.* Eukaryot Cell, 2008. **7**(2): p. 319-27.

50. Doering, T.L., *How sweet it is! Cell wall biogenesis and polysaccharide capsule formation in Cryptococcus neoformans.* Annu Rev Microbiol, 2009. **63**: p. 223-47.

51. O'Meara, T.R. and J.A. Alspaugh, *The Cryptococcus neoformans capsule: a sword and a shield.* Clin Microbiol Rev, 2012. **25**(3): p. 387-408.

52. Chang, Y.C. and K.J. Kwon-Chung, *Isolation, characterization, and localization of a capsule-associated gene, CAP10, of Cryptococcus neoformans.* J Bacteriol, 1999. **181**(18): p. 5636-43.

53. Chang, Y.C. and K.J. Kwon-Chung, *Isolation of the third capsule-associated gene, CAP60, required for virulence in Cryptococcus neoformans.* Infect Immun, 1998. **66**(5): p. 2230-6.

54. Chang, Y.C., L.A. Penoyer, and K.J. Kwon-Chung, *The second capsule gene of cryptococcus neoformans, CAP64, is essential for virulence.* Infect Immun, 1996. **64**(6): p. 1977-83.

55. Chang, Y.C. and K.J. Kwon-Chung, *Complementation of a capsule-deficient mutation of Cryptococcus neoformans restores its virulence.* Mol Cell Biol, 1994. **14**(7): p. 4912-9.

56. Cherniak, R. and J.B. Sundstrom, *Polysaccharide antigens of the capsule of Cryptococcus neoformans.* Infect Immun, 1994. **62**(5): p. 1507-12.

57. Del Poeta, M., *Role of phagocytosis in the virulence of Cryptococcus neoformans.* Eukaryot Cell, 2004. **3**(5): p. 1067-75.

58. Grijpstra, J., et al., *The Cryptococcus neoformans cap10 and cap59 mutant strains, affected in glucuronoxylomannan synthesis, differentially activate human dendritic cells.* FEMS Immunol Med Microbiol, 2009. **57**(2): p. 142-50.

59. Yauch, L.E., J.S. Lam, and S.M. Levitz, *Direct inhibition of T-cell responses by the Cryptococcus capsular polysaccharide glucuronoxylomannan.* PLoS Pathog, 2006. **2**(11): p. e120.

60. Villena, S.N., et al., *Capsular polysaccharides galactoxylomannan and glucuronoxylomannan from Cryptococcus neoformans induce macrophage apoptosis mediated by Fas ligand.* Cell Microbiol, 2008. **10**(6): p. 1274-85.

61. Rocha, J.D., et al., *Capsular polysaccharides from Cryptococcus neoformans modulate production of neutrophil extracellular traps (NETs) by human neutrophils.* Sci Rep, 2015. **5**: p. 8008.

62. Chaka, W., et al., *Induction of TNF-alpha in human peripheral blood mononuclear cells by the mannoprotein of Cryptococcus neoformans involves human mannose binding protein.* J Immunol, 1997. **159**(6): p. 2979-85.

63. Dong, Z.M. and J.W. Murphy, *Cryptococcal polysaccharides bind to CD18 on human neutrophils.* Infect Immun, 1997. **65**(2): p. 557-63.

64. Pericolini, E., et al., *Cryptococcus neoformans capsular polysaccharide component galactoxylomannan induces apoptosis of human T-cells through activation of caspase-8.* Cell Microbiol, 2006. **8**(2): p. 267-75.

65. Moyrand, F., T. Fontaine, and G. Janbon, *Systematic capsule gene disruption reveals the central role of galactose metabolism on Cryptococcus neoformans virulence.* Mol Microbiol, 2007. **64**(3): p. 771-81.

66. Miller, M.B. and B.L. Bassler, *Quorum sensing in bacteria.* Annu Rev Microbiol, 2001. **55**: p. 165-99.

67. Sahin, E., *Swarm robotics: From sources of inspiration to domains of application.* Swarm Robotics, 2005. **3342**: p. 10-20.

68. Meighen, E.A., *Enzymes and Genes from the Lux Operons of Bioluminescent Bacteria.* Annual Review of Microbiology, 1988. **42**: p. 151-176.

69. Kempner, E.S. and F.E. Hanson, *Aspects of light production by Photobacterium fischeri.* J Bacteriol, 1968. **95**(3): p. 975-9.

70. Eberhard, A., *Inhibition and activation of bacterial luciferase synthesis.* J Bacteriol, 1972. **109**(3): p. 1101-5.

71. Nealson, K.H., T. Platt, and J.W. Hastings, *Cellular control of the synthesis and activity of the bacterial luminescent system.* J Bacteriol, 1970. **104**(1): p. 313-22.

72. Henke, J.M. and B.L. Bassler, *Three parallel quorum-sensing systems regulate gene expression in Vibrio harveyi.* J Bacteriol, 2004. **186**(20): p. 6902-14.

73. Bassler, B.L., and Melissa B. Miller., *"Quorum sensing."* in *The prokaryotes.* 2013, Springer Berlin Heidelberg. p. 495-509.

74. Ng, W.L. and B.L. Bassler, *Bacterial quorum-sensing network architectures.* Annu Rev Genet, 2009. **43**: p. 197-222.

75. Waters, C.M. and B.L. Bassler, *Quorum sensing: cell-to-cell communication in bacteria.* Annu Rev Cell Dev Biol, 2005. **21**: p. 319-46.

76. Hoover, S.E., et al., *A new quorum-sensing system (TprA/PhrA) for Streptococcus pneumoniae D39 that regulates a lantibiotic biosynthesis gene cluster.* Mol Microbiol, 2015.

77. Lanigan-Gerdes, S., et al., *Identification of subtilisin, Epr and Vpr as enzymes that produce CSF, an extracellular signalling peptide of Bacillus subtilis.* Mol Microbiol, 2007. **65**(5): p. 1321-33.

78. Lazazzera, B.A., *The intracellular function of extracellular signaling peptides.* Peptides, 2001. **22**(10): p. 1519-27.

79. Puchkov, E.O., *Intercellular Signaling in Microbial World: A Panoramic View.* BIOCHEMISTRY (MOSCOW) SUPPLEMENT SERIES A: MEMBRANE AND CELL BIOLOGY, 2016. **10**(1): p. 33-42.

80. Kugler, S., et al., *Phenotypic variation and intracellular parasitism by histoplasma Capsulatum.* Proc Natl Acad Sci U S A, 2000. **97**(16): p. 8794-8.

81. Kruppa, M., *Quorum sensing and Candida albicans.* Mycoses, 2009. **52**(1): p. 1-10.

82. Hornby, J.M., et al., *Quorum sensing in the dimorphic fungus Candida albicans is mediated by farnesol.* Appl Environ Microbiol, 2001. **67**(7): p. 2982-92.

83. Chen, H., et al., *Tyrosol is a quorum-sensing molecule in Candida albicans.* Proc Natl Acad Sci U S A, 2004. **101**(14): p. 5048-52.

84. Nickerson, K.W., A.L. Atkin, and J.M. Hornby, *Quorum sensing in dimorphic fungi: farnesol and beyond.* Appl Environ Microbiol, 2006. **72**(6): p. 3805-13.

85. Sprague, G.F., Jr. and S.C. Winans, *Eukaryotes learn how to count: quorum sensing by yeast.* Genes Dev, 2006. **20**(9): p. 1045-9.

86. Navarathna, D.H., et al., *Effect of farnesol on a mouse model of systemic candidiasis, determined by use of a DPP3 knockout mutant of Candida albicans.* Infect Immun, 2007. **75**(4): p. 1609-18.

87. Juhas, M., L. Eberl, and B. Tummler, *Quorum sensing: the power of cooperation in the world of Pseudomonas.* Environ Microbiol, 2005. **7**(4): p. 459-71.

88. Dandekar, A.A., S. Chugani, and E.P. Greenberg, *Bacterial quorum sensing and metabolic incentives to cooperate.* Science, 2012. **338**(6104): p. 264-6.

89. Schuster, M., et al., *Acyl-homoserine lactone quorum sensing: from evolution to application.* Annu Rev Microbiol, 2013. **67**: p. 43-63.

90. Turovskiy, Y., et al., *Quorum sensing: fact, fiction, and everything in between.* Adv Appl Microbiol, 2007. **62**: p. 191-234.

91. Redfield, R.J., *Is quorum sensing a side effect of diffusion sensing?* Trends Microbiol, 2002. **10**(8): p. 365-70.

92. West, S.A., et al., *Quorum sensing and the confusion about diffusion.* Trends Microbiol, 2012. **20**(12): p. 586-94.

93. Gama, J.A., et al., *Immune subversion and quorum-sensing shape the variation in infectious dose among bacterial pathogens.* PLoS Pathog, 2012. **8**(2): p. e1002503.

94. Taminiau, B., et al., *Identification of a quorum-sensing signal molecule in the facultative intracellular pathogen Brucella melitensis.* Infect Immun, 2002. **70**(6): p. 3004-11.

95. Terwagne, M., et al., *Quorum sensing and self-quorum quenching in the intracellular pathogen Brucellamelitensis.* PLoS One, 2013. **8**(12): p. e82514.

96. Carnes, E.C., et al., *Confinement-induced quorum sensing of individual Staphylococcus aureus bacteria.* Nat Chem Biol, 2010. **6**(1): p. 41-5.

97. Boedicker, J.Q., M.E. Vincent, and R.F. Ismagilov, *Microfluidic confinement of single cells of bacteria in small volumes initiates high-density behavior of quorum sensing and growth and reveals its variability.* Angew Chem Int Ed Engl, 2009. **48**(32): p. 5908-11.

98. Hanna, N., et al., *The virB operon is essential for lethality of Brucella microti in the Balb/c murine model of infection.* J Infect Dis, 2011. **203**(8): p. 1129-35.

99. Qazi, S.N., et al., *agr expression precedes escape of internalized Staphylococcus aureus from the host endosome.* Infect Immun, 2001. **69**(11): p. 7074-82.

100. Feldmesser, M., et al., *Cryptococcus neoformans is a facultative intracellular pathogen in murine pulmonary infection.* Infect Immun, 2000. **68**(7): p. 4225-37.

101. Shao, X., et al., *An innate immune system cell is a major determinant of species-related susceptibility differences to fungal pneumonia.* J Immunol, 2005. **175**(5): p. 3244-51.

102. Kechichian, T.B., J. Shea, and M. Del Poeta, *Depletion of alveolar macrophages decreases the dissemination of a glucosylceramide-deficient mutant of Cryptococcus neoformans in immunodeficient mice.* Infect Immun, 2007. **75**(10): p. 4792-8.

103. Panepinto, J.C. and P.R. Williamson, *Intersection of fungal fitness and virulence in Cryptococcus neoformans.* FEMS Yeast Res, 2006. **6**(4): p. 489-98.

104. Chrisman, C.J., M. Alvarez, and A. Casadevall, *Phagocytosis of Cryptococcus neoformans by, and nonlytic exocytosis from, Acanthamoeba castellanii.* Appl Environ Microbiol, 2010. **76**(18): p. 6056-62.

105. Bunting, L.A., J.B. Neilson, and G.S. Bulmer, *Cryptococcus neoformans: gastronomic delight of a soil ameba.* Sabouraudia, 1979. **17**(3): p. 225-32.

106. Casadevall, A., *Amoeba provide insight into the origin of virulence in pathogenic fungi.* Adv Exp Med Biol, 2012. **710**: p. 1-10.

107. Steenbergen, J.N., H.A. Shuman, and A. Casadevall, *Cryptococcus neoformans interactions with amoebae suggest an explanation for its virulence and intracellular pathogenic strategy in macrophages.* Proc Natl Acad Sci U S A, 2001. **98**(26): p. 15245-50.

108. Liu, O.W., et al., *Systematic genetic analysis of virulence in the human fungal pathogen Cryptococcus neoformans.* Cell, 2008. **135**(1): p. 174-88.

109. Kozel, T.R., et al., *Role of the capsule in phagocytosis of Cryptococcus neoformans.* Rev Infect Dis, 1988. **10 Suppl 2**: p. S436-9.

110. Kozel, T.R. and E.C. Gotschlich, *The capsule of cryptococcus neoformans passively inhibits phagocytosis of the yeast by macrophages.* J Immunol, 1982. **129**(4): p. 1675-80.

111. Kozel, T.R. and J. Cazin, *Nonencapsulated Variant of Cryptococcus neoformans I. Virulence Studies and Characterization of Soluble Polysaccharide.* Infect Immun, 1971. **3**(2): p. 287-94.

112. Bulmer, G.S. and M.D. Sans, *Cryptococcus neoformans. II. Phagocytosis by human leukocytes.* J Bacteriol, 1967. **94**(5): p. 1480-3.

113. Shoham, S., et al., *Toll-like receptor 4 mediates intracellular signaling without TNF-alpha release in response to Cryptococcus neoformans polysaccharide capsule.* J Immunol, 2001. **166**(7): p. 4620-6.

114. Garcia-Rodas, R. and O. Zaragoza, *Catch me if you can: phagocytosis and killing avoidance by Cryptococcus neoformans.* Fems Immunology and Medical Microbiology, 2012. **64**(2): p. 147-161.

115. Chow, S.K. and A. Casadevall, *Evaluation of Cryptococcus neoformans galactoxylomannan-protein conjugate as vaccine candidate against murine cryptococcosis.* Vaccine, 2011. **29**(10): p. 1891-8.

116. Chun, C.D., J.C. Brown, and H.D. Madhani, *A major role for capsule-independent phagocytosis-inhibitory mechanisms in mammalian infection by Cryptococcus neoformans.* Cell Host Microbe, 2011. **9**(3): p. 243-51.

117. Diamond, R.D. and J.E. Bennett, *Growth of Cryptococcus neoformans within human macrophages in vitro.* Infect Immun, 1973. **7**(2): p. 231-6.

118. Levitz, S.M., et al., *Cryptococcus neoformans resides in an acidic phagolysosome of human macrophages.* Infect Immun, 1999. **67**(2): p. 885-90.

119. Feldmesser, M., S. Tucker, and A. Casadevall, *Intracellular parasitism of macrophages by Cryptococcus neoformans.* Trends Microbiol, 2001. **9**(6): p. 273-8.

120. Voelz, K., D.A. Lammas, and R.C. May, *Cytokine signaling regulates the outcome of intracellular macrophage parasitism by Cryptococcus neoformans.* Infect Immun, 2009. **77**(8): p. 3450-7.

121. Ma, H., et al., *Expulsion of live pathogenic yeast by macrophages.* Curr Biol, 2006. **16**(21): p. 2156-60.

122. Leopold Wager, C.M., et al., *Cryptococcus and Phagocytes: Complex Interactions that Influence Disease Outcome.* Front Microbiol, 2016. **7**: p. 105.

Chapter 2

Regulation of *Cryptococcus neoformans* Virulence

Summary

Our current understanding of regulatory networks that allow fungal pathogens to correctly adapt to and replicate in host environments is quite limited compared to the sophisticated understanding of these regulatory mechanisms in bacterial pathogens. Using the genetically-tractable fungal pathogen, *Cryptococcus neoformans*, we were able to implement Chromatin Immunoprecipitation and sequencing (ChIP-Seq) on a number of transcription factors required for virulence. The binding targets for these virulence regulators revealed a transcriptional network with a surprising number of overlapping targets. We propose to screen these transcriptional targets as candidate novel virulence factors.

Introduction

Until recently, the cryptococcal polysaccharide capsule was the only mechanism known by which *C. neoformans* avoided phagocytosis. As discussed above, the capsule's properties have been extensively studied to determine how *C. neoformans* resists phagocytosis in the absence of antibodies, such as the likely environment during early infection in the human lung [1]. While not common, capsule-deficient clinical strains have been reported [2-4] and an acapsular mutant has been identified that is hypervirulent in a mouse model [5]. This suggested a novel virulence mechanism that compensates for the loss of the capsule. However, large-scale efforts to discover new virulence mechanisms were limited due to technical difficulties in performing random insertional mutagenesis to screen for new genes involved in pathogenicity [6]. In 2008, our laboratory knocked out a quarter of the *C. neoformans* genome using biolistic transformation and screened these knockouts for virulence defects [7]. This screen revealed the Gat201 transcription factor, whose knockout strain exhibited dramatic increases in phagocytosis by macrophages. Additionally, these increased levels of phagocytosis were much higher than those seen in capsule-deficient strains.

Subsequently, Chromatin Immunoprecipitation followed by hybridization to custom microarrays (ChIP-Chip) identified a large regulatory network, including at least 6 other transcription factors and over 100 genes, controlled by Gat201 [8]. Three of these regulators have been implicated in cryptococcal virulence [7-9], implying that *C. neoformans* implements a network of regulators to control pathogenicity. The majority of these potential Gat201-regulated genes were knocked out and the strains were screened for phagocytosis levels. Gat201's knockout phenotype was partially recapitulated by two proteins found to be regulated by it. They were another transcription factor, Gat204, and a protein called Barwin-like Protein 1 (Blp1),

which contains a double-psi beta-barrel (DPBB) structural domain similar to that in the plant defense protein barwin (see Chapter 4). When these two proteins were knocked out together, they recapitulated almost half of the *gat201*Δ phenotype.

We characterized the binding targets of three of 12 virulence regulators and determined that three of those transcription factors (Gat201, Gat204, and Liv3) share a large number of regulatory targets, comprising a network. We propose to screen these targets to efficiently characterize more virulence-related phenotypes.

Results

We reasoned that virulence factors would be enriched in the regulatory targets of Gat201, a key transcription factor required for virulence and the inhibition of phagocytosis by macrophages [7, 8]. Our previous ChIP-Chip studies of Gat201 identified targets important for phagocytosis inhibition and infection [8]. To develop an extended network, we employed the more sensitive and higher resolution ChIP-Seq method (Figure 1A). Previous studies of fungal pathogens suggest that genes whose promoters are bound by more than one transcription factor regulating a particular process often share that function [10-12]. Thus, we selected two additional transcription factors previously identified as Gat201 targets and implicated in virulence, Gat204 and Liv3 [7, 8], for ChIP-Seq. All ChIP-Seq experiments were done in mammalian tissue culture conditions in which Gat201 has been shown to control transcription and to bind DNA [8].

The peak assignment strategy used to associate binding peaks seen by ChIP-Seq to individual targets genes is robust and the vast majority (>75% of peaks) are assigned to genes in this manner. To further validate the datasets, I determined whether peaks for each dataset fell between two genes that are both oriented in the same direction (Type 1), between genes that are

divergent (Type 2), or in an intergenic region that lies downstream of two genes (Type 3) (Figure S1A). The prediction for transcription factor ChIP-Seq is that the vast majority of binding peaks would fall in promoter regions, (either Type 1 or Type 2 intergenic regions). While intergenic regions throughout the entire genome are evenly distributed between all three types, all of the ChIP-Seq datasets are heavily biased toward Type 1 or Type 2 intergenic regions (Figure S1B).

We defined regulatory targets as genes whose promoters were bound in all three biological replicates of ChIP-Seq for each transcription factor (Figure S2A-C). Analysis revealed that Gat201, Gat204, and Liv3 constitute a transcription factor network, sharing characteristics of other published regulatory networks [13, 14]. Gat201, Gat204, and Liv3 targets (Table 1) overlap significantly ($p < 10^{-300}$ by chi-squared test), with 225 shared by all three regulators, a group we refer to as 'central targets' (Figure 1B). Using RNA-Seq analysis of deletion mutants, we found that 42% of all binding events in the network cause an increase or decrease in target transcript levels, consistent with reported properties of other networks [12, 15, 16] (Figure 2A&B, Table 2). Each transcription factor binds its own promoter and the promoter of the other two regulators (Figure 3A), a characteristic common to many networks [10, 13, 14]. As predicted by their DNA-binding domains, de novo motif finding using the ChIP-Seq data (Figure 3B) shows that Gat201 and Gat204 have typical specificities of GATA family transcription factors [17] (Figure S2C). Liv3, a Wor1-ortholog, produced a DNA binding motif reminiscent of the *Candida albicans* Wor1 motif [18] (Figure 3C).

When comparing the overlap of targets with some of the other virulence regulators that I examined (Liv1, Liv2, Liv4, and Snt1), Snt1 is the only virulence regulator that has a significant overlap of regulatory targets with the Gat201 virulence network's target (Figure 4). Strikingly, 73 of the 225 central targets of this virulence network are also bound by the chromatin regulator,

Snt1, which represents an 8-fold enrichment over chance in the size of the overlap ($p < 7.154 \times 10^{-48}$). This protein is predicted to be part of the Set3 chromatin–modifying complex. In *C. neoformans*, deletion mutants for members of this complex were found to be attenuated for virulence [7]. In *S. Cerevisiae*, *SET3* has been characterized to regulate transcriptional targets through overlapping ncRNA transcription [19]. These findings suggest the possibility that Gat201 network targets might be, at least in part, regulated in a similar manner. Future work will be needed to examine such a potential mechanism.

Discussion

Here, we characterized a transcription factor network in *C. neoformans* composed of three transcription factors, all required for cryptococcal virulence. Since the genes in this network are regulated by transcription factors involved in virulence, it is reasonable to hypothesize that the genes in the network are potential virulence factors, especially those genes whose promoters are bound by all three transcription factors. While the beginning of this network has been characterized, binding targets include additional transcription factors, which will need to be examined to further flush out this regulatory network. Additionally, examination of this network in further conditions will be required to fully understand regulation of virulence in *C. neoformans*. Here, I characterized the Gat201-Gat204-Liv3 network in tissue culture conditions exclusively. Although Gat201 was previously found to not bind promoters in rich media [8], there may be other in vitro conditions in which this network is active. As described in Chapter 3, Liv3 does appear to regulate genes in saturated cultures. Gat201 and Gat204 have not been examined in these conditions yet. Additionally, determining the regulatory targets of

Gat201, Gat204, and Liv3 in the host environment would lead to a much deeper understanding of how *C. neoformans* uses this network to regulate its virulence.

Above, I describe that Snt1's regulatory targets overlap significantly with those of the Gat201-Gat204-Liv3 network. This raises the interesting possibility that the Set3 complex mediates part of this network's regulatory function. In *S. cerevisiae*, the Set3 complex regulates transcription through overlapping ncRNAs [19]. Recently, approximately 1000 candidate ncRNAs were described in *C. neoformans* [20]. These RNAs could be part of the mechanism by which Set3 complex regulates transcription. Alternatively, overlapping transcriptions of coding sequences could also be involved in this type of transcriptional regulation. This type of regulation is likely important for cryptococcal virulence since previous work in the lab found that deletion mutants in the Set3 complex were attenuated in a mouse model of virulence [7]. Further work will be required to further understand the mechanism by which Snt1 regulates transcription, the interaction between Snt1 and the Gat201-Gat204-Liv3 network, and the role that chromatin modifications by the Set3 complex play in virulence.

As part of the ongoing *C. neoformans* full genome deletion collection project being undertaken in the lab, we deleted a large number of the targets in this network and have screened those targets and additional mutants for plate phenotypes, including melanin production and sensitivity to growth at high temperatures and growth on cell wall stressors. We propose screening these mutants as a pool to efficiently characterize their phenotypes.

Experimental Procedures

Cryptococcal strain construction

Gene deletions were generated using nourseothricin (NAT) resistance (*natR*) cassettes and proteins were tagged with CBP-2X Flag epitope tags using nourseothricin (NAT) resistance cassettes as previously described [21]. Strains constructed in this study are labeled in Table 3. Gat201, Gat204, and Liv3 strains are derived from the CM18 parent for consistency with previous publications.

Chromatin immunoprecipitation and RNA-Seq cultures

C. neoformans cultures were grown in 50 mL YPAD (1% yeast extract, 2% Bacto-peptone, 2% glucose, 0.015% L-tryptophan, 0.004% adenine) overnight. 50 ODs were washed 1x with water and resuspended in 15 mL Dulbecco's Modified Eagle Media (DMEM). This suspension was transferred to 150mm x 25mm tissue culture treated plates already containing 5 mL DMEM. Cultures were incubated sitting at 37ºC, 5% CO_2 for 8 hours for ChIP-Seq and 24 hrs for RNA-Seq.

Chromatin immunoprecipitation

C. neoformans cultures were grown and immunoprecipitation was performed as previously published [8]. Cultures were crosslinked by addition of 1% formaldehyde (Sigma) and incubation at room temperature for 15 min, at which point 125 mM glycine was added for 5 min to stop the reaction. Cells were washed 2x in ice cold water, snap frozen, and lyophilized overnight in a Freezone 4.5 freeze dry system (Labconco). Fifty OD_{600} units of cells were resuspended in 0.5 ml ChIP lysis buffer (50 mM HEPES-KOH pH 7.5, 140 mM NaCl, 1 mM

EDTA, 1% Triton X-100, 0.1% sodium deoxycholate, and a fungal protease inhibitor cocktail). Cells were lysed in a Mini-Beadbeater (BioSpec Products) with 0.5 mm zirconia beads (BioSpec Products) for 15 cycles of 1.5 min each with 5 min rest on ice between cycles. Cell lysate was transferred to a new tube and centrifuged for 10 min at 15k x *g*. The resulting chromatin pellet was resuspended in 250 μl ChIP lysis buffer and sonicated for four 15 min cycles (High setting; 30 sec on, 60 sec off) in a Bioruptor waterbath sonicator (Diagenode). After sonication, cell debris was removed by centrifugation at 21k x *g* for 10 min at 4ºC and the supernatant was brought to 1.5 ml in ChIP lysis buffer and snap frozen. Immunoprecipitation was performed at 4˚C overnight in 0.5 ml chromatin aliquots using 2.5 μl of anti-FLAG M2 antibody (F3165, Sigma). Antibodies were bound by addition of 25 μl pre-washed Protein G DYNAbeads (Invitrogen) (pre-washes included 2x with PBS, 3x with ChIP lysis buffer, then resuspend to 4x original volume in ChIP lysis buffer with fungal protease inhibitor cocktail). After a 3 hr incubation with rotation at 4˚C, the beads were washed twice with 1 ml ChIP lysis buffer, twice with 1 ml high salt ChIP lysis buffer (ChIP lysis buffer with 500 mM NaCl), twice with 1 ml wash buffer (10 mM Tris-Cl pH 8.0, 0.25 M LiCl, 0.5% NP-40, 0.5% sodium deoxycholate, 1 mM EDTA), and once with 1 ml TE buffer (10 mM Tris-Cl pH 8.0, 1 mM EDTA). Each wash was performed for 5 min at room temperature. Beads were eluted with 100 μl elution buffer (50 mM Tris-Cl pH 8.0, 10 mM EDTA, 1% SDS) at 70˚C for 15 min with mixing every 2 min, followed by a second elution at room temperature for 1 min with 150 μl TE buffer with 0.67% SDS and 334 μg/ml proteinase K (Sigma). Input samples (50 μl) were combined with 200 μl TE buffer with 1% SDS and 250 μg/ml proteinase K. All samples were incubated overnight at 65˚C, followed by addition of 1250 μl buffer NTB and DNA purification using a NucleoSpin Gel

Clean-up column (Macherey-Nagel). Purified DNA was treated with RNaseA (Ambion) and used as input for sequencing library construction.

ChIP-seq library construction

The DNA yield of a single immunoprecipitation reaction from 500 μl lysate—or 100 ng WCE DNA—was blunted by treatment with the End-It DNA End-Repair Kit (Epicentre) and then A-tailed using Klenow fragment (New England Biolabs) according to manufacturers' instructions, with column purifications after each step. Next, barcoded Illumina adaptors (33 nM) were ligated to the DNA using 1200U Rapid T4 DNA Ligase (Enzymatics) in a 20 μl reaction that was incubated at room temperature for 30 min. The DNA was column purified and PCR amplified using 1U Phusion DNA polymerase (New England Biolabs), 2 M betaine, 75 μM dNTPs, and 0.4 μM of each primer in a 50 μl reaction. Cycling conditions were: 98˚C for 3 min; 15 cycles of 98˚C for 1 min 20 sec, 65˚C 30 sec, 72˚C 30 sec; 72˚C 5 min. The reaction was size selected for products between 200-350 bp using SPRI beads [22]. Library quality and concentration were determined by High Sensitivity DNA Bioanalyzer analysis (Agilent) and qPCR using KAPA Library Quant Standards (KAPA Biosystems), respectively. For each genotype, library construction was performed for 3 biological replicates.

ChIP-Seq analysis

ChIP-seq data were aligned using Bowtie1 [23] and the Seriesoftubes package [24]. We allowed up to two mismatches within the seed sequence and, if a read could align equally well to multiple loci, it was discarded from analysis. Indexed, sorted bam files were created for each dataset using SAMtools [25] and bedgraph files were created using BEDtools [26, 27]. ChIP-Seq peaks

were called using MACS2 [28]. If a peak fell in an intergenic region, it was assigned to the downstream gene (more than one assignment was allowed if the peak fell in a divergent promoter). Peaks were also assigned to promoters of MiscRNAs if they fell within 850 bp (the average size of intergenic regions) upstream of a miscRNA [20]. Chromosomal traces were plotted using Integrative Genomics Viewer 2.0.30 (Broad Institute). Overlap between biological replicates was high (Table 4) but, for subsequent analysis, we only included genes whose promoters had at least one ChIP-Seq peak in each of the three biological replicates analyzed (Figure 1, Table 1). We validated the quality of the Gat201 datasets by comparing genes identified as targets in this study with the previous Gat201 ChIP-Chip study. 58 of the 62 previously characterized Gat201 targets were present in our data as well [8].

Calling sequence motifs

The sequence of ChIP-Seq peaks that were present in all 3 biological replicates (defined as any portion of the peak overlapping between datasets, the meta-peak was extended to include all overlapping peaks between datasets) were used for de novo motif generation. Peaks were sorted by the number of reads that aligned to each peak and the top 100 peaks were used as input to Gimsan [29]. Motifs were generated for widths of 5, 6, 8, and 14 bps for both strands represented by the sequences and the program was run for 10 cycles. The length of the motif reported for each genotype was determined by the lowest p-value for the resultant motifs. The logo for previously published GATA transcription factor DNA binding motifs was generated from previously published data [17] using Weblogo [30].

RNA-Seq Library Preparation

Total RNA was isolated and libraries prepared as described previously [31]. Cell pellets were lyophilized overnight and then RNA was isolated using TRIzol (Invitrogen). To obtain mRNA, 50-200 μg of total RNA (isolated as described above) was purified using the Oligotex mRNA mini kit (Qiagen). For each RNA sample, two successive rounds of purification were performed. Input RNA quality and mRNA purity were verified by Bioanalyzer Pico RNA chips (Agilent). The purified RNA (120 ng) was treated by on-column DNase digestion as described previously [32], then used to prepare sequencing libraries using the NEBNext Ultra Directional RNA Library Prep Kit (New England Biolabs). Libraries were analyzed for quality and average size on Bioanalyzer High Sensitivity DNA chips (Agilent) and quantified by qPCR with KAPA Library Quant Standards. Libraries were sequenced on the HiSeq 2500 platform (Illumina).

RNA-Seq Analysis

RNA-seq data, which included two biological replicates per genotype, were aligned using Tophat [33]. Expression analysis for each transcription factor mutant was performed as follows: First, the number of reads aligning to an entire mRNA was counted. For each genotype examined, any region with <20 reads in the mutant or wild-type sample was excluded from analysis. Next, counts were compared between datasets after normalizing the datasets using the TMM algorithm [34]. Gene expression profiles for each transcription factor mutant are contained in Table 2. Fold changes averaged between the two replicates and genes were considered significantly changed if they were >1.5-fold or <0.67-fold changed between datasets.

Acknowledgements

I thank members of the Madhani lab for helpful discussions and Nguyen Nguyen for media preparation. I thank Eric Dang for his initial work to develop the ChIP-Seq protocol in the Madhani lab. This work was supported by a grant from the National Institute of Allergy and Infectious Disease (R01AI096869) and a fellowship from the National Heart, Lung, and Blood Institute (F30HL120496-01A1). CMH and HDM designed the study. CMH performed the experiments and HDM supervised the work.

Figures and Tables

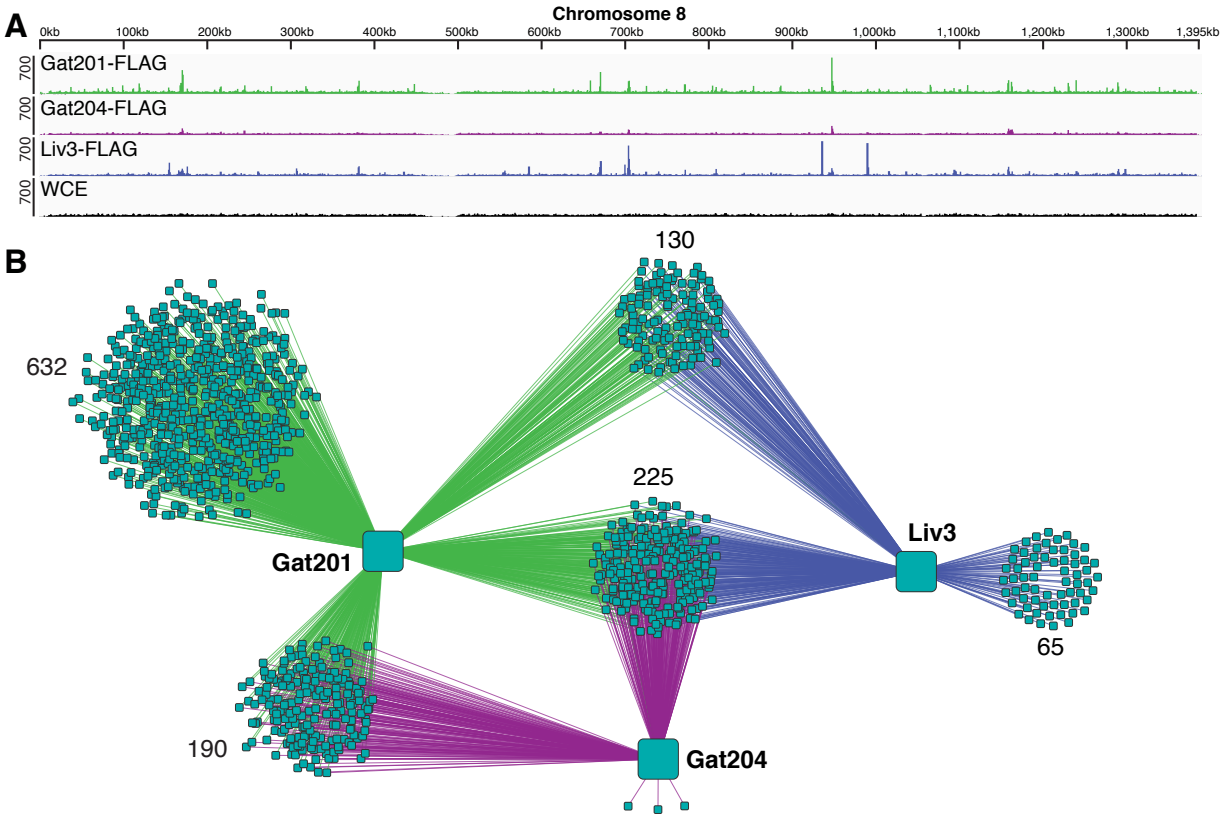

Figure 1

Figure 1: The Gat201-Gat204-Liv3 regulatory network

a) Representative ChIP-Seq data from chromosome 8. The y-axis represents number of reads.

b) Network diagram showing promoters bound by each regulator.

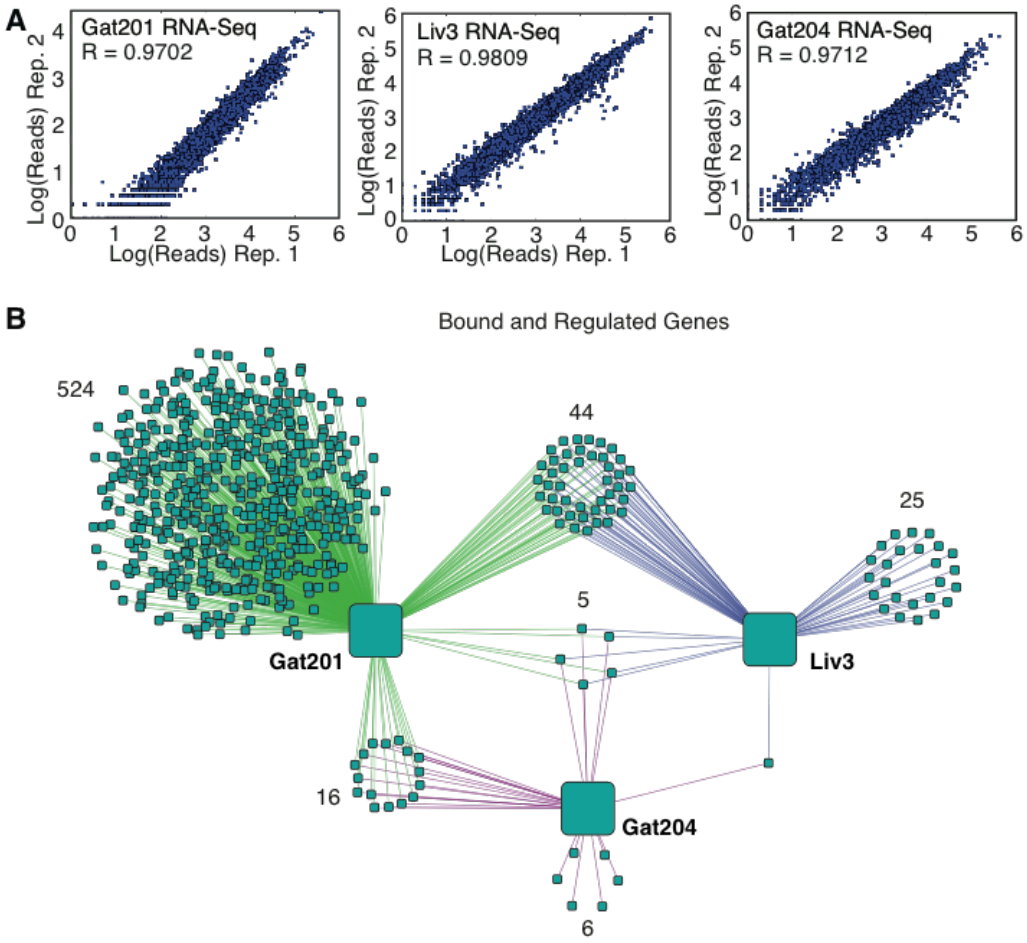

Figure 2

Figure 2: Expression profiling of Gat201-Gat204-Liv3 network

a) Scatterplots of RPKMs in two biological replicates of RNA-Seq datasets. Each point represents a gene.

b) Bound and regulated network diagram. This diagram shows genes whose promoters were bound by each transcription factor and whose expression is changed by greater than 1.5-fold in either direction in the transcription factor deletion mutant compared to wild type.

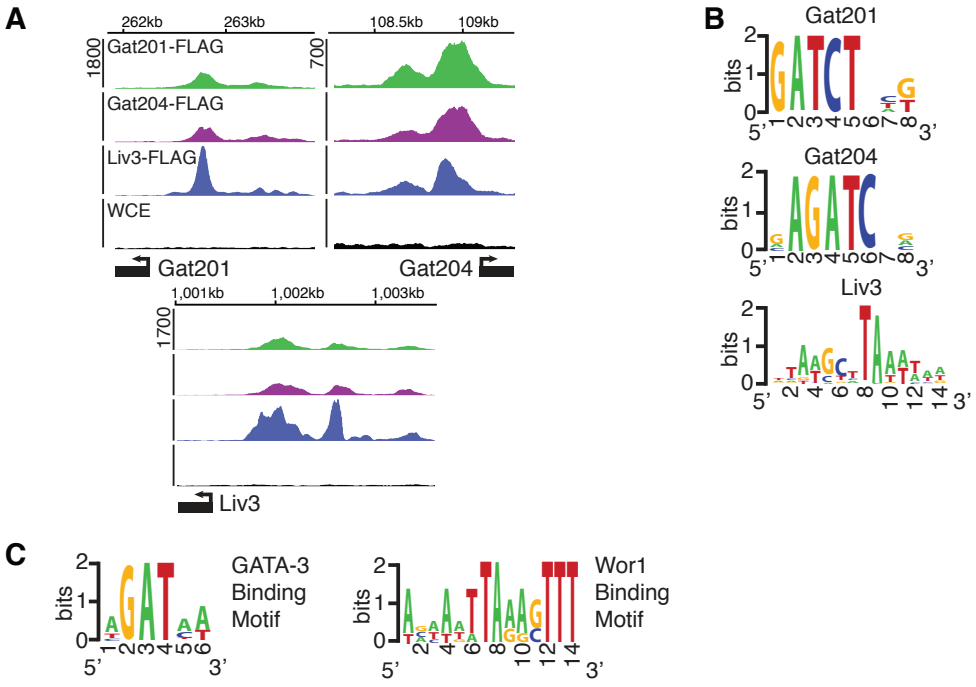

Figure 3

Figure 3: Binding motifs of the Gat201-Gat204-Liv3 virulence network

a) ChIP-Seq traces for Gat201, Gat204, and Liv3 at the promoter of each regulator. The y-axis represents number of reads.

b) Binding motifs derived from Gat201, Gat204, and Liv3 ChIP-Seq datasets.

c) DNA binding motifs for GATA-3 transcription factors and the *C. albicans* Wor1 transcription factor.

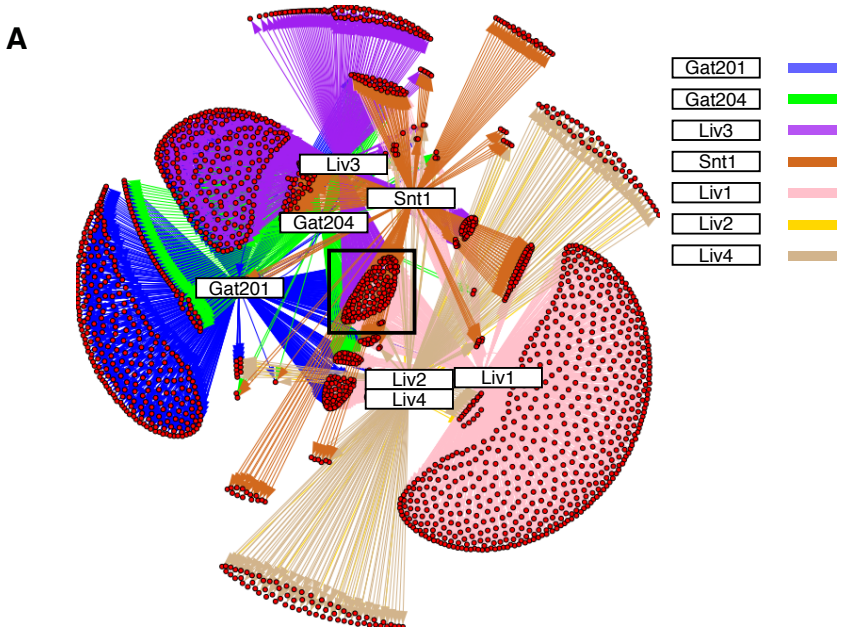

Figure 4

Figure 4: Expanded virulence transcription factor network in *C. neoformans*

a) A network composed of ChIP-Seq targets for seven total transcription factors involved in cryptococcal virulence.

Table 1: Gat201, Gat204, and Liv3 ChIP-Seq profiles, Related to Figure 1, Extended Experimental Procedures

ChIP-Seq: Genes whose promoters were bound in all three biological replicates are listed with the average enrichment of ChIP signal at their promoters over input sample. The same ChIP-Seq peak was allowed to be assigned to multiple genes' promoters. The prefix "3P" indicates the intergenic region downstream of a given gene and was used to connote intergenic regions that were downstream of two convergent genes.

Table 1 is available on the Cell Host and Microbe website due to large size.

Table 2: Expression profiles of *gat201*Δ, *gat204*Δ, and *liv3*Δ, Related to Figure 1, Extended Experimental Procedures

RNA-Seq: Fold change (mutant/wildtype, log2 scale) in transcript level was determined by RNA-Seq using two biological replicates and listed in columns B and C. The fold change was averaged and converted to log2 scale in column D. For the genes whose promoters were bound by a regulator in the ChIP-Seq analysis, the average enrichment over input is listed.

Table 2 is available on the Cell Host and Microbe website due to large size.

Table 3: Strains used in this study, Related to Experimental Procedures

Strain #	Name	Species	Genotype	Parent	Source
CM18	-	*C. neo.*	H99 (wildtype)	-	1
CM205	Gat201-FLAG	*C. neo.*	*gat201-CBP-2xFLAG-NatR*	CM18	2
CM1522	Gat204-FLAG	*C. neo.*	*gat204-CBP-2xFLAG-NatR*	CM18	5
CM174	Liv3-FLAG	*C. neo.*	*liv3-CBP-2xFLAG-NatR*	CM18	4
D1725	*gat201*Δ	*C. neo.*	*gat201*Δ*::NatR*	CM18	3
D1521	*gat204*Δ	*C. neo.*	*gat204*Δ*::NatR*	CM18	2
D1715	*liv3*Δ	*C. neo.*	*liv3*Δ*::NatR*	CM18	3
			Sources:		
			1= Gift of J. Lodge		
			2= Chun, Brown [8]		
			3= Liu, Chun [7]		
			4= This study		

Table 4: Correlation between ChIP-Seq Biological Replicates, Related to Extended Experimental Procedures

Aligned sequences from transcription factor ChIP-Seq data were divided up into consecutive non-overlapping 1 kb windows and coverage was compared between two replicates as described in the table. The R-value of Pearson Correlation is reported for each comparison.

Gat201	Dataset 1	Dataset 2	Dataset 3
Dataset 1	1	0.9754	0.9740
Dataset 2		1	0.9791
Dataset 3			1
Gat204	Dataset 1	Dataset 2	Dataset 3
Dataset 1	1	0.9523	0.9353
Dataset 2		1	0.9979
Dataset 3			1
Liv3	Dataset 1	Dataset 2	Dataset 3
Dataset 1	1	0.9490	0.8898
Dataset 2		1	0.9088
Dataset 3			1

Supplemental Figures

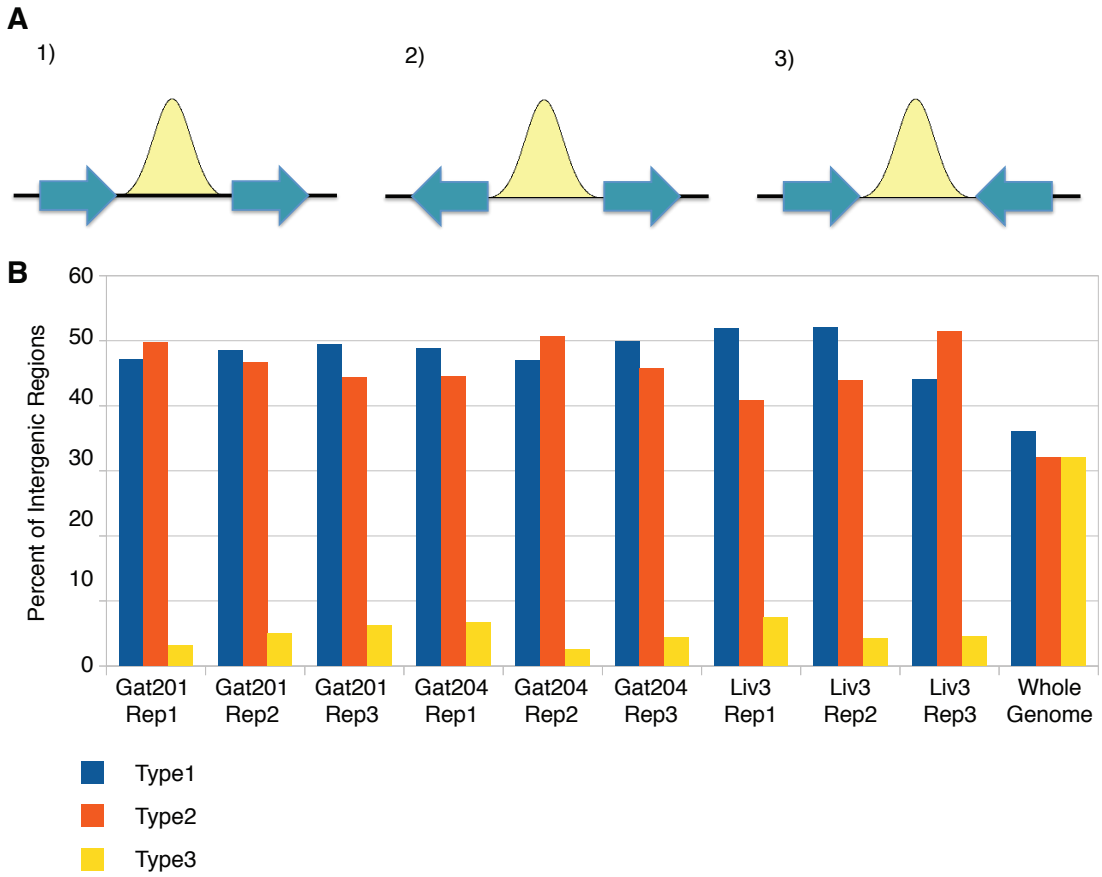

Figure S1

Figure S1: Further characterization of the Gat201 transcriptional network, Related to Figure 1

a) Intergenic classification. Each class is defined by the orientation of the genes flanking the intergenic region.

b) Intergenic classification of ChIP-Seq datasets. The intergenic regions that contained binding peaks in each dataset were classified and graphed here, along with a comparison of all the intergenic regions in the whole genome.

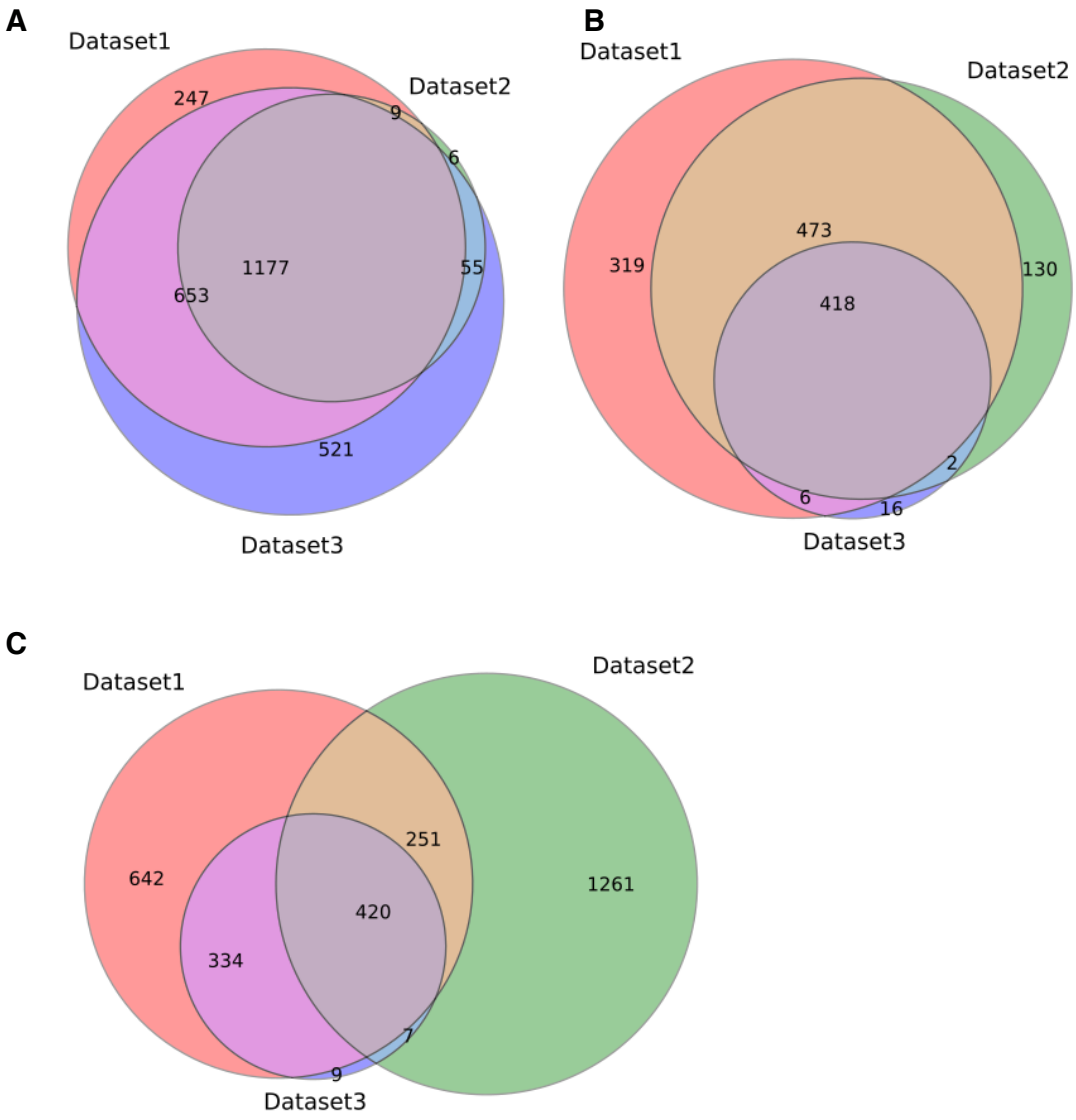

Figure S2

Figure S2: ChIP-Seq target overlap for replicates of the Gat201 transcriptional network, Related to Figure 1

a) Number of targets shared between ChIP-Seq datasets for Gat201, b) Gat204, and c) Liv3.

Works Cited

1. Claudia Monari, F.B.A.V., *Glucuronoxylomannan exhibits potent immunosuppressive properties.* FEMS Yeast Research, 2006. **6**: p. 537-542.
2. HA Torres, V.P., Il Raad, DP Dontoyiannis, *Proven pulmonary cryptococcosis due to capsule-deficient Cryptococcus neoformans does not differ clinically from proven pulmonary cryptococcosis due to capsule-intact Cr. neoformans.* Mycoses, 2005. **48**(1): p. 21-24.
3. Kozel, T.R. and J. Cazin, *Nonencapsulated Variant of Cryptococcus neoformans I. Virulence Studies and Characterization of Soluble Polysaccharide.* Infect Immun, 1971. **3**(2): p. 287-94.
4. Laurenson, I.F., J.D. Ross, and L.J. Milne, *Microscopy and latex antigen negative cryptococcal meningitis.* J Infect, 1998. **36**(3): p. 329-31.
5. O'Meara, T.R., et al., *Interaction of Cryptococcus neoformans Rim101 and protein kinase A regulates capsule.* PLoS Pathog, 2010. **6**(2): p. e1000776.
6. Idnurm, A., et al., *Cryptococcus neoformans virulence gene discovery through insertional mutagenesis.* Eukaryot Cell, 2004. **3**(2): p. 420-9.
7. Liu, O.W., et al., *Systematic genetic analysis of virulence in the human fungal pathogen Cryptococcus neoformans.* Cell, 2008. **135**(1): p. 174-88.
8. Chun, C.D., J.C. Brown, and H.D. Madhani, *A major role for capsule-independent phagocytosis-inhibitory mechanisms in mammalian infection by Cryptococcus neoformans.* Cell Host Microbe, 2011. **9**(3): p. 243-51.
9. Jung, W.H., et al., *Iron regulation of the major virulence factors in the AIDS-associated pathogen Cryptococcus neoformans.* PLoS Biol, 2006. **4**(12): p. e410.

10. Beyhan, S., et al., *A temperature-responsive network links cell shape and virulence traits in a primary fungal pathogen.* PLoS Biol, 2013. **11**(7): p. e1001614.

11. Perez, J.C., C.A. Kumamoto, and A.D. Johnson, *Candida albicans commensalism and pathogenicity are intertwined traits directed by a tightly knit transcriptional regulatory circuit.* PLoS Biol, 2013. **11**(3): p. e1001510.

12. Nobile, C.J., et al., *A recently evolved transcriptional network controls biofilm development in Candida albicans.* Cell, 2012. **148**(1-2): p. 126-38.

13. Sorrells, T.R. and A.D. Johnson, *Making Sense of Transcription Networks.* Cell, 2015. **161**(4): p. 714-723.

14. Hughes, T.R. and C.G. de Boer, *Mapping yeast transcriptional networks.* Genetics, 2013. **195**(1): p. 9-36.

15. Whitfield, T.W., et al., *Functional analysis of transcription factor binding sites in human promoters.* Genome Biol, 2012. **13**(9): p. R50.

16. Fisher, W.W., et al., *DNA regions bound at low occupancy by transcription factors do not drive patterned reporter gene expression in Drosophila.* Proc Natl Acad Sci U S A, 2012. **109**(52): p. 21330-5.

17. Ko, L.J. and J.D. Engel, *DNA-binding specificities of the GATA transcription factor family.* Mol Cell Biol, 1993. **13**(7): p. 4011-22.

18. Lohse, M.B., et al., *Distinct class of DNA-binding domains is exemplified by a master regulator of phenotypic switching in Candida albicans.* Proc Natl Acad Sci U S A, 2010. **107**(32): p. 14105-10.

19. Kim, T., et al., *Set3 HDAC mediates effects of overlapping noncoding transcription on gene induction kinetics.* Cell, 2012. **150**(6): p. 1158-69.

20. Janbon, G., et al., *Analysis of the genome and transcriptome of Cryptococcus neoformans var. grubii reveals complex RNA expression and microevolution leading to virulence attenuation.* PLoS Genet, 2014. **10**(4): p. e1004261.

21. Chun, C.D. and H.D. Madhani, *Applying genetics and molecular biology to the study of the human pathogen Cryptococcus neoformans.* Methods Enzymol, 2010. **470**: p. 797-831.

22. Rohland, N. and D. Reich, *Cost-effective, high-throughput DNA sequencing libraries for multiplexed target capture.* Genome Res, 2012. **22**(5): p. 939-46.

23. Langmead, B., *Aligning short sequencing reads with Bowtie.* Curr Protoc Bioinformatics, 2010. **Chapter 11**: p. Unit 11 7.

24. Schiller, B.J., *Data Biology: A quantitative exploration of gene regulation and underlying mechanisms.* 2013.

25. Li, H., et al., *The Sequence Alignment/Map format and SAMtools.* Bioinformatics, 2009. **25**(16): p. 2078-9.

26. Quinlan, A.R., *BEDTools: The Swiss-Army Tool for Genome Feature Analysis.* Curr Protoc Bioinformatics, 2014. **47**: p. 11 12 1-11 12 34.

27. Quinlan, A.R. and I.M. Hall, *BEDTools: a flexible suite of utilities for comparing genomic features.* Bioinformatics, 2010. **26**(6): p. 841-2.

28. Zhang, Y., et al., *Model-based analysis of ChIP-Seq (MACS).* Genome Biol, 2008. **9**(9): p. R137.

29. Ng, P. and U. Keich, *GIMSAN: a Gibbs motif finder with significance analysis.* Bioinformatics, 2008. **24**(19): p. 2256-7.

30. Crooks, G.E., et al., *WebLogo: a sequence logo generator.* Genome Res, 2004. **14**(6): p. 1188-90.

31. Dumesic, P.A., et al., *Product binding enforces the genomic specificity of a yeast polycomb repressive complex.* Cell, 2015. **160**(1-2): p. 204-18.

32. Zhang, Z., et al., *Strand-specific libraries for high throughput RNA sequencing (RNA-Seq) prepared without poly(A) selection.* Silence, 2012. **3**(1): p. 9.

33. Trapnell, C., et al., *Differential gene and transcript expression analysis of RNA-seq experiments with TopHat and Cufflinks.* Nat Protoc, 2012. **7**(3): p. 562-78.

34. Oshlack, A., M.D. Robinson, and M.D. Young, *From RNA-seq reads to differential expression results.* Genome Biol, 2010. **11**(12): p. 220.

Chapter 3

Convergently-evolved peptide-based cell-cell signaling system required for the virulence of a eukaryotic pathogen

Summary

Qsp1 is a peptide of unknown function secreted by the fungal meningitis pathogen *Cryptococcus neoformans*, a major driver of mortality in HIV/AIDS. We identified *QSP1* as a direct target of three transcription factors required for virulence. Indeed, we find that *qsp1*Δ mutants are attenuated for infection, display dramatically slowed tissue accumulation, and are more readily controlled by primary macrophages. We further demonstrate that Qsp1 mediates autoregulatory signaling that modulates the activities of secreted proteases and promotes cell wall function at high cell densities. Production of the peptide requires its release from a secreted precursor by a cell-associated protease. Remarkably, Qsp1 sensing requires an oligopeptide transporter, and cytoplasmic expression of the mature Qsp1 peptide complements multiple phenotypes of the deletion mutant. We conclude that the virulence of *C. neoformans* requires an autoregulatory peptide that is matured extracellularly, but functions intracellularly. This mechanism, unprecedented in eukaryotes, provides avenues for therapeutic development.

Introduction

Disseminated fungal infections are among the most difficult to diagnose and treat, causing death in 30-50% of cases [1-4]. Compounding this challenge, antifungal drug development has been slow; only a single new class of antifungal agents, the echinocandins, has been introduced in the last two decades [5]. While there are more than one million fungal species estimated to exist [6], the majority of disseminated infections are caused by a limited number of species, notably *Candida albicans*, *Aspergillus fumigatus*, and *Cryptococcus neoformans* [2, 7]. Our work focuses on *Cryptococcus neoformans*, the most common cause of fungal meningitis. This single species causes 950,000 cases and 625,000 deaths annually, an estimated 40% of all HIV-related mortality [8]. *C. neoformans* is a member of a pathogen species complex that includes *C. neoformans var grubii* (serotype A) and *C. neoformans var. neoformans* (serotype D) [9]. We primarily study *C. neoformans var grubii*, which is responsible for ~90% of infections in the HIV/AIDS patient population [10, 11]. Investigations of *C. neoformans* pathogenesis have focused on three virulence traits: melanin production [12], growth at human body temperature [13], and production of a polysaccharide capsule [14]. However, as with other fungal pathogens, our knowledge of the specializations that allow *C. neoformans* to thrive within mammalian hosts is limited compared to our sophisticated understanding of bacterial pathogenesis.

Many bacterial pathogens require autoregulatory quorum sensing (QS) systems for virulence, which are regarded as attractive therapeutic targets [15, 16]. In classical bacterial QS paradigms, cells secrete a signal and monitor its concentration to sense cell number and/or diffusion [17, 18], and use this information to regulate diverse biological functions [19]. In gram-negative bacteria, the most common secreted signals are acyl homoserine lactones (AHLs) [20], whereas gram-positive bacteria generally utilize peptides [21].

While several quorum sensing-like phenomena have been described in fungal pathogens, our understanding of their roles and mechanisms of action are limited, and whether any are required for virulence remains an open question [22]. A candidate QS signal in *C. neoformans* was identified in studies of a mutant *C. neoformans* Serotype D strain lacking the co-repressor Tup1 [23]. The authors observed that *tup1*Δ strains, but not wild-type strains, failed to grow when a low number of cells were spread on agar plates. Purification of the activity from *tup1*Δ culture supernatants revealed an 11 amino acid peptide that was able to rescue this low-density plating defect. They suggested that this peptide, which was active at nanomolar concentrations, could be part of a QS system in *C. neoformans* and named it Qsp1 (Quorum Sensing-Like Peptide 1). Unfortunately, no phenotype for a *qsp1*Δ strain was reported and the reason *tup1*Δ strains require Qsp1 is not known. Furthermore, a similar low-density plating defect was not observed in a Serotype A strain lacking *TUP1* [24]. Thus, the normal function of Qsp1 remained unknown.

Through studies aimed at extending a virulence-associated regulatory network, we identified *QSP1* as a direct target of three transcription factors implicated in virulence. This finding, in addition to the importance of QS in bacterial virulence, prompted us to address the following outstanding questions: 1) Is Qsp1 produced by wild-type cultures? 2) Does Qsp1 accumulate with cell density, as is typical for bacterial QS signals? 3) Does Qsp1 have density-dependent functions? 4) Is Qsp1 required for virulence? and 5) What factors are required for cells to produce and respond to Qsp1?

We show that Qsp1 is indeed produced by wild-type cells and accumulates as cell density increases. We demonstrate that Qsp1 is required for virulence, pulmonary colonization, and accumulation within macrophages. Furthermore, we find that Qsp1 promotes normal colony

morphology, cell wall ultrastructure and stress resistance, and modulates the activities of multiple secreted proteases. Transcriptional profiling revealed that Qsp1 controls gene expression selectively at high cell densities and that exogenously-added synthetic Qsp1 can complement the phenotypes of *qsp1*Δ cells, demonstrating autoregulatory function. To identify additional components of the Qsp1 pathway, we constructed a large library of targeted gene deletion strains and screened them using colony morphology as a phenotype. One mutant identified corresponds to a cell-associated serine protease that we demonstrate to be required for the production of Qsp1 from a secreted precursor. Another mutant was *tup1*Δ, already known to interact with *QSP1* in Serotype D. The screen further identified a predicted oligopeptide transporter, which we show is required for cells to respond to Qsp1. This observation raised the possibility that Qsp1 functions intracellularly after being imported into cells. Indeed, cytoplasmic expression of Qsp1 complements multiple phenotypes of the deletion mutant. These studies reveal a peptide-based autoregulatory mechanism, previously unknown in eukaryotes, in which a signal is produced by extracellular proteolysis of a self-made protein but functions intracellularly. Its importance for the virulence of an important human fungal pathogen offers potential avenues for therapeutic development.

Results

QSP1 is a direct target of three virulence regulators

Based on the transcription factor network described in Chapter 2, we anticipated the central targets of the Gat201-Gat204-Liv3 network would be enriched for genes encoding virulence factors. A prominent target, *QSP1,* is a gene encoding a small secreted peptide [23] (Figure 1A, Figure S1A). Strikingly, our RNA-Seq analysis revealed that *QSP1* produces the single most abundant transcript in cells grown in tissue culture conditions (Figure 1B). *QSP1* is predicted to encode a peptide precursor containing a signal sequence and a 24 amino acid pro-peptide (Qsp24), the C-terminal 11 amino acids of which encode the mature Qsp1 peptide [23] (Figure 1C). To determine whether this abundant transcript templates the production of high amounts of the mature peptide, we raised polyclonal rabbit antisera against Qsp1 (Figure S1B). Qsp1 is readily detected in wild-type culture supernatants by immunoblotting, producing a signal that comigrates with the synthetic peptide (Figure S1C). We next developed a quantitative ELISA to measure the concentration of Qsp1 in culture supernatants, and this analysis revealed that the peptide accumulates with cell density to micromolar concentrations (Figure 1D).

QSP1 is required for virulence

As a highly expressed, central target of the Gat201-Gat204-Liv3 network, *QSP1* was a candidate virulence factor. We first assessed whether the *qsp1*Δ mutant displays a growth defect in vitro. However, we observed no defects in the growth of *qsp1*Δ cells after plating on media containing oxidative, nitrosative, pH, iron starvation, osmotic, or cell wall stressors (Figure S1D&E). Next, we assessed virulence of two independently derived *qsp1*Δ mutants using an

established intranasal infection model in A/J mice [25, 26]. We found that *qsp1*Δ mutants are significantly attenuated compared to wild type. Mean survival time for mice infected with wild-type *C. neoformans* was 14.6 days whereas mean survival times for mice infected with *qsp1*Δ-1 or *qsp1*Δ-2 mutants were 24.2 and 23.2 days, respectively (Figure 2A). Since A/J mice have a C5 complement deficiency [27, 28], we tested whether *qsp1*Δ mutants were also attenuated in an immunocompetent mouse strain, C57Bl/6 [29]. We obtained similar results in this mouse background: wild-type-infected mice displayed a mean survival time of 17.6 days, while *qsp1*Δ-1- and *qsp1*Δ-2-infected mice had mean survival times of 27.1 days and 25.4 days, respectively (Figure S2A).

In *C. neoformans*, virulence-attenuated mutants fall into several classes. One group, including *gat201*Δ and *gat204*Δ [30], comprises mutants deficient in early pulmonary accumulation. Another group, including a urease-deficient strain, *ure1*Δ*,* corresponds to mutants that accumulate normally in the lung but are deficient in dissemination [31]. To differentiate between these two groups, we quantified the cryptococcal viable cell counts (CFUs) in lung homogenates obtained from mice infected with either wild-type or *qsp1*Δ strains. Compared to wild type, *qsp1*Δ mutants accumulated to approximately three-fold fewer CFUs at day four after infection and to 20-fold fewer CFUs at day 13 (Figure 2B). Control experiments demonstrate that these defects were not due to a defect in initial seeding of the tissue (Figure S2B). In addition to the fitness defect during early infection, we examined whether *qsp1*Δ strains had a phenotype during central nervous system infection, using an intracisternal infection model in immunosuppressed rabbits [32]. This model has been used to identify mutants unable to establish chronic meningitis, which are instead rapidly cleared from the meninges [33, 34]. However, we

detected no significant difference in cerebrospinal fluid CFUs between wild type and *qsp1*Δ (Figure S2C), indicating similar fitness in the central nervous system.

Investigations of the cryptococcal *rim101*Δ mutant demonstrate that it alters the host immune response, thereby impacting its virulence [35, 36]. Cryptococcal infections that result in a Th2-dominant T-cell response tend to favor *C. neoformans* [37, 38], while Th1-dominant responses more effectively clear the fungus [39]. We therefore examined whether there is an altered inflammatory response during *qsp1*Δ infection. We determined the number and type of leukocytes recruited to lungs after infection with wild-type or *qsp1*Δ strains using flow cytometry-based profiling of tissue homogenate (Figure 2C). Consistent with the lower pulmonary burden found after infection with *qsp1*Δ mutants, there were fewer leukocytes recruited. However, the majority of leukocytes were eosinophils, as in samples obtained from lungs of mice infected with wild type, indicating a Th2-polarized infection [40]. We also assessed the level of cytokines in lungs and found no differences between wild-type and mutant infections at early or late time points (Figure 2D). As predicted by the leukocyte recruitment data, the type 2 cytokines (IL-4, IL-5, and IL-13) [38] dominated at 3.5 days after infection and IL-13 was the most abundant cytokine 13 days after infection. These data are consistent with studies of T cell polarization during wild-type *C. neoformans* infections [41, 42].

While the general Th1/Th2 polarization is unchanged, this finding does not preclude Qsp1 impacting the interaction between *C. neoformans* and specific leukocytes. In particular, we examined the interaction between the *qsp1*Δ mutant and macrophages, the most abundant immune cells in the alveolar space [43]. Hosts susceptible to cryptococcal infection display decreased survival when depleted of macrophages [44, 45] and macrophages contribute to cryptococcal dissemination [46, 47]. First, we measured phagocytosis rates of wild-type and

*qsp1*Δ strains using bone marrow-derived macrophages (BMDMs) as described previously [26, 48] (Figure S2D). We observed no difference between wild type and *qsp1*Δ mutants when cryptococcal cells were unopsonized (Figure 2E, Figure S2E) or opsonized with a monoclonal antibody against the capsule (Figure 2F, Figure S2E). We reasoned that *qsp1*Δ cells may have altered fitness after phagocytosis in the high-density environment of the phagolysosome [49]. Therefore, we measured the ability of the *qsp1*Δ mutant to accumulate within macrophages [48, 50] (Figure S2F). After phagocytosis, we observed that wild-type cells accumulated intracellularly significantly faster than *qsp1*Δ cells, which displayed approximately two-fold fewer CFUs 24- and 48-hrs after infection (Figure 2G). These observations indicate that *qsp1*Δ cells are more readily controlled by BMDMs than wild type.

Intercellular signaling by Qsp1

Since *qsp1*Δ strains are attenuated for virulence, we continued to seek additional phenotypes for the mutant. We serendipitously observed that *qsp1*Δ mutants form dry, wrinkled colonies at room temperature, in contrast to smooth, mucoid colonies produced by wild type (Figure 3A). This colony phenotype provided an opportunity to assay Qsp1 function. Specifically, we developed a confrontation assay in which recipient strains were grown as colonies near a patch of donor strain cells. We found that, when *qsp1*Δ cells are confronted by a wild-type patch of cells, they grow to produce smooth colonies (Figure 3B). We reasoned that this effect was due to Qsp1 diffusing from the donor. Indeed, synthetic Qsp1 was sufficient to cause *qsp1*Δ cells to produce smooth colonies (Figure S3A). To determine whether this effect was specific to Qsp1, we synthesized and tested the predicted proQsp1 (Qsp24) and pro-region (Qsp13) peptides. We also synthesized a peptide in which the 11 amino acids of Qsp1 are

scrambled (Scrambled Qsp1). We found that Qsp24 is sufficient to complement the *qsp1*Δ colony phenotype but Qsp13 and scrambled Qsp1 are not (Figure S3A), suggesting Qsp1 is sufficient and necessary for normal colony morphology. To assess structure-function relationships in Qsp1, we synthesized mutant peptides, including all possible single amino acid substitutions to alanine/glycine for large side-chains or to tryptophan for small side-chains. We also synthesized N- and C- terminal truncations of Qsp1 (Table S6, Experimental Procedures). None of the truncations display colony morphology-altering activity (data not shown). All but three positions in Qsp1 are sensitive to substitution (Figure S3B), indicating a strong requirement for specific residues for function.

Modulation of canonical virulence factors by Qsp1

Other cryptococcal mutants have been reported to form dry colonies, mostly mutants lacking capsule [51, 52] or mutants that are hyphal [53]. However, *qsp1*Δ cells grow exclusively in the yeast form and they stain normally with an anti-capsular monoclonal antibody (mAb339) (data not shown). *C. neoformans* cells display much larger capsules during mammalian infection [54] than those seen under standard laboratory conditions [55], and large capsules can be induced by specific in vitro conditions [56]. Therefore, we subjected wild-type and *qsp1*Δ cells to capsule-inducing conditions and quantified capsule size. At 37ºC, *qsp1*Δ mutants formed capsules that were similar to wild type. However, at room temperature, *qsp1*Δ mutant cells had larger capsules than wild type (Figure 3C, Figure S3C). While the capsule enlargement of *qsp1*Δ mutants at room temperature is potentially informative for understanding their colony phenotype, the capsule size of the mutant is normal at 37ºC, the temperature of the mammalian host.

Cell wall-associated melanin is another well-studied virulence factor of *C. neoformans*, and is typically assayed by spotting cells from a liquid culture on an agar plate containing L-DOPA, a phenolic precursor to melanin. *lac1*Δ *lac2*Δ mutants lack both laccase enzymes responsible for melanin and therefore remain light-colored on L-DOPA plates. We found that *qsp1*Δ mutants displayed altered melanization at 37ºC, but the phenotype curiously depended on the condition of cultures used to inoculate the assay (Figure 3D). Using cells from saturated liquid cultures, we observed that *qsp1*Δ cells are hypomelanized and that this defect could partially be rescued by addition of synthetic Qsp1. Conversely, *qsp1*Δ cells grown on filters on solid medium and then transferred to L-DOPA plates are hypermelanized (Figure 3D). Thus, Qsp1 is not essential for melanization and, under some conditions, negatively regulates this virulence factor. *lac1*Δ cells are attenuated for virulence but mouse lungs infected with this mutant show altered leukocyte recruitment and cytokine levels compared to wild type [57]. As the *qsp1*Δ mutant does not display such changes, it is unlikely that the attenuated virulence of the *qsp1*Δ mutant is due solely to changes in melanization.

Qsp1 impacts multiple secreted endoprotease activities

A secreted metalloprotease has been shown to be required for cryptococcal invasion of the central nervous system [58] and we have recently identified a secreted aspartyl protease required for cryptococcal virulence (S.C.C., et. al., unpublished observations). In work to be described elsewhere, we developed fluorogenic peptide substrates (Figure S3D) to assay secreted serine, aspartyl, and metallo endoprotease activities in *C. neoformans* and identified the genes encoding each activity (S.C.C., et. al., unpublished observations). We examined the impact of Qsp1 on these activities in *C. neoformans*. In wild-type culture supernatants from tissue culture

conditions, secreted metalloprotease and serine endoprotease activites dominate while secreted aspartyl endoprotease activity dominates when cultures are grown in minimal media (S.C.C. et al, unpublished observations). *qsp1*Δ mutants have decreased secreted aspartyl endoprotease activity in minimal media and increased secreted serine endoprotease and metalloprotease activities in tissue culture conditions compared to wild type (Figure 3E). Growing cultures in the continuous presence of synthetic Qsp1 restored the serine and aspartyl endoprotease activities (Figure 3E).

Qsp1 regulates the transcriptome at high cell-density

To determine whether Qsp1 regulates gene expression, we initially performed a low-coverage RNA-Seq experiment comparing wild type and *qsp1*Δ cells grown in log-phase and saturated culture conditions. We observed 100 genes differentially expressed in *qsp1*Δ compared to wild-type saturated cultures but only five differentially-expressed genes in log-phase cultures (Figure 4A), indicating a density-dependent impact on the transcriptome. We next performed a high-coverage experiment comparing saturated wild-type and *qsp1*Δ cultures, and identified 1749 differentially expressed genes. Notably, this set of Qsp1-regulated genes is significantly enriched for genes that encode proteins of the cell wall/extracellular proteome of *C. neoformans* (Figure 4B) [59], and a number of *QSP1*-regulated genes are known or predicted to be involved in cell wall biogenesis or regulation (Figure S4A).

***qsp1*Δ mutants display density-dependent cell wall defects**

Further motivating investigation of the cell wall, changes in the cryptococcal cell wall have been shown to impact colony morphology [60], melanization [61, 62], and capsule behavior

[62-64], each of which are altered in *qsp1*Δ mutants. We assessed cell wall structure of wild-type and *qsp1*Δ cells by thin section transmission electron microscopy as described previously [35] (Figure 4C). We observed that *qsp1*Δ cells display significantly thinner cell walls than wild type (Figure 4D). Previous studies have shown that wild-type cell walls are organized into distinct layers, typical of fungi [14, 65]. The number and width of layers appears to be dynamic and dependent on conditions, as in other fungi [66, 67]. We observed distinct layers in 90% of the wild-type cell walls examined. In contrast, we observed layers in about 60% of *qsp1*Δ cell walls (Figure 4E).

As described, *qsp1*Δ mutants do not display plating defects on agar containing the cell wall perturbants Calcofluor White, caffeine, or SDS. However, we reasoned that this assay, in which single cells are deposited and then allowed to form colonies, would not capture phenotypes that occur at high cell density. Therefore, we analyzed cell wall function in dense conditions by incubating saturated cultures with cell wall stressors and examining the viability of cells after incubation by plating. We found that *qsp1*Δ mutants display a dramatic loss of viability relative to wild type when exposed to high concentrations of SDS and caffeine (Figure 4F, Figure S4C). This phenotype could be rescued if cells were grown continuously in the presence of the synthetic Qsp1 before the assay. In contrast, exponentially-growing cultures display no difference in viability between the two genotypes. This density-dependent effect is specific to cell wall stressors, as we did not observe increased killing of saturated *qsp1*Δ cultures upon acidified nitrite or hydrogen peroxide treatment (Figure S4B, Figure S4C). Since the *qsp1*Δ capsule and cell wall phenotypes are reminiscent of mutants lacking chitin or chitosan, we quantified chitin and chitosan content of cell walls but found that wild type and *qsp1*Δ mutants display similar profiles (Figure S4D).

A transcription factor functions downstream of Qsp1

In our analysis of the 100 most changed transcripts in *qsp1*Δ cells, we observed a significant enrichment for regulatory targets of the transcription factor Liv3, which binds the Qsp1 promoter as described above (Figure S4E). To test whether Liv3 mediates some or all of the Qsp1 response, we constructed a *qsp1*Δ *liv3*Δ deletion mutant and performed RNA-Seq analysis. To test the role of Liv3 independently of effects Liv3 might have on synthesis, secretion or processing of Qsp1, we profiled the transcriptomes of *qsp1*Δ and *qsp1*Δ *liv3*Δ both grown to saturation in either the presence or absence of synthetic Qsp1. We identified 851 differentially-expressed genes in *qsp1*Δ mutants grown in the presence of synthetic Qsp1 compared to *qsp1*Δ mutants grown in the absence of synthetic Qsp1 (Figure 4G). These strongly overlap with genes identified when wild-type and *qsp1*Δ cells are compared (Figure 4G). In contrast, we observed only 282 differentially-expressed genes in the *qsp1*Δ *liv3*Δ mutant grown with synthetic Qsp1 compared to without (Figure 4G). Thus, Liv3 mediates a majority (66%) of the transcriptional response to Qsp1.

Given these results, we assessed whether *liv3*Δ mutants share the colony phenotype of *qsp1*Δ. Indeed, we observe *liv3*Δ mutants have a dry colony phenotype at room temperature (data not shown) but which is most pronounced at 30ºC (Figure S4F). Like *qsp1*Δ mutants, *liv3*Δ mutants form smooth colonies when grown at 37ºC (Figure S4F). Further supporting a downstream role for Liv3 *liv3*Δ mutants cannot be complemented by a nearby patch of wild-type cells (Figure S4G) or by the synthetic Qsp1 peptides (Figure S4H). In addition, expression of Liv3 using the strong copper-regulated p*CTR4* promoter [68] bypasses the dry colony phenotype of *qsp1*Δ cells (Figure 4H).

Forward genetic screen for mutants in the *QSP1* pathway

We sought additional components of the Qsp1 signaling pathway. Since *QSP1* is part of the Gat201-Gat204-Liv3 network (see Chapter 2), we hypothesized that other network members may encode such components. Therefore, we attempted to construct a deletion mutant for each of the 1010 direct targets of Gat201, Gat204, and/or Liv3. We screened the 705 mutants successfully created for a dry colony phenotype and profiled melanin, capsule, and cell morphology for the nine mutants identified (Table S2). One of the mutants corresponds to *liv3*Δ, confirming observations described above. We screened an additional 1407 mutants produced while constructing a complete deletion collection for *C. neoformans* (the 2112 strains constructed and screened have been deposited to the Fungal Genetics Stock Center). Of these, we identified six additional mutants with the dry colony phenotype (Table S2), including three known acapsular mutants [*cap10*Δ*, cap60*Δ*,* and *cap64*Δ [52, 69, 70]] and one mutant defective in capsule attachment [*pbx1*Δ [71, 72]].

Pqp1 is a protease required for Qsp1 processing

Among the mutants with a dry colony phenotype was a predicted secreted subtilisin-like serine protease encoded by *CNAG_00150* (Figure 5A). Since only a peptide corresponding to the C-terminal 11 amino acids of the larger predicted proQsp1 (Qsp24) peptide was detected in culture supernatants in prior studies [23], we hypothesized that *CNAG_00150* encodes the protease responsible for cleaving the predicted proQsp1 species. Furthermore, we found that the colony phenotype of *qsp1*Δ *pqp1*Δ mutant could be complemented by synthetic Qsp1 but not by synthetic Qsp24 (Figure 5B), suggesting that cells lacking Pqp1 are defective in processing

synthetic Qsp24 into Qsp1 but are able to respond to Qsp1 itself. Below, we refer to this protease as proQsp1 Protease 1 (Pqp1).

Using synthetic Qsp1 and Qsp24, we determined that, while the anti-Qsp1 antibody recognizes both peptides, they cannot be distinguished by mobility after SDS-PAGE and immunoblotting. To resolve these species, we used one-dimensional isoelectric focusing gel electrophoresis (IEFGE). In both rich and minimal media, we identified a band with identical mobility as synthetic Qsp1 in wild-type supernatants but that band was not detected in *pqp1*Δ or *qsp1*Δ supernatants. In *pqp1*Δ supernatants from rich media, we observed a band migrating at a more basic pI but its mobility differed from synthetic Qsp24 (Figure 5C).

We propose that the band present in *pqp1*Δ supernatants could be consistent with two Qsp1 precursors, Qsp15 and Qsp16, which represent the C terminal 15 or 16 amino acids of proQsp1. When we synthesized synthetic with those sequences and analyzed them by IEFGE, their mobility was very similar to that of the Qsp1 species in *pqp1*Δ supernatants (Figure S5C). However, no peaks or spectra were detected in the mass spectrometry data that corresponded with these unmodified peptide species. We hypothesize that the larger band appearing in *pqp1*Δ supernatants may be a modification to these precursors. By mass spectrometry, we were able to identify peaks and spectra consistent with glycosylated species of both Qsp15 and Qsp16 (data not shown). Additionally, peaks and spectra consistent heavily glycosylated Qsp1 was also detected (data not shown). We examined this possibility of Qsp1 species' glycosylation using a C-terminally CBP-2XFlag-tagged Qsp1 construct, which exhibited smearing upon analysis by PAGE followed by anti-Flag immunoblotting. When treated with PNGase, this smear collapsed to a single band, consistent with glycosylation (Figure S5D). I have not attempted to replicate these results, so they will need to be repeated. Smearing is not apparent when the wild type Qsp1

peptide is analyzed by PAGE followed by immunoblotting with the anti-Qsp1 antisera, perhaps indicating that the anti-Qsp1 antisera does not detect the putative glycosylated species.

Since we observed that synthetic Qsp24 complements the colony morphology defect of *qsp1*Δ cells, this possible glycosylation may not be necessary for processing. To test this explicitly, we added synthetic Qsp24 to *qsp1*Δ cultures and analyzed the products by IEFGE and immunoblotting (Figure S5A). Consistent with processing, we observed the appearance of a band that comigrated with synthetic Qsp1. This band did not appear when synthetic Qsp24 was added to *qsp1*Δ*pqp1*Δ cultures (Figure 5D).

To confirm these results, we analyzed peptide species in culture supernatants by LC-MS/MS and identified peaks (Figure 5E) and spectra (Figure 5F) corresponding to the Qsp1 species in samples generated from the supernatant of a wild-type culture. However, we did not observe peaks or spectra corresponding to Qsp1 in *qsp1*Δ or *pqp1*Δ culture supernatants (Figure 5E), supporting the model that Pqp1 is required for maturation of the endogenous precursor. No peak corresponding to Qsp24 was identified in culture supernatants from any genotype examined, again consistent with a modification of this putative precursor that has yet to be defined.

Pqp1 was previously identified as an extracellular but surface-associated protein [59]. Therefore, we quantified proQsp1 processing activity by cells and cell-free supernatants using a proQsp1-like substrate that contained the presumptive cleavage site between a fluorophore and a quencher (Figure S5B). We found that approximately 90% of protease activity against this substrate is cell-associated, although a small amount of activity accumulates in supernatants over time (Figure 5G). A small amount of residual cleavage (10-20% of wild type) was found in *pqp1*Δ mutant cells, presumably due to one or more unknown proteases that cleave at some

position in the peptide (this assay does not measure cleavage at a specific site). To test whether any other proteases are essential for Qsp1 biogenesis or action, we analyzed nine additional mutants lacking predicted secreted proteases (Table S3), and found that none display a dry colony phenotype.

TUP1 interacts with *QSP1* in a density-dependent manner in Serotype A

Another mutant with a dry colony phenotype was the *tup1*Δ mutant in Serotype A. While the *tup1*Δ mutant in Serotype D was not reported to have a dry colony phenotype, it was published to be unable to form colonies when plated on agar plates below a particular cell density. We tested whether the *tup1*Δ mutant in Serotype A had a similar phenotype and found that, at room temperature, the *tup1*Δ mutant was delayed in forming single colonies when streaked for single colonies on agar plates (Figure 6A) or when plated at a 100-fold dilution of saturated cultures (Figure 6B). Adding synthetic Qsp1 peptide to the agar plate, also significantly improved the *tup1*Δ mutant's plating defect phenotype. This same density-dependent plating defect is not present for the *tup1*Δ mutant when it is grown at 30ºC or 37ºC (Figure 6A). We attempted to rescue the *tup1*Δ plating defect by growing the mutant on agar plates with added chemicals, including copper sulfate and diamide. Copper sulfate in agar plates appeared to rescue the *tup1*Δ while diamide did not (Figure S6A). However, I have not attempted to replicate these results so they need to be repeated.

One hypothesis for *tup1*Δ's colony phenotype defect is that the mutant overproduces a toxic metabolic side-product like hydrogen peroxide or superoxide. I tested whether the *tup1*Δ mutant, two independent *qsp1*Δ mutants, and another dry mutant discussed below (*opt1*Δ) had any defect in production of hydrogen peroxide. However, none of the mutants had a consistent

phenotype for hydrogen peroxide production across more than five repetitions of the same experiment (data not shown). Given the high level of biological noise, it is difficult to conclude whether any of these mutants overproduce or underproduce hydrogen peroxide compared to wild type. Next, I examined superoxide production for the same mutants as discussed above and the *fre7*Δ mutant since *FRE7* is predicted to contain a NOX/DUOX domain by sequence homology [73, 74]. Although *fre7*Δ did not have a defect in superoxide production, *tup1*Δ did produce almost 4-fold less superoxide anion than wild type (Figure 6C). This activity was predominantly cell-associated and completed ablated by addition of bovine superoxide dismutase (Figure 6C). No other mutants tested showed a defect in superoxide anion production.

Given *tup1*Δ's density-dependent colony formation defect and its superoxide anion production defect, I tested the ability of the *tup1*Δ mutant to survive within bone marrow-derived macrophages (BMDMs) using the intracellular growth assay described above. In this assay, *tup1*Δ had 3-fold fewer surviving cells than wild type after 24 hours of co-culture with the BMDMs (Figure 6D). This effect was seen in both macrophage supernatants and macrophage lysates (Figure S6B & C). Additionally, this same effect was apparent when using BMDMs that were unstimulated or stimulated with interferon-gamma.

A predicted oligopeptide transporter required for peptide sensing

We began our search for downstream components in the *QSP1* signaling pathway by analyzing all published mutants in G protein coupled receptors and two-component receptors (Table S3). None showed a dry colony phenotype (data not shown). However, our screen identified a gene encoding a predicted oligopeptide transporter, which we named *OPT1* (Figure S7A). Further suggesting a connection, the *QSP1* and *OPT1* genes are located next to each other

in the genome and both display binding of Gat201, Gat204, and Liv3 to their promoters (Figure 7A). Significantly, *opt1*Δ mutants show nearly all of the phenotypes of *qsp1*Δ mutants. Like *qsp1*Δ mutants, *opt1*Δ mutants form dry colonies and are hypercapsular at room temperature (Figure 7B&C, Figure S7B). *opt1*Δ mutants display the same melanization pattern as *qsp1*Δ mutants at 37˚C (Figure S7C). Additionally, *opt1*Δ mutants show viability defects in saturated cultures exposed to SDS and caffeine that are indistinguishable from those of *qsp1*Δ mutants (Figure 7D, Figure S7D), despite no plating defects on any stress conditions tested (Figure S7E&F). Finally, *opt1*Δ mutants display no differences in unopsonized (Figure 7E) or opsonized (Figure 7F) uptake by BMDMs compared to wild type, but have a two-fold intracellular proliferation defect after phagocytosis by BMDMs, similar to *qsp1*Δ mutants (Figure 7G).

Although the phenotypes of *opt1*Δ mutants closely mirror those of *qsp1*Δ mutants, *opt1*Δ mutants differ in two important respects: 1) They can produce Qsp1 and 2) They fail to respond to Qsp1. The dry colony phenotype of *opt1*Δ mutants cannot be complemented by wild-type patches (Figure 7H). However, *opt1*Δ patches can complement nearby *qsp1*Δ colonies, indicating that *opt1*Δ mutants still produce Qsp1. Using our ELISA assay, we found that *opt1*Δ mutants produce wild-type amounts of Qsp1 in culture supernatants at cell densities up to OD 4.5. At higher densities, we observed less accumulation (Figure S7G). However, the colony morphology phenotype of *opt1*Δ mutants and the sensitivity of saturated *opt1*Δ cultures to cell wall stressors are not phenotypes due to a defect in Qsp1 production since they cannot be complemented by addition of synthetic Qsp1 (Figure 7I & Figure S7H).

Qsp1 functions intracellularly

The requirement of Opt1, a predicted oligopeptide transporter, for the response to Qsp1 but not for its production suggests that Qsp1 may be imported to act within cells. Therefore, we replaced the *QSP1* gene with an N-terminal fusion of ubiquitin to the mature Qsp1 peptide to express a precursor (iUbi-Qsp1) (Figure 8A) predicted to be cleaved by endogenous ubiquitin proteases to release the mature Qsp1 peptide cytoplasmically [75]. We controlled the expression of this precursor using the strong copper-repressed p*CTR4* promoter [76]. As expected from the lack of a signal sequence in the construct, these strains did not produce detectable extracellular Qsp1 when assayed using confrontation assays (data not shown). Strikingly, expression of the iUbi-Qsp1 construct by growth on inducing media produces a wild-type colony phenotype while copper-induced repression of the gene recapitulates the dry colony phenotype of the *qsp1*Δ mutant (Figure 8B). Importantly, the media conditions used to regulate the p*CTR4* promoter do not alter the colony phenotypes of wild-type or *qsp1*Δ cells (Figure 8B). Furthermore, we observed that iUbi-Qsp1 complements other phenotypes of the *qsp1*Δ mutant, namely the capsule size changes (Figure 8C) and SDS/caffeine sensitivity (Figure 8D). The requirement of *OPT1* for Qsp1 action together with the ability of iUbi-Qsp1 to complement multiple *qsp1*Δ phenotypes provide strong evidence for intracellular site of action for Qsp1.

Discussion

Meeting the challenge of invasive fungal infections requires an understanding of the attributes of each pathogen that enable its success in the host. In this paper, we describe a peptide-based cell-cell signaling system required for the virulence of *Cryptococcus neoformans*, the most common cause of fungal meningitis and a major driver of mortality in HIV/AIDS. To our knowledge, this work represents the first decisive evidence that autoregulatory signaling is required for fungal virulence. In addition, our studies reveal that the signaling peptide, Qsp1, is formed by extracellular proteolysis of a precursor, but that sensing of Qsp1 occurs intracellularly, a signaling mechanism without precedent in eukaryotes.

A secreted peptide required for virulence in a eukaryotic pathogen

The original functional isolation of Qsp1 relied on a serotype-specific effect, namely that deletion of the *TUP1* gene created a dependency on the secreted peptide for growth [23, 24]. However, no phenotypes for the *qsp1*Δ mutant were reported nor was it demonstrated that wild-type cells produce Qsp1. Our studies showing that three virulence regulators bind to the *QSP1* promoter prompted us to further investigate this peptide. Strikingly, we found that *qsp1*Δ cells are substantially attenuated for lethal disease in the murine inhalation model and show a dramatic reduction in tissue burden in the lungs, the initial site of infection. We ruled out several explanations for the attenuated virulence phenotype of *qsp1*Δ cells. They do not display in vitro plating defects under any condition tested and growth in the host is not generally defective as *qsp1*Δ cell counts reached wild-type levels in a central nervous system infection model. Additionally, our studies of the adaptive immune response to infection did not reveal any detectable change in the dysfunctional Th2 polarization that characterizes cryptococcal disease.

As macrophages are key determinants of the outcome of *C. neoformans* infection, we compared the interactions of wild-type and *qsp1*Δ cells with primary macrophages and observed a two-fold defect in intracellular accumulation of *qsp1*Δ cells compared to wild type. We observed no difference in phagocytosis rates, suggesting a specific role for Qsp1 after uptake. Macrophages are thought to have multiple functions in cryptococcal infection, including a protective role in killing *C. neoformans* as well as contributing to its dissemination. For both functions, the pathogen would presumably gain an advantage by optimizing survival in this cell type. The *qsp1*Δ mutant's intracellular accumulation defect could explain its virulence defect as other cryptococcal mutants with decreased accumulation inside macrophages are attenuated in an intranasal model of infection [77-79]. An intriguing possibility is that confinement in the phagolysosome leads to the accumulation of high local concentrations of Qsp1, thereby triggering its action [49].

Qsp1 mediates autoregulatory signaling

Our identification of a dry colony phenotype for *qsp1*Δ cells enabled us to test whether it could be complemented by Qsp1-producing cells or by synthetic peptide. Both of these approaches demonstrate that the 11 amino acid mature Qsp1 peptide is a cell-cell signaling molecule that is produced by *C. neoformans* and acts on cryptococcal cells, thereby mediating an autoregulatory function. RNA-seq analysis confirms this view that Qsp1 acts on cryptococcal cells themselves. Genetic analysis indicates that the impact of *QSP1* on the transcriptome is density-dependent, suggesting that it functions when the peptide accumulates to high concentrations. These observations are also consistent with our finding that only saturated cultures show sensitivity to stress conditions.

Having recently defined the secreted protease activities of *C. neoformans* (S.C. et al., unpublished observations), we extended our analysis to test the role of Qsp1. We observed Qsp1-dependent changes in three major endoprotease activities. Qsp1 promotes an aspartyl protease activity that we have found in other studies to be required for virulence (S.C.C. et al., unpublished observations). In contrast, Qsp1 limits metalloprotease and serine protease activities, which may be deleterious at high cell densities.

The outer surface of fungi is the cell wall, a dynamic and highly organized protective organelle that impacts virtually all transactions with the environment. It was therefore notable that genes encoding extracellular/cell-wall proteins were significantly enriched among those regulated by *QSP1* at high cell density. In addition, *PLB1*, a gene encoding a phospholipase required for cell wall integrity and virulence, was among genes activated by Qsp1. The dry colony phenotype of *qsp1*Δ cells also pointed to a role in cell wall structure. Indeed, our thin-section EM studies of cell wall ultrastructure revealed changes in thickness and organization in *qsp1*Δ mutants. Furthermore, we observed a concomitant density-dependent change in the resistance of *qsp1*Δ cells to killing by cell wall stressors. To our knowledge, our studies provide the first example in fungi of a mutant that does not synthesize an autoregulatory molecule that exhibits a density-dependent phenotype.

Production of the signal requires a cell-associated serine protease

We used the *qsp1*Δ rough colony phenotype to perform a forward genetic screen for additional components of the pathway. As part of an ongoing effort to construct a complete gene deletion collection, we prioritized targets of the Gat201-Gat204-Liv3 network and also included a large number of additional genes. We ultimately constructed and screened 2112 gene deletion

strains and identified 15 mutants that form dry colonies. One corresponded to a predicted subtilase-like serine protease *CNAG_00150*, which we named *PQP1*. Many lines of evidence support the view that Pqp1 is the protease that cleaves a Qsp1 precursor to produce the 11 amino acid mature Qsp1 peptide: 1) *pqp1*Δ cells fail to produce Qsp1. 2) While *qsp1*Δ's dry colony phenotype can be complemented by addition of either Qsp1 or a predicted precursor, proQsp1, only mature Qsp1 can complement *pqp1*Δ cells. 3) An exogenously-added predicted Qsp1 precursor can be processed by a cell-associated activity present in wild-type and *qsp1*Δ strains but not mutants lacking Pqp1. 4) Deletion of genes coding for all other predicted secreted endoproteases did not yield any mutants with a dry colony phenotype. Although reconstitution of Pqp1 activity using recombinant protein will ultimately be required, our studies strongly imply that Pqp1 is the protease responsible for processing a Qsp1 precursor to the functional Qsp1 signaling molecule.

Qsp1 rescues *tup1*Δ's density-dependent defect in forming single colonies

As in Serotype D, the tup1Δ mutant in Serotype A cannot form single colonies as quickly as wild type when plated at a low density. This plating defect is helped, although not completely alleviated, by addition of the Qsp1 synthetic peptide. Since Qsp1 affects *tup1*Δ's phenotype, it appears that *TUP1* and *QSP1* share a related function. However, perhaps not surprisingly since it is a general transcriptional corepressor, *tup1*Δ is a pleiotropic mutant. The *tup1*Δ mutant has decreased superoxide anion production compared to wild type and also does not survive as well inside of BMDMs. We do not currently know whether these two phenotypes are correlated but it is possible that cryptococcal superoxide anion production is required for *C. neoformans* to

survive inside of BMDMs. Further work will be required to determine whether this hypothesis is true.

Reception requires a predicted oligopeptide transporter: intracellular action of Qsp1

Additional mutants isolated based on their dry colony phenotypes were not complemented by synthetic Qsp1, making them candidates for factors involved in the response to Qsp1. Among these, the *opt1*Δ mutant shares the full constellation of *qsp1*Δ phenotypes, including temperature-dependent changes in colony morphology, capsule production, melanin changes, defective growth within macrophages, and density-dependent sensitivity to cell wall stressors. The notable difference is that, rather than being defective in producing the signal, the *opt1*Δ mutant is defective in responding to the signal. As the *opt1*Δ mutant precisely mirrors the *qsp1*Δ mutant but is defective in signal reception, we reason that Opt1 functions in the response to Qsp1. The predicted protein sequence of Opt1 places it in a well-characterized family of oligopeptide transporters [80], leading us to hypothesize that Opt1 transports Qsp1 into cells. The model that Opt1 transports Qsp1 would explain why no other candidates for cells surface receptors tested displayed a dry colony phenotype.

To test this hypothesis, we constructed a strain to conditionally express the mature Qsp1 peptide intracellularly (iUbi-Qsp1). As expected, the iUbi-Qsp1 strain does not secrete Qsp1. Nonetheless, it displays a wild-type colony morphology upon induction, indicating that expression of mature Qsp1 intracellularly complements the null colony morphology phenotype. Significantly, we observed that iUbi-Qsp1 also complements additional phenotypes of the *qsp1*Δ mutant: capsule size alterations and sensitivity to cell wall stressors. Together with the

requirement of a predicted oligopeptide transporter for the cellular response to Qsp1, these data provide strong evidence that Qsp1 functions intracellularly after being imported.

Evolution of peptide-based autoregulatory signaling

QSP1 and *OPT1* form a two-gene cluster in *C. neoformans*, raising the possibility that they were recently acquired by horizontal gene transfer. However, phylogenetic analysis (Figure S6I) indicates that *OPT1* was present in the ancestor of present day *Tremellaceae*, the basidiomycete family that harbors the *Cryptococcus* species complex. Moreover, genes encoding candidate Qsp1 precursors lie adjacent to *OPT1* in *Filobasidiella depauparata*, *Tsuchiyaea wingfieldii, and Cryptococcus amylolentus* (Table S4). These findings suggest that the Qsp1 system likely evolved prior to the emergence of the pathogenic *Cryptococcus neoformans*/*Cryptococcus gattii* species complex. This conclusion is germane because, while bacterial QS molecules are typically sensed by cell surface receptors, in a handful of gram-positive species the response to a quorum sensing peptide requires a multisubunit oligopeptide permease [81, 82]. The permease enables import of the peptide and its binding to intracellular receptors [81, 83]. Furthermore, in some of these species, the mature peptide is produced by C-terminal cleavage of a precursor by a cell wall-associated peptidase. As our analysis indicates that none of the components involved appear to have a proximal bacterial ancestor, it is clear that the eukaryotic system evolved independently, presumably due to its adaptive value. What might explain this remarkable instance of convergent evolution? Both eukaryotic and prokaryotic microbes secrete proteases to obtain peptide nutrients that are then taken up by peptide transporters. Presumably, self-made secreted proteins are processed to some extent by the same proteases. If a peptide resulting from digestion of a self-made protein were produced that also

had an intracellular activity after import (e.g. binding to a protein and modulation of its activity), this would effectively result in the birth of an autoregulatory system. Notably, the predicted Qsp1-like sequences encoded by the *Tsuchiyaea wingfieldii and Cryptococcus amylolentus* genomes appear to be part of larger proteins, suggesting that the ancestral *QSP1* system may indeed have involved the production of a signaling peptide from proteolysis of a larger secreted protein. As there are numerous other contexts where secreted proteins, proteases, and peptide transporters coexist, including the human small intestine, this signaling mechanism could be widespread and important.

Experimental Procedures

Materials

Strains (Table S5) were grown in YPAD (1% yeast extract, 2% Bacto-peptone, 2% glucose, 0.015% L-tryptophan, 0.004% adenine), YNB, or DMEM at temperatures specified in the text.

Gene nomenclature and identification

C. neoformans genes were defined by Broad Institute (Cambridge, MA) annotations of the *var. grubii* H99 genome (http://www.broadinstitute.org/annotation/genome/cryptococcus_neoformans/MultiHome.html). Genes are named as "CNAG_#." Domains were detected using PFAM and SMART with default settings. We propose renaming the reported *CQS1* gene [23] to *QSP1* in accordance with *C. neoformans* gene naming guidelines [84].

Cryptococcal strain construction

Gene deletions were generated using nourseothricin (NAT) resistance (*natR*) cassettes and proteins were tagged with CBP-2X Flag epitope tags using nourseothricin (NAT) resistance cassettes as previously described [26]. Strains constructed in this study are labeled in Table S5. The strains reported are derived from the KN99α wild type since that isolate is more closely related to the H99 clinical isolate [85].

RNA-Seq Library Preparation

Total RNA was isolated and libraries prepared as described previously [86]. Cultures for RNA-Seq were grown at 30ºC for 48 hours to saturation. 1mL of saturated culture was harvested by

centrifugation for 1 minute at 3000 rpm, discarding supernatant, and immediately freezing the pellet in liquid nitrogen. Cell pellets were lyophilized overnight and then RNA was isolated using TRIzol (Invitrogen). To obtain mRNA, 50-200 μg of total RNA (isolated as described above) was purified using the Oligotex mRNA mini kit (Qiagen). For each RNA sample, two successive rounds of purification were performed. Input RNA quality and mRNA purity were verified by Bioanalyzer Pico RNA chips (Agilent). The purified RNA (120 ng) was treated by on-column DNase digestion as described previously [87], then used to prepare sequencing libraries using the NEBNext Ultra Directional RNA Library Prep Kit (New England Biolabs). Libraries were analyzed for quality and average size on Bioanalyzer High Sensitivity DNA chips (Agilent) and quantified by qPCR with KAPA Library Quant Standards. Libraries were sequenced on the HiSeq 2500 platform (Illumina).

RNA-Seq Analysis

RNA-seq data, which included at least two biological replicates per genotype, were aligned using Tophat [88]. The number of reads aligning to an entire mRNA was counted. Then, the DESeq R package [89] was used to determine which genes were differentially expressed between mutants. Gene expression profiles for saturated conditions are listed in Table S1. Genes with an adjusted p-value < 0.05 were considered significantly changed. Data analysis was performed on 2-3 replicates per condition.

LC-MS/MS Identification of Qsp1 Species

Peptides were extracted from the sample by addition of 90% methanol and 1% acid. The supernant was remove and dried down. Dried supernant was resuspended in 5% acetonitrile and

0.1% formic acid. The extracted peptide samples were analyzed on a Q Exactive mass spectrometer and a Fusion Orbitrap tribrid mass spectrometer (Thermo). Samples were injected directly onto a 15cm, 100µm ID column packed with 5µm ODS-AQ C18 resin (YMC). Samples were separated at a flow rate of 400nl/min on an Easy nLCII (Thermo). Buffer A was 5% acetonitrile and 0.1% formic acid and B was 80% acetonitrile and 0.1% formic acid in water. A one hour reverse phase gradient was used as follows: a gradient of 5-15%B over 5min, an increase to 90%B over 55min. Column was re-equilibrated with 10µl of buffer A prior to the injection of sample. Peptides were eluted directly from the tip of the column and nanosprayed directly into the mass spectrometer by application of 2.5kV voltage at the back of the column. The Q Exactive was operated in a data dependent mode. Full MS^1 scans were collected at 70K resolution with a mass range of 400 to 2000 m/z and an AGC target of $1e^6$. MS^2 scans were collected at 17.5K resolution and an AGC target of $1e^5$ and normalized collision energy of 25. Maximum fill times were set to 10ms and 120ms for MS and MS/MS scans respectively. Quadrupole isolation at 2m/z was used, an underfill ratio of 0.1% was utilized and dynamic exclusion was enabled with exclusion duration of 15 sec. The Fusion Orbitrap tribrid was also subsequently used to collect MS/MS spectra with CID and EThcD to confirm sequence of identified peptides. Data was analyzed by Skyline and manual MS/MS validation.

Colony Morphology Assay and Patch Complementation

Strains were streaked for single colonies on thin YPAD plates (poured so that molten agar/YPAD just covered the bottom of the plate and then allowed to dry for 2 days in room air). Strains were grown until single colonies formed at the specified temperature. For complementation assays, YPAD plates were made as described above and one strain (receiving

strain) was streaked for singles on one half of the plate and then the donor strain was patched on the other side of the plates. Both strains were grown until the recipient strain formed single colonies. For assays involving *liv3*Δ, the assays were conducted at 30ºC. All other assays were performed at room temperature. Colony morphologies were photographed using an Epson Perfection V350 Photo scanner. Colony morphology assays for the copper-repressible and BCS-inducible promoter were performed on YPAD plates containing 25 μM $CuSO_4$ and 1 mM ascorbic acid (promoter off) or YPAD plates containing 200 μM bathocuproine disulphonate (promoter on).

Testing Mutations of Qsp1 Synthetic Peptide

All assays were performed at room temperature unless otherwise specified. Peptides for Qsp1 mutational analysis (Table S6) were synthesized by Peptide 2.0. All peptides were resuspended to 10mM concentration in 100% DMSO and then diluted to 10 μM in water. Biological activity of each peptide sequence was tested by spotting 5 μL of overnight cultures of the *qsp1*Δ strain grown at 30ºC and then 5 μL of the diluted peptide being tested on top of the culture spot. After growth at room temperature, complementation was indicated by the spot growing up smooth whereas uncomplemented spots grew up rough.

Antibody production

A peptide corresponding to the Qsp1 sequence with an N-terminal cysteine (CNFGAPGGAYPW) was synthesized by Peptide2.0 to a purity of >98%. The peptide was conjugated to keyhole limpet hemocyanin and used to immunize rabbits in an 84-day protocol (Covance).

ELISA for Qsp1 in Supernatants

Cell-free supernatants were isolated from growing cultures of the indicated phenotypes in YNB media + 2% glucose. 50 μL of supernatants or synthetic Qsp1 peptide in YNB media + 2% glucose (for the standard curve) were added to wells of 96-well white opaque polystyrene plates (Thermo Scientific #15042) and incubated at room temperature for 3 hours. The supernatants were removed and blotted dry on a stack of paper towels. Wells were blocked with 200 μL of 5% milk in PBS for 2 hours at room temperature. Wells were washed 2x with 200 μL of PBS (blotting dry between washes). Wells were incubated with 100 μL of primary antibody (5% milk in PBS with 1:1000 dilution of rabbit anti-Qsp1 serum) overnight at 4ºC. Wells were washed 3x with 200 μL of PBS (blotting dry between washes). Wells were incubated with 200 μL of secondary antibody (5% milk in PBS with 1:8000 dilutions of HRP-conjugated goat anti-rabbit secondary antibody (Bio-Rad)) for 1 hr at room temperature. Wells were washed 4x with 200 μL of PBS (blotting dry between washes) and then incubated with 100 μL of SuperSignal West chemiluminescent substrate (Pierce). Signal was immediately quantified using the luminescence protocol on a Tecan Infinite M200 plate reader.

Dot Blots Against Qsp1

Peptides were synthesized by Peptide 2.0 to a purity of >98%. 1-3 μL suspensions of peptide dilutions in PBS were spotted onto a hydrated Hybond-P membrane (Amersham) and left to air dry overnight. After rehydration, the membrane was blocked by incubation in 5% milk in TBST for 1 hr at room temperature, followed by 1 hr in 5% milk in TBST supplemented with anti-Qsp1 rabbit serum (1:1,000). The membrane was washed three times for 10 min each in TBST, then

incubated for 1 hr in 5% milk in TBST supplemented with HRP-conjugated goat anti-rabbit secondary antibody (Bio-Rad, 1:8,000), washed three times for 10 min each in TBST, and visualized using SuperSignal PicoWest chemiluminescent substrate (Pierce).

Immunoblotting

To assess Qsp1 or proteases in supernatants, cell-free supernatants from the specified media and growth conditions were lyophilized overnight until dry and resuspended in 1x SDS Sample Buffer (10% glycerol, 60 mM Tris/HCl pH 6.8, 2% SDS, 0.01% bromophenol blue, 1.25% beta-mercaptoethanol). To assess proteases in cellular lysates, the specified amount of ODs of cells were spun down and supernatant removed. The cell pellet was lyophilized dry overnight and resuspended in lysis buffer (50 mM Tris pH 6.8, 1 mM EDTA, 1.83 mM DTT, with a fungal protease inhibitor cocktail). Cells were bead beat 3 x 5 min with 3 minutes rest on ice in between cycles and then 32 μL of 4X SDS Sample Buffer (40% glycerol, 240 mM Tris/HCl pH 6.8, 8% SDS, 0.04% bromophenol blue, 5% beta-mercaptoethanol) were added to the lysates. Samples in SDS Sample Buffer were boiled for 5 mins at 100ºC and then analyzed by SDS-PAGE. Immunoblotting utilized the following antibodies: mouse monoclonal anti-FLAG (Sigma F3165, 1:3,000), rabbit polyclonal anti-*Cryptococcus* Qsp1 (1:1,000). Secondary antibodies included HRP-conjugated goat anti-mouse (Bio-Rad, 1:8,000) and HRP-conjugated goat anti-rabbit (Bio-Rad, 1:2,000).

PNGase Treatment

After cell lysates were prepared as described above, 9 μL of sample were combined with 1 μL 10X Glycoprotein Denaturing Buffer (5% SDS, 400 mM DTT) and denatured at 95ºC for 5

minutes. This reaction was chilled on ice and pulsed in centrifuge to collect liquid at bottom of the tube. Then, 2 µL of 10% NP-40, 6 µL H2O, and 2 µL 10X GlycoBuffer 2 (500 mM sodium phosphate, pH 7.5) were added to the 10 µL product from the previous step. 1 µL of PNGase F (NEB) was added to each sample and the reactions were incubated at 37ºC for 1 hour, immediately followed by the addition of 4X sample buffer and immunoblotting as described above.

Fluorescent Substrate Protease Activity Assay

Protease assays were performed with the specified substrates as previously described [90]. For all protease activity assays, specified substrates were mixed with conditioned media or cells (as stated) at 20 µM concentration, mixed, and fluorescence was monitored over the course of an hour in a Biotek Synergy H4 Hybrid Multi-Mode Microplate Reader. To assay metalloprotease activity, cell-free supernatants from cultures incubated in DMEM were mixed with the iFret1 substrate (K(AMC)-PLGKQVEY-K(DNP)). Activity detected in this condition was abolished by addition of the metalloprotease inhibitor 1,10-phenanthroline. To assay aspartyl protease activity, cell-free supernatants from cultures grown in YNB were mixed with the iFret2 substrate ((AMC)-GSPAFLA-K(DNP)-dA). All activity from this condition is abolished by addition of the aspartyl protease inhibitor pepstatin A. To assay serine protease activity, cell-free supernatants from cultures incubated in YNB were mixed with the Marp1 substrate ((AMC)-PKRLSALL-K(DNP)). All activity from this condition was abolished by addition of the serine protease inhibitor, antipain. Pqp1 protease activity were assayed with a Qsp1-like peptide with the sequence K(MCA)-VKSNNFGA-K(DNP)-RR . All assays for Pqp1 activity were conducted

with YNB conditioned media or cells grown in YNB. All fluorophore/quencher peptides were synthesized by CPC Scientific at 80% purity.

Capsule Induction and Measurement

Capsule was induced as previously described [91] with minor changes: after transfer to 10% Sabouraud's medium buffered to pH 7.3 with 50 mM MOPS, capsule was induced at 37ºC overnight or at room temperature for 3-4 days (until visible capsule was induced on wildtype cells).

Melanin Assessment

Cultures grown to saturation in liquid YPAD medium were spotted onto melanin-inducing plates containing 100 mg/mL L-DOPA (L-dihydroxyphenylalanine, Sigma) and grown at the specified temperatures. Accumulation of pigment was observed over 1-3 days. Peptides in this assay were used at 1μM concentration. For melanin production on a solid substrate, patches of cells were pregrown for four days on sterile filter papers laid on top of YPAD plates and then transferred to melanin-inducing plates containing 100 mg/mL L-DOPA. Accumulation of pigment was observed over the next 1-3 hours.

Saturation Stress Assays

Cells were grown to log phase or saturation (48 hour cultures) in YPAD at 30ºC. Saturated cultures were used at their current concentrations and log phase cultures were adjusted to 7 ODs/mL by concentration (no fresh media added). 50μL of saturated or log phase cells were inoculated into a 2-fold dilution series of various stressors (150μL of stressors at various

concentrations). The stressors were SDS (Sigma) (undiluted starting at 10%), caffeine () (undiluted starting at 100 mg/mL), H_2O_2 (Sigma) (undiluted starting at 30%), acidified sodium nitrite (Sigma) (undiluted starting at 3M), acidified with 50mM succinic acid to pH 4, and water. Cells were incubated at room temperature with most stressors for 3 hours (caffeine at 37ºC for 20 hours) and then plated on YPAD plates and grow at room temperature for 3 days to assess viability. A 6-fold dilution series of cells incubated for 3 hours in water was plated in parallel as a control for number of cells added to assay.

Cell Wall Analysis by TEM and Quantification

48-hr saturated YPAD cultures or 24-hr DMEM cultures (as prepared for RNA-Seq) were prepared to examine cell wall ultrastructure as previously described [64]. Samples were analyzed by Wandy Beatty at the Washington University Molecular Microbiology Imaging Facility.

Chitin and Chitosan Assays

Three biological replicates of each genotype were grown in YPD for 48 hours at the specified temperatures. Three technical replicates for each biological replicate were used for cell wall preparation and chitin and chitosan quantification as described in [61].

Growth Assays

Serial dilutions were spotted on YNB plates and YNB plates with the following additives: 2.5 mM caffeine (Sigma), 1.5 mg/mL Calcafluor White (Sigma), 1.5 M NaCl, 1 M Sorbitol, 2 mM $NaNO_2$ acidified to pH 4 with 25 mM succinic acid, acidified to pH 4 with 25 mM succinic acid, alkalized to pH 7 with 25 mM MOPS buffer, 1 mM H_2O_2, and 2 mM H_2O_2. Serial dilutions were

also spotted on LIM plates [56] and LIM plates with 100 mM $FeCl_3$ and 1 mM ascorbic acid. Plates were grown at 30ºC for 2 days and then photographed.

Intranasal Infection Model

Mouse lung infections were performed as previously described [26]. For monotypic infections, *C. neoformans* strains were grown in liquid YNB + 2% glucose cultures overnight at 30ºC. Cells were counted using a hemacytometer and 2 x 10^6 cells were washed twice in PBS and resuspended in 1 mL of PBS. 5-6 week-old female A/J (NCI) mice or 6 week-old female C57BLk/6 (NCI) mice were anesthetized by intraperitoneal injection of ketamine (75 mg/kg) and medetomidine (0.5-1.0 mg/kg). The mice were then suspended from a silk thread by their front incisors and 50μL of the inoculum (1 x 10^5 cells) were slowly pipetted into the nares. After 10 minutes, the mice were lowered and the anesthesia was reversed by intraperitoneal injection of atipamezole (1.0-2.5 mg/kg). For survival curves, 8-10 mice were infected per inoculum. The concentrations of the inocula were confirmed by plating serial dilutions. Mice were monitored several times a week until onset of symptoms (weight loss, ruffled fur, abnormal gait) and then monitored daily. Mice that displayed signs of severe morbidity (weight loss > 15% of starting weight, abnormal gait, hunched posture, ruffled fur, swelling of the cranium) were sacrificed by CO_2 inhalation followed by cervical dislocation. For Colony Forming Unit (CFU) analysis, lungs, spleens, and brains were removed and homogenized in 5 mL sterile PBS. Serial dilutions of each organ sample were plates on Sabouraud agar plates containing 40 μg/mL gentamicin and 50 μg/mL carbenicillin. This protocol was reviewed and approved by the UCSF Institutional Animal Care and Use Committee.

Rabbit Meningitis Model

Rabbit intrathecal infections were performed as previously described [32]. Yeast strains (KN99α, *qsp1Δ*-1, and *qsp1Δ*-2) were inoculated in 20 ml of YPD broth and grown at 30°C shaking incubator for 2 days. The cells were pelleted at 3000 rpm at RT for 5 min, washed twice in PBS pH 7.4, resuspended in 5 ml of PBS, and counted with a hemacytometer. The cell density was adjusted to $3.3x10^8$ cells/ml in PBS to produce an inoculum of 10^8 cells/0.3ml. The inoculum was assessed for colony forming units (CFUs)/ml by plating 200 ul of a 10^6 dilution on YPD agar. New Zealand White (NZW) male rabbits (4 rabbits/group) were inoculated intracisternally with 10^8 cells in a volume of 0.3 ml using a 5/8" gauge needle and a 3ml syringe. Cerebral spinal fluid (CSF) was collected at days 4, 7, and 11 post-inoculation and 10-fold dilutions were assessed for CFUs on YPD agar. Prior to the cisternal inoculations and CSF taps rabbits were sedated with an IM injection of a mixture of ketamine (46 mg/kg) and xylazine (6 mg/kg). To induce and maintain immunosuppression rabbits were given an IM injection of hydrocortisone acetate (5 mg/kg) one day prior to inoculation and daily during the infection. All work was done according to IACUC protocol A003-14-01.

Leukocyte Recruitment

Lung leukocytes were isolated as previously described [92]. Briefly, lungs were excised and minced to generate approximately 1 mm^3 pieces. The lung mince was incubated in HBSS (Invitrogen, Grand Island, NY) + 1.3 mM EDTA solution for 30 min at 37°C with agitation, and then transferred to RPMI-1640 (Invitrogen) medium supplemented with 5% Fetal Bovine Serum (FBS) (Invitrogen) and 150 U/ml type I collagenase (Invitrogen) and incubated for 1 h at 37°C with agitation. The cells were passed through a 70 μm filter, pelleted, and resuspended in 44%

Percoll-RPMI medium (GE Life Sciences, Pittsburgh, PA). A Percoll density gradient was created (44% top, 67% bottom), and the samples were centrifuged for 20 min at 650 x *g*. The leukocytes at the interface were removed, washed 2 times with RPMI medium, and resuspended in PBS + FBS at a concentration of 10^7 cells/ml.

Flow Cytometry Analysis of Leukocytes

5% (i.e. 500,000 cells) of the sample was stained with the following antibodies: Ly6G (RB6-8C5, APC-eFluor 780, eBioscience), Ly6C (HK1.4, eFluor 450, eBioscience), CD11b (M1/70, BV650, Biolegend), CD11c (N418, BV605, Biolegend), NK1.1 (PK136, AF700, Biolegend), CD3 (17A2, PE-Cy5, Biolegend), CD4 (RM4-5, FITC, Biolegend), CD19 (6D5, PE-Cy7, Biolegend), Sca1 (D7, APC, Biolegend), and Siglec F (E50-2440, PE, BD Biosciences). Cells were identified as the following: Th cells = CD11b- CD3+ CD4+. Eosinophils = CD11b+ CD11c- Siglec F+. Innate lymphoid cells = lineage- Sca1+. Dendritic cells and macrophages = CD11b+ CD11c+ Siglec F-. B cells = Siglec F- CD11b- CD11c- CD19+. Natural killer cells = Siglec F- CD11c- NK1.1+. Neutrophils = CD11b+ CD11c- Ly6G+. Monocytes = CD11b+ Ly6C+ Siglec F-. CD8+ T cells = Siglec F- CD11b- CD3+ CD4-. Dendritic cell subsets were determined using the following antibodies and gating strategy. CD3 (17A2, PE-Cy5, Biolegend), CD19 (6D5, PE-Cy5, Biolegend), Siglec F (E50-2440, APC, BD Biosciences), CD64 (X54-5/7.1, PE, Biolegend), MHCII (M5/114.15.2, AF700, Biolegend), CD11c (N418, BV605, Biolegend), CD11b (M1/70, BV650, Biolegend), CD103 (2E7, e450, eBioscience), FcεRI (MAR-1, PE-Cy7, Biolegend). Cells were identified as the following: Dump = CD3+, CD19+, Siglec F+. Monocyte-derived DC = Dump-, CD64+, CD11c+, MHCII+, CD11b+,

CD103-, FcεRI+. CD103+ cDC = Dump-, CD64-, CD11c+, MHCII+, CD103+, CD11b-. CD11b+ cDC = Dump-, CD64-, CD11c+, MHCII+, CD11b+, CD103-.

Lung Cytokines

Lungs from mice 4 and 13-days post-infection were excised, snap frozen in liquid nitrogen, and homogenized in 3 mL of T-PER (Thermo Fisher Scientific) with Complete Protease Inhibitor Cocktail (Roche, Indianapolis, IN). The lung homogenate was pelleted, and the supernatant was collected and stored at -80°C until analysis. Samples were diluted 1:4 in assay buffer immediately before processing. Cytokines were quantified using Luminex technology according to manufacturer instructions (Bio-Rad, Hercules, CA).

Macrophage Uptake (Opsonized and Unopsonized)

Macrophage uptake and intracellular proliferation assays were performed as previously described [48] with minor changes described below. Bone-marrow derived macrophages (BMDMs) were isolated from the bone marrow of C57BL/6 mice and cultured for 7 days in BMDM growth media containing DMEM H-21, 20% v/v FBS, 2mM glutamine, 0.11 mg/mL sodium pyruvate, and 10% MCSF derived from A549 cell supernatants in the presence of penicillin/streptomycin. 10,000 BMDMs were seeded per well in a 96-well plate (Costar) and stimulated with 100 ng/mL Interferon-γ (Roche) for 24 hours before infection and maintained under stimulation throughout infection. Overnight cultures of *C. neoformans*, grown in YPAD, were washed once in DMEM and then resuspended in BMDM growth media. For opsonized experiments, cells were opsonized with mAb1255 (10μg/mL) at 37ºC for 1 hour prior to infection. Uptake experiments were done at an MOI of 10 (plated serial dilutions of inoculum to confirm MOI) and uptake was assessed

after 24hrs co-culture at 37ºC, 5% CO_2 and 3 washes with PBS to remove non-adherent *C. neoformans* cells. >200 BMDMs quantified per well, with 6 wells per genotype.

Macrophage Killing Assay

BMDMs were prepared as described above and 100,000 cells were seeded per well in a 24-well plates (Corning 353047). BMDMs were stimulated with Interferon-γ as described above and then infected with opsonized *C. neoformans* (see above) at an MOI of 0.1 (plated serial dilutions of inoculum to confirm MOI). After 24 hours co-cultures at 37ºC, 5% CO_2, supernatants were removed and serial dilutions were plated for CFUs. Macrophages were lysed in 500 µL sterile water, sitting at 37ºC for 15 minutes. Wells were washed with an additional 500 µL sterile water and combined with lysate, yielding 1mL lysate. Serial dilutions of this lysate were plated for CFUs. The ratio of CFUs over input was quantified and this value was analyzed by bootstrapping, generating 95% confidence intervals. Non-overlapping 95% confidence intervals were considered significantly different; $p < 0.05$.

Lucigenin Superoxide Production

Cells from saturated cultures were harvested and washed twice with assay buffer (25mM glycine, 0.5% glucose, pH 9.5). Supernatant samples were isolated by spinning out cells and transferring cell-free supernatant to a fresh tube. 50 µL of washed cells or supernatant were transferred to black 96-well plates (Corning 3991). 150 µL of assay buffer containing 133.3 µM lucigenin was added to each 50 µL sample and luminescence was detected using a Tecan M1000 plate reader over the course of an hour, integrating the signal over two seconds.

Internal Qsp1 Strain Construction

The upstream flanking region to the Qsp1 promoter was amplified with the primer pair Q1C8_20F(DKS) and Qsp1.65R(DKS). The Ctr4 promoter was amplified using the primer pair Qsp1.66F(DKS) and Qsp1.77R(DKS). The ubiquitin gene was amplified using the promoter pair Qsp1.78F(DKS) and Qsp1.C2_2R_DKS. The mature Qsp1 and terminator sequences were amplified using the primer pair Qsp1.C2_3F_DKS and Q1C1_2R. The Nat marker was amplified with the primer pair Qsp1.C1_3F_DKS and Qsp1.C1_3R_DKS. The downstream flanking region was amplified with the primer pair Qsp1.C1_4F_DKS and Qsp1.C1_4R_DKS. These four segments were combined with the pRS316 plasmid backbone using homologous recombination in *S. cerevisiae* to form a plasmid. The construct was digested out of the plasmid backbone and transformed into *C. neoformans* to create the internal Qsp1 strain. Transformants were verified using primers flanking each integration site and the primers Ctr4prom_orfcheckF_92F_DKS and qsp1_orfcheckR_DKS.

Primer Name	Primer Sequence
Q1C8_20F(DKS)	GTA AAA CGA CGG CCA GTG AAT TGT AAT ACG ACT CAC TAT AGG GCG AAT TGG TTT AAA TAA TGA TGC AAG CGG GAT ACT TAG
Qsp1.65R(DKS)	GACCATCGATAAGCTTGATTTGGCGAGAGAGAA GAGAGTGTTTTTCTCTC
Qsp1.66F(DKS)	GAGAGAAAAACACTCTCTTCTCTCTCGCCAAATC AAGCTTATCGATGGTC
Qsp1.77R(DKS)	CATACGTCTTGACGAAGATCTGCATATGGATTG GTGAAGTCGTTGTCGTA
Qsp1.78F(DKS)	TACGACAACGACTTCACCAATCCATATGCAGAT CTTCGTCAAGACGTATG
Qsp1.C2_2R_DKS	TACCACCACCGGGGGCGCCGAAGTTTCCACCGC GGAGACGGAGGA
Qsp1.C2_3F_DKS	TCTTGTCCTCCGTCTCCGCGGTGGAAACTTCGGC GCCCCCGGTGG
Q1C1_2R	CGCTCTCCAGCTCACATCCTCGCAGCGTTGTCGA GGGATGACGGATGTTGG
Qsp1.C1_3F_DKS	CAACATCCGTCATCCCTCGACAACGCTGCGAGG ATGTGAGCTGGA

Qsp1.C1_3R_DKS	TTTGCGCCTGCATGTGCTGCACATTGGTTTATCTGTATTAACACGGAAGAGATGT
Qsp1.C1_4F_DKS	TCTTCCGTGTTAATACAGATAAACCAATGTGCAGCACATGCAGGC
Qsp1.C1_4R_DKS	CAGGAAACAGCTATGACCATGATTACGCCAAGCTCGGAATTAACCCTCACTAAAGGGTTTAAACTTGAGAAGGAAGAGGTTTGCTTGGT
Ctr4prom_orfcheckF_92F_DKS	GTGTGGATGGATGGCAAGG
qsp1_orfcheckR_DKS	AAAGAGGATGTTGGGAATGG

Acknowledgements

We thank members of the Madhani lab for helpful discussions, Nguyen Nguyen for media preparation, members of the laboratory of Jeff Cox (Samantha Bell, Trevor Parry, and Robert Watson) for kind gifts of bone-marrow derived macrophages and reagents, and Joe Heitman for strains. This work was supported by a grant from the National Institute of Allergy and Infectious Disease (R01AI096869) and a fellowship from the National Heart, Lung, and Blood Institute (F30HL120496-01A1). Mass spectrometry experiments were supported by the National Center for Research Resources (P41RR011823), the National Institute of General Medical Sciences (P41GM103533), and the National Institute on Aging (R01AG027463). Rabbit experiments were supported by NIAID grant R01AI73896.

CMH and HDM designed the study. DS performed experiments shown in Figure 7 & S3B. AIG performed experiments shown in Figure 3D, 5B, 5C, 5D, S1F, 6C, and Table S3. AIG, IC, and SP created the knockout collection for screening. SCC and CC performed experiments shown in Figure 3E and provided protocols and guidance for assays shown in Figure 5G. DW and KN performed experiments shown in Figure 2C & 2D. JKD, JJM, and JRY mass spectrometry analyses shown in Figure 5. DT and JP performed experiment shown Figure S2C. RU and JKL performed the experiment shown in Figure S4D. CAC performed sequence and phylogeny analysis in Figure S6I and Table S5. CMH performed experiments shown in Figures 1-6 and S1-S6. CMH and HDM wrote the manuscript. All authors contributed to editing the manuscript.

Figures and Tables

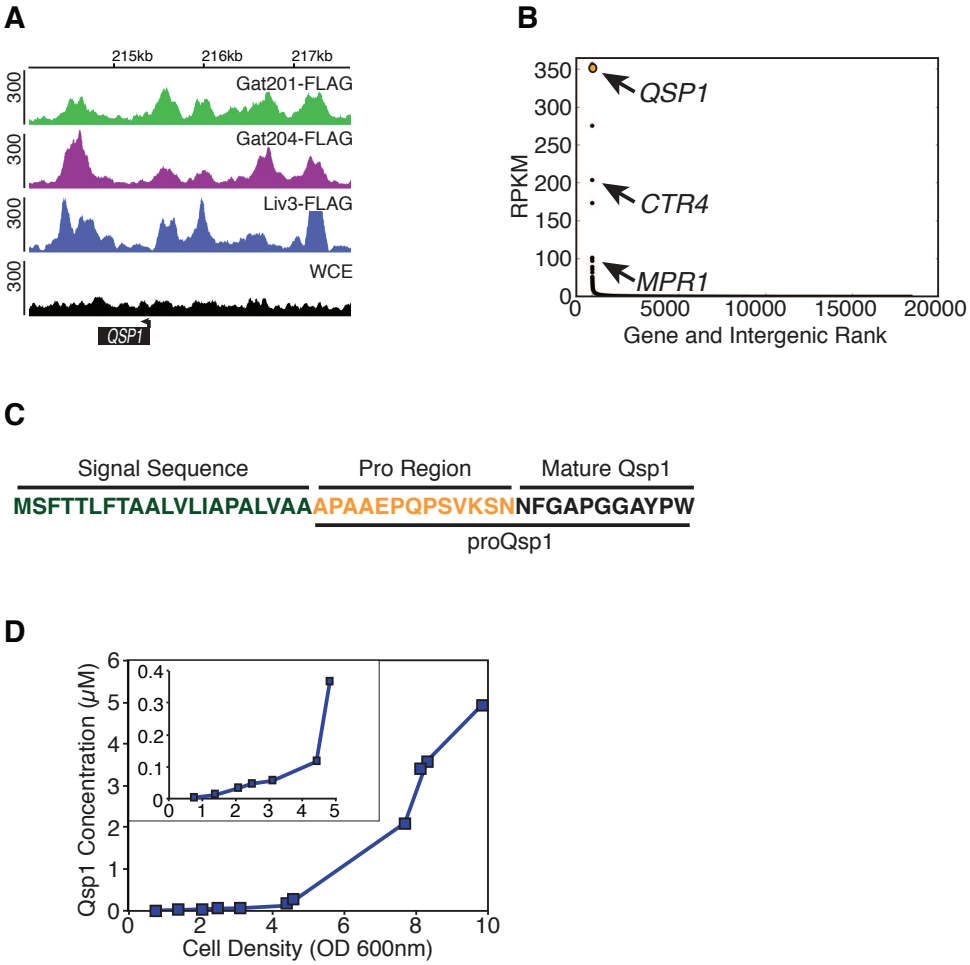

Figure 1

Figure 1: Qsp1 is a Transcriptional Target of Three Virulence Regulators

a) ChIP-Seq data for Gat201, Gat204, and Liv3 at the promoter of *QSP1*.

b) Plot of the rank and RPKM for each gene in a wild-type strain grown in tissue cultures conditions.

c) Schematic of predicted precursor encoded by *QSP1*. Signal sequence predicted by SignalP [93].

d) Qsp1 accumulation in wild-type culture supernatants as measured by ELISA. Inset: Qsp1 accumulation at lower cell densities.

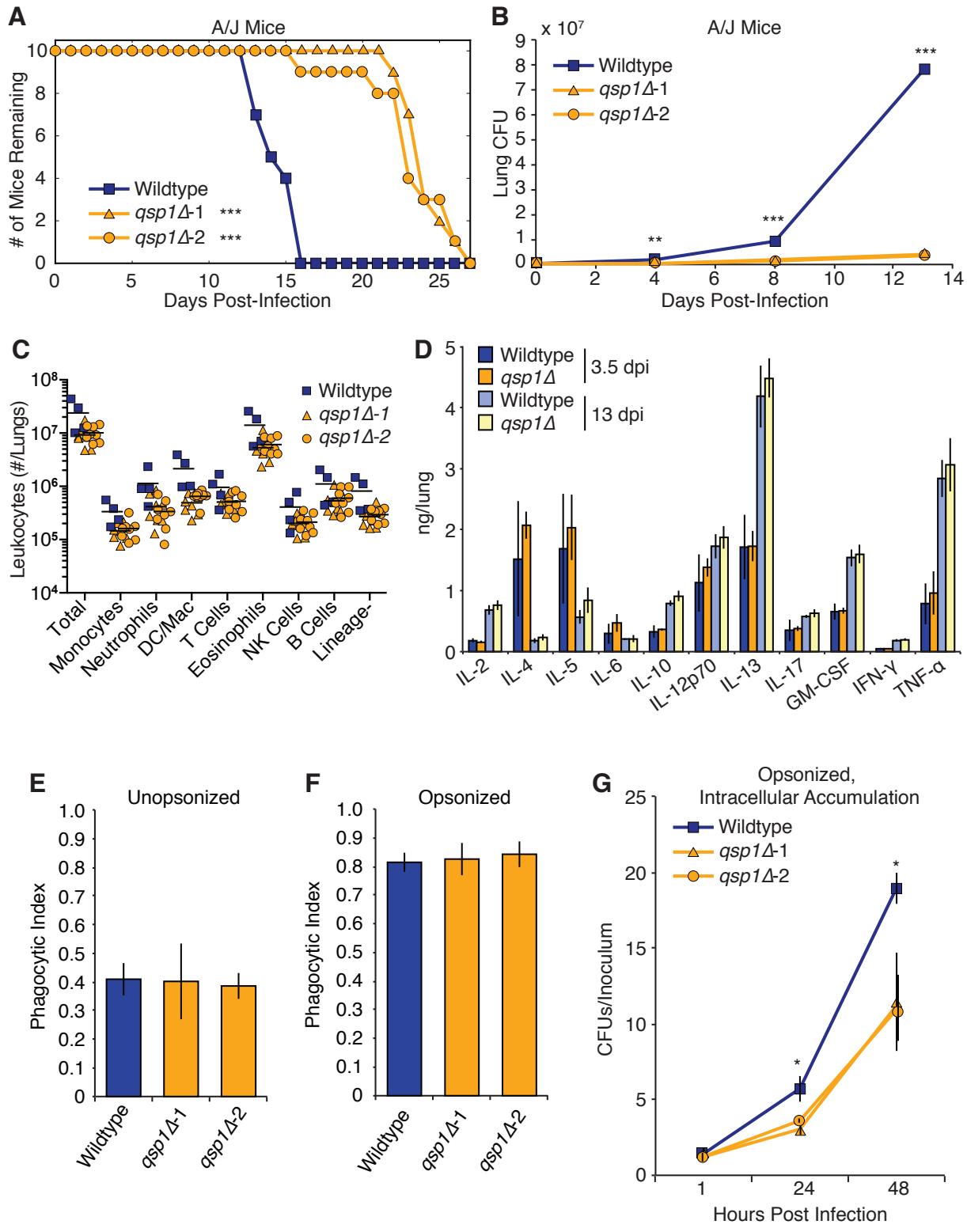

Figure 2

Figure 2: Qsp1 is required for virulence and accumulation within macrophages

a) Survival analysis. Ten A/J mice were infected per genotype. Significance was determined using a log rank test. ** indicates $p < 10^{-4}$.

b) Lung burden analysis. Nine A/J mice were infected per genotype. At specified times, lung CFUs of three mice per genotype were measured and CFUs for each *qsp1*Δ mutant were compared to wild type by student t-test. ** indicates $p<10^{-3}$ and *** indicates $p<10^{-4}$.

c) Leukocyte recruitment. Four C57BL/6 mice were infected with wild type and eight C57BL/6 mice per *qsp1*Δ strains. 18 days after infection, number and class of immune cells present in the lungs were analyzed by flow cytometry.

d) Cytokine analysis. Ten C57BL/6 mice were infected per genotype. Full lungs were analyzed for cytokines at specified timepoints. Error bars are S.D.

e) Phagocytic index of unopsonized and f) opsonized *C. neoformans*. >1200 BMDMs quantified per genotype. Error bars are S.D.

g) Intracellular accumulation. CFUs isolated from BMDM cell lysates at specified times after infection, normalized to starting inoculum. Error bars represent 95% confidence intervals constructed by bootstrapping. Bootstrap analysis was used to test the difference between wild type and each *qsp1*Δ mutant. * indicates a result with p value < 0.05.

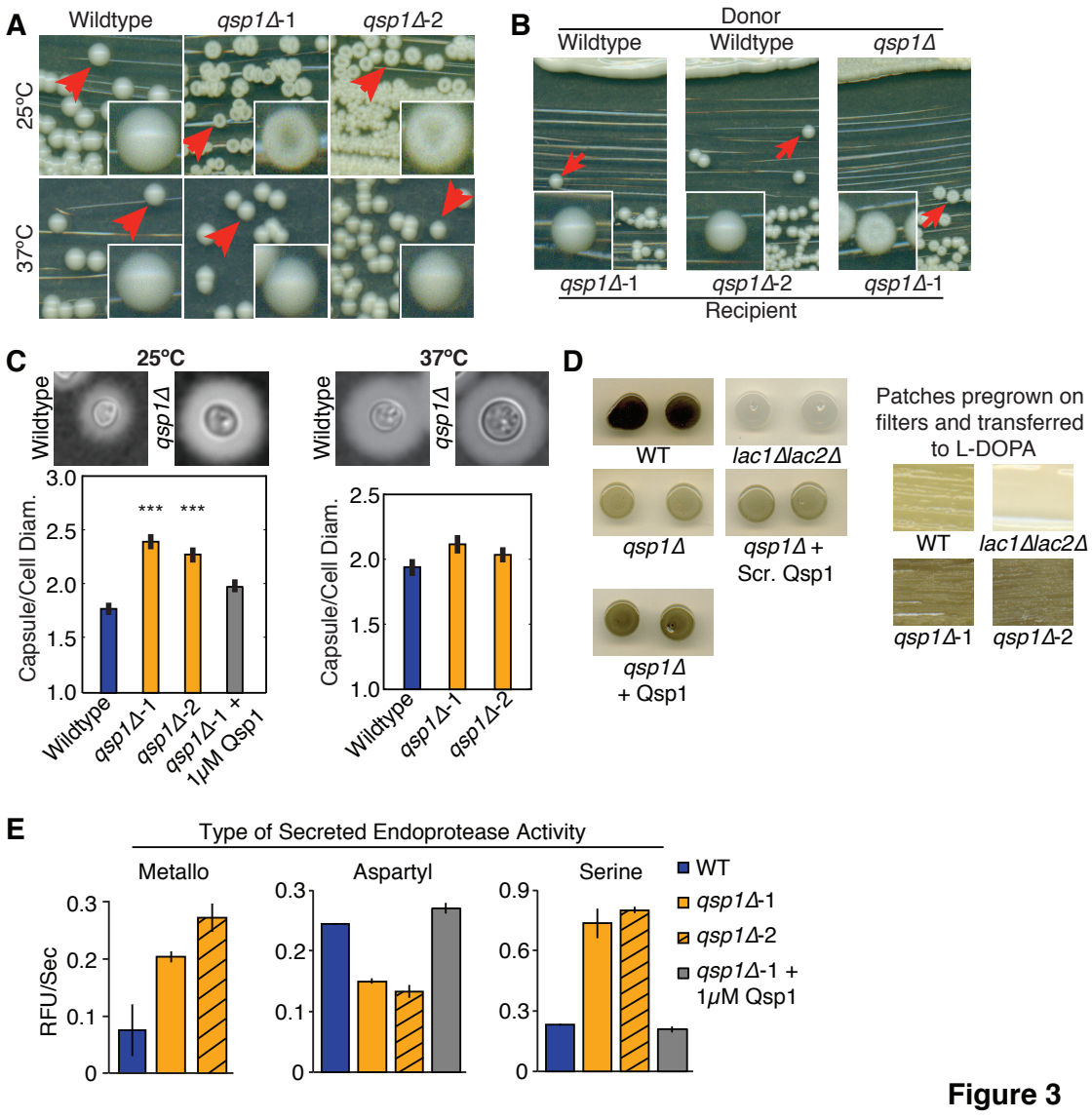

Figure 3

Figure 3: Impact of Qsp1 on virulence-related phenotypes

a) Colony morphology of wild-type and *qsp1*Δ strains grown at specified temperatures.

b) Complementation assays. Patches of donor cells were grown at room temperature next to single colonies of recipient cells.

c) Capsule quantification. Representative pictures of cryptococcal capsule stained with india ink. >100 cells per genotype used for capsule size determination. Mutants were compared to wild type using student t-tests. *** indicates $p < 10^{-5}$. Error bars are S.E.

d) Melanin assay. All assays performed on L-DOPA plates at 37˚C. Left: Cells were grown in liquid culture with or without synthetic peptides before spotting. Right: Patches were grown on sterile filters and transferred to L-DOPA plates.

e) Secreted protease activities. *qsp1*Δ mutants were compared to wild type by student t-tests. Error bars are S.D.

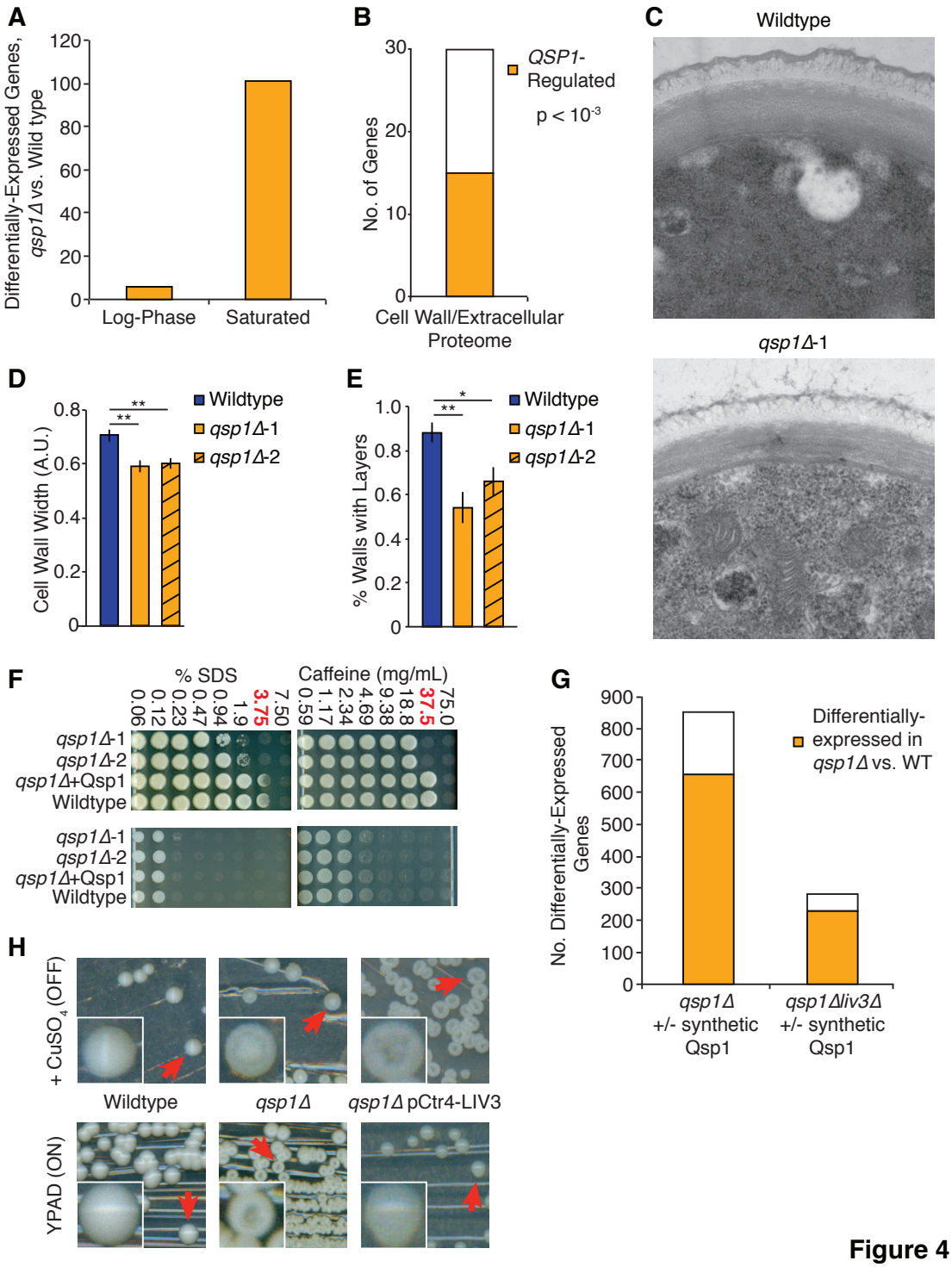

Figure 4

Figure 4: Qsp1 has density-dependent impacts on gene expression and cell wall integrity

a) Density-dependent RNA-Seq. Expression profiling was performed on *qsp1*Δ and wild type log-phase and saturated cultures. The number of differentially-expressed genes

(p_{adj}<0.05 by DESeq) in the *qsp1*Δ sample compared to wild type is shown for both conditions.

b) The overlap of *QSP1*-regulated genes with the published cell wall and secreted proteome [59] are shown. *QSP1*-dependent genes are 2.3-fold are significantly enriched ($p < 10^{-3}$ by the hypergeometric distribution).

c) Transmission electron microscopy. Representative micrographs of wild-type and *qsp1*Δ cells from tissue culture conditions.

d) Quantification of cell wall width and e) the percentage of cells with visible cell wall layers. 50 cells per genotype. Mutants were compared to wild type by student t-tests. ** indicates $p < 0.001$ and * indicates $p < 0.01$. Error bars are S.D.

f) Stress assays. Saturated and log phase cultures were incubated with indicated levels of stressors and plated for viability. Concentrations at which *qsp1*Δ viability is most different from wild type are in red.

g) *LIV3*-dependent genes. Expression profiling was performed for *qsp1*Δ and *qsp1*Δ*liv3*Δ saturated cultures grown with or without 1 μM synthetic Qsp1 peptide. The number of differentially-expressed genes is shown, with genes that were also differentially expressed in *qsp1*Δ versus wildtype in yellow.

h) *LIV3* suppression of *qsp1*Δ dry colony phenotype. Constitutive expression of *LIV3* using a copper-repressible promoter in a *qsp1*Δ mutant causes the mutant to form shiny colonies.

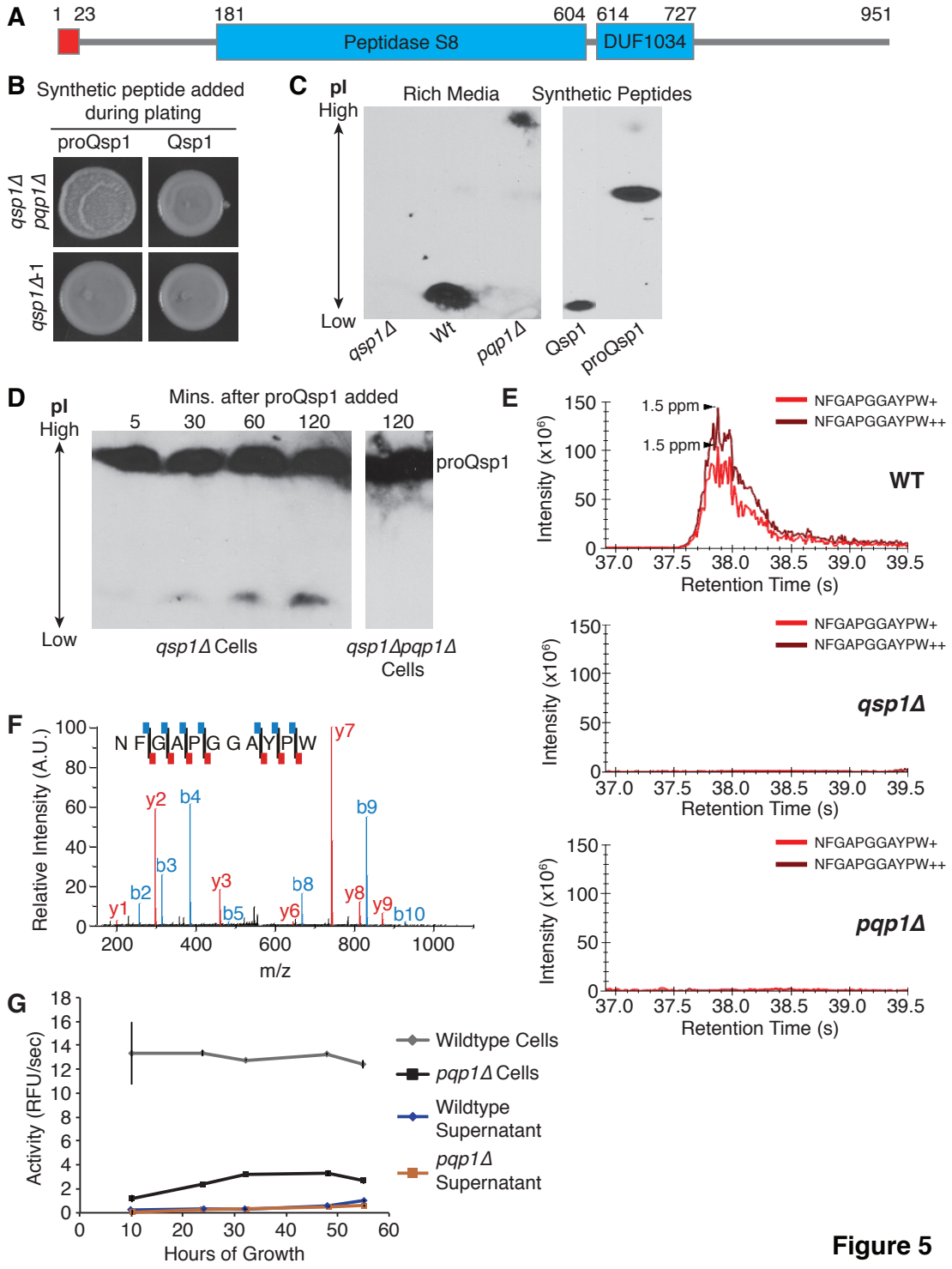

Figure 5

Figure 5: Pqp1 is required for Qsp1 precursor processing

a) Predicted structure of Pqp1 protein.

b) Spotting assays. Cultures were spotted with specified synthetic peptide stock and grown at room temperature.

c) Qsp1 secretion assays. Isoelectric focusing gel electrophoresis and immunoblotting against Qsp1/Qsp24 in culture supernatants and Qsp1/Qsp24 synthetic peptides.

d) Predicted Qsp1 precursor cleavage assays. Synthetic Qsp24 was incubated with cultures of specified strains. Supernatants were isolated and then analyzed for cleavage by isoelectric focusing gel electrophoresis and immunoblotting against Qsp1/Qsp24.

e) Extracted ion chromatogram of Qsp1 from LC/MS of culture supernatants.

f) Qsp1 MS2 spectra. Mass spectrometry of Qsp1 showing the fragment ions identified. Each fragment detected is shown with red (y ions) or blue (b ions) lines on the peptide sequence.

g) Pqp1 activity assay. Shown are rates of cleavage of Qsp1-like substrate by cells or cell-free supernatants in wild-type and *pqp1*Δ cultures. Error bars are S.D.

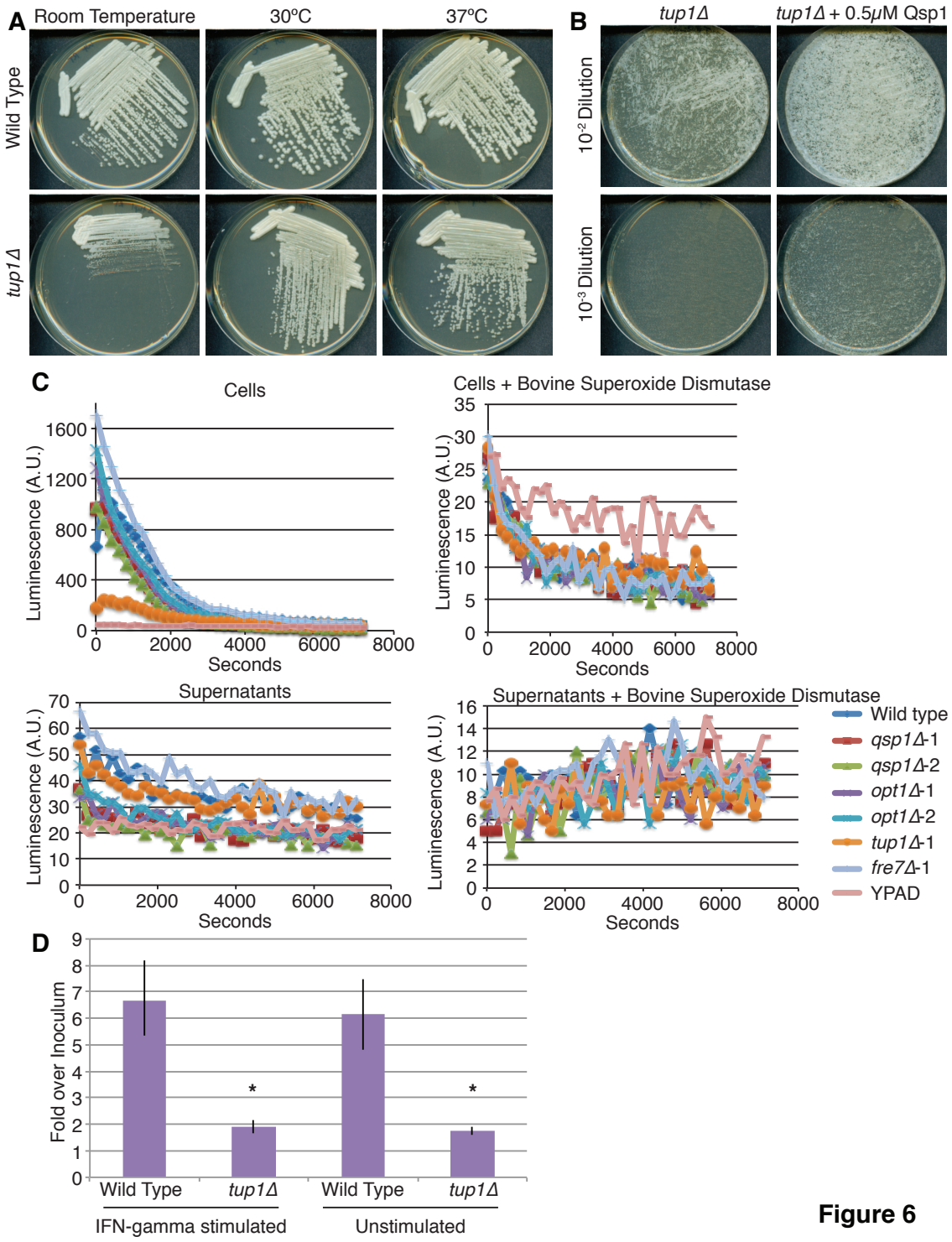

Figure 6

Figure 6: *tup1*Δ's density-dependent plating defect exists in Serotype A

a) Plating Assay. Specified strains were streaked for single colonies on YPAD agar plates and grown at the indicated temperatures for 48 hours.

b) Serial Dilution Plating. *tup1*Δ mutants were plated at the indicated dilutions with and without synthetic Qsp1 peptides.

c) Lucigenin superoxide anion production assay. Superoxide production was measured over one hour after lucigenin substrate was added to specified samples.

d) Macrophage intracellular accumulation assay. CFUs isolated from BMDM cells at specified times after infection, normalized to starting inoculum. Error bars represent 95% confidence intervals constructed by bootstrapping. Bootstrap analysis was used to test the difference between wild type and mutants. * indicates p value < 0.05.

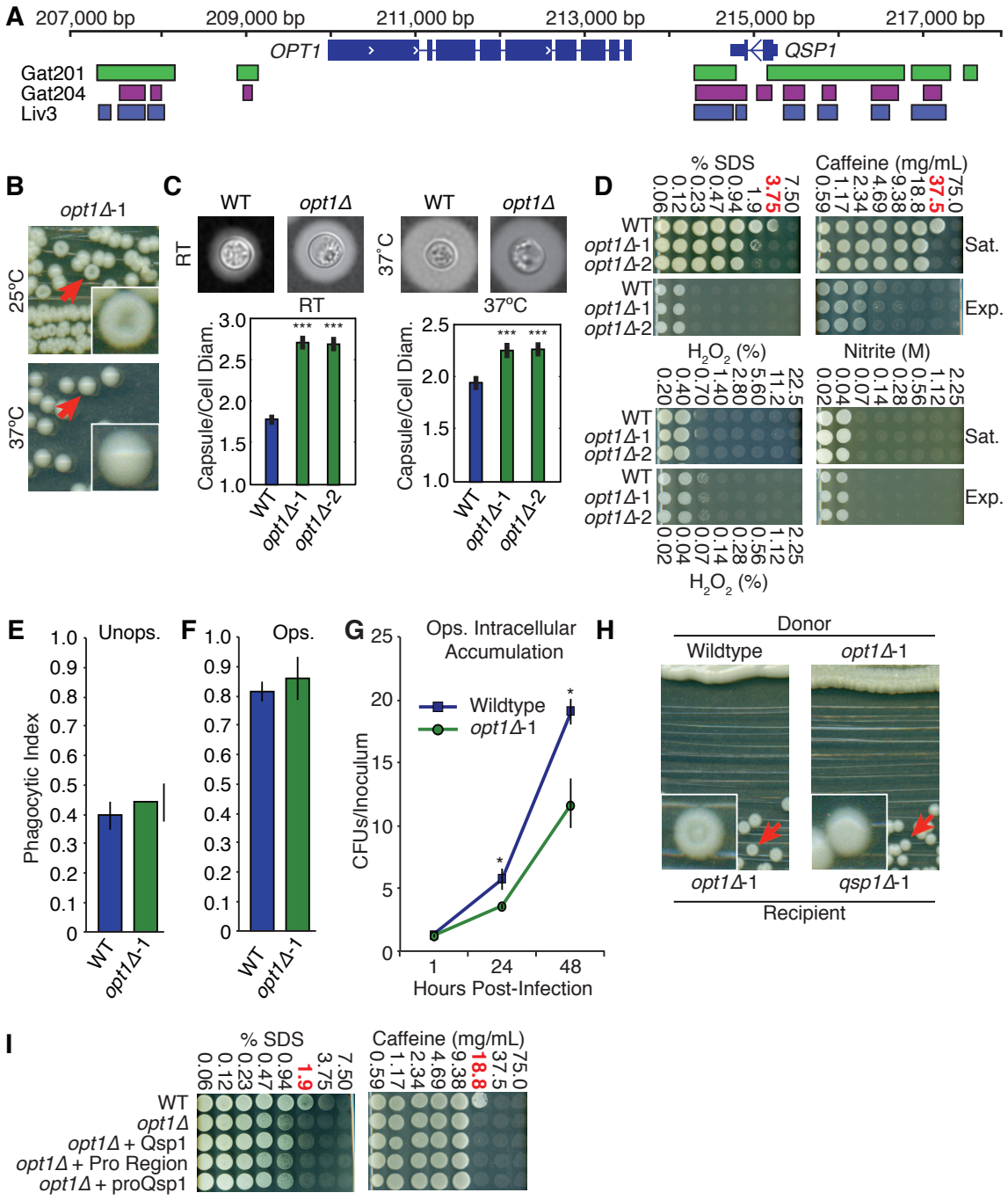

Figure 7

Figure 7: A predicted oligopeptide transporter is required for cells to respond to Qsp1

a) Transcription factor binding sites in intergenic regions surrounding *QSP1* and *OPT1*.

b) Colony morphology of the *opt1*Δ mutant.

c) Capsule sizes. Representative pictures of cryptococcal capsule stained with india ink. >100 cells per genotype were used in quantification. Mutants were compared to wild type using student t-tests. *** indicates $p < 10^{-5}$. Wild-type data from Figure 3 included for comparison. Error bars are S.E.

d) Stress assays. Saturated and log phase cultures were incubated with indicated levels of stressors and plated for viability. Wild-type data from Figure 4 included for comparison. Concentrations at which *opt1*Δ viability is most different from wild type are in red.

e) Phagocytic index of unopsonized and f) opsonized *C. neoformans*. >1200 BMDMs quantified per genotype. Wild-type data from Figure 2 is included for comparison. Error bars are S.D.

g) Macrophage intracellular accumulation assay. CFUs isolated from BMDM cells at specified times after infection, normalized to starting inoculum. Wild-type data from Figure 2 included for comparison. Error bars represent 95% confidence intervals constructed by bootstrapping. Bootstrap analysis was used to test the difference between wild type and mutants. * indicates p value < 0.05.

h) Complementation assays. Patches of donor cells are grown at room temperature next to single colonies of recipient cells.

i) Stress assays: Saturated wild-type and *opt1*Δ cultures were grown in the absence or presence of synthetic peptides and incubated with SDS or caffeine and plated for viability. Concentrations at which *opt1*Δ viability is most different from wild type are in red.

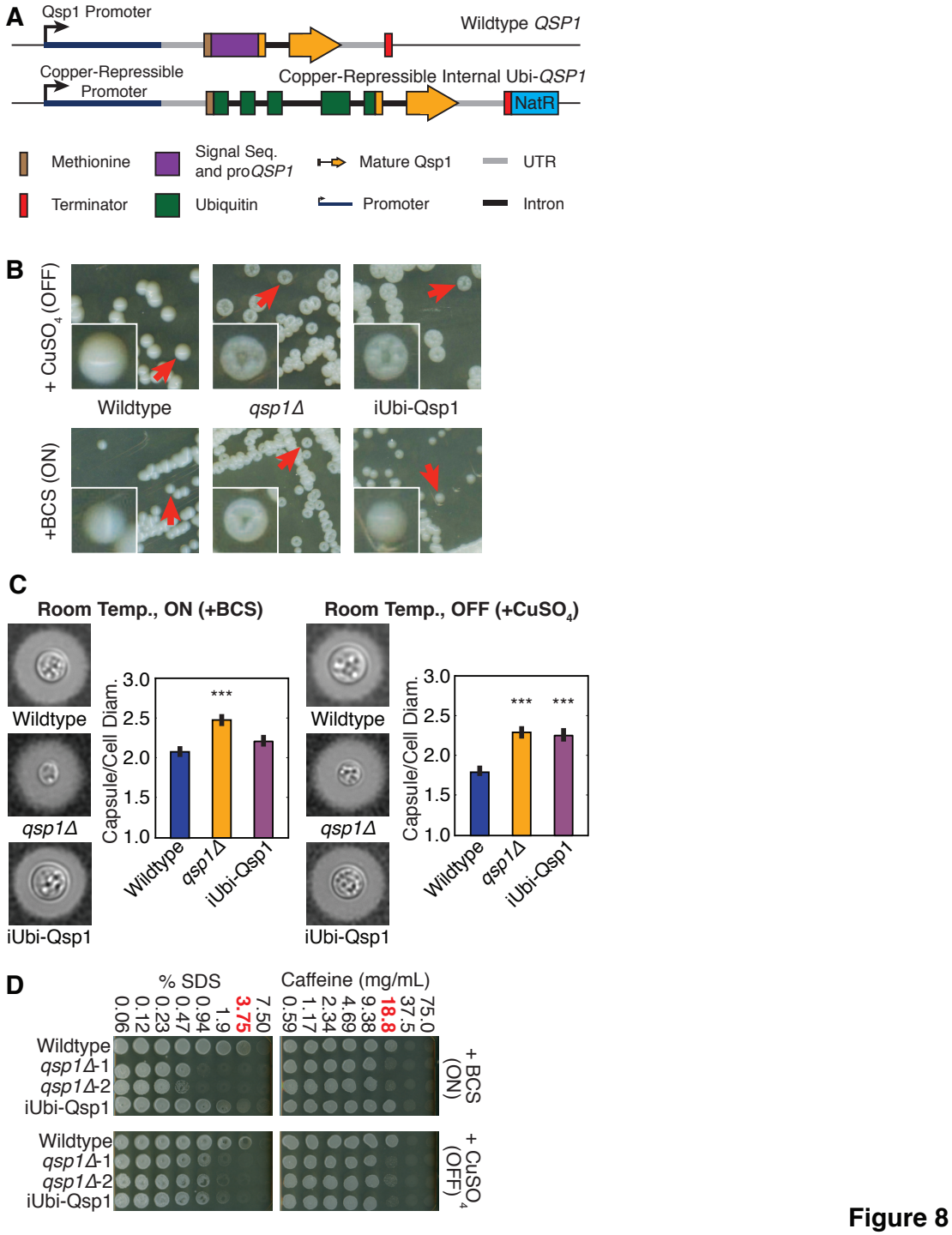

Figure 8

Figure 8: Cytoplasmic expression of QSP1 complements multiple *qsp1*Δ phenotypes

a. Schematic of the wild-type *QSP1* locus and the internal Qsp1 expression construct, iUbi-Qsp1.

b. Colony morphology phenotype. The room temperature colony morphology of wild type, *qsp1*Δ, and the iUbi-Qsp1 are shown, in conditions that induce and repress the promoter.

c. Capsule quantification. Representative pictures of cryptococcal capsule stained with india ink. >100 cells per genotype and condition used for capsule size determination. Mutants were compared to wild type using student t-tests. *** indicates $p < 10^{-5}$. Error bars are S.E.

f) Stress Assays. Saturated wild-type, qsp1Δ, and iUbi-Qsp1 cultures were grown in conditions which either induce or repress the expression of cytoplasmic Qsp1 and then incubated with stressors and plated for viability. Concentrations at which *qsp1*Δ viability is most different from wild type are in red.

Supplemental Figures and Tables

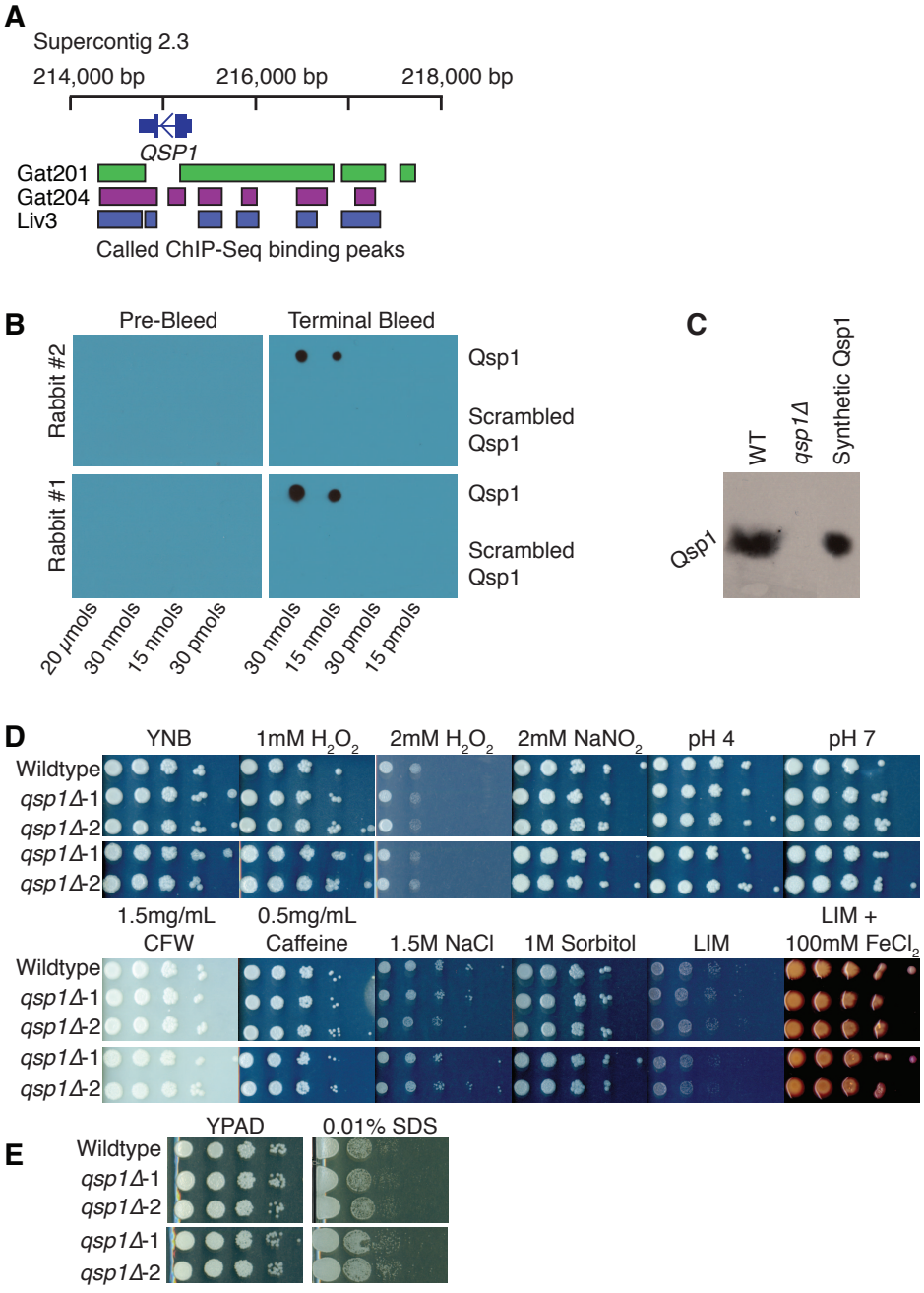

Figure S1

Figure S1: Initial phenotyping of *QSP1*, Related to Figure 1

a) Transcription factor binding sites in intergenic regions surrounding *QSP1*.

b) Dot blots. Polyclonal antisera raised against the Qsp1 peptide were tested against the synthetic Qsp1 and scrambled Qsp1 peptides. Pre-bleed and final bleed for both rabbits shown here.

c) Qsp1 in culture supernatants. Cultures were grown at room temperature for 24 hours, then adjusted to OD 4.5 and grown for another 24 hours. All cultures finished at 15 ODs/mL and 3 mLs of supernatants were harvested as described in the methods and analyzed by immunoblotting.

d) Growth assays. 10-fold dilution series were spotted on YNB plates with specified stressors added. *qsp1*Δ strains were spotted on plates with (above) and without (below) wild type to control for complementation effects.

e) SDS growth assay. 10-fold dilution series were spotted on YPAD plates with and without SDS added.

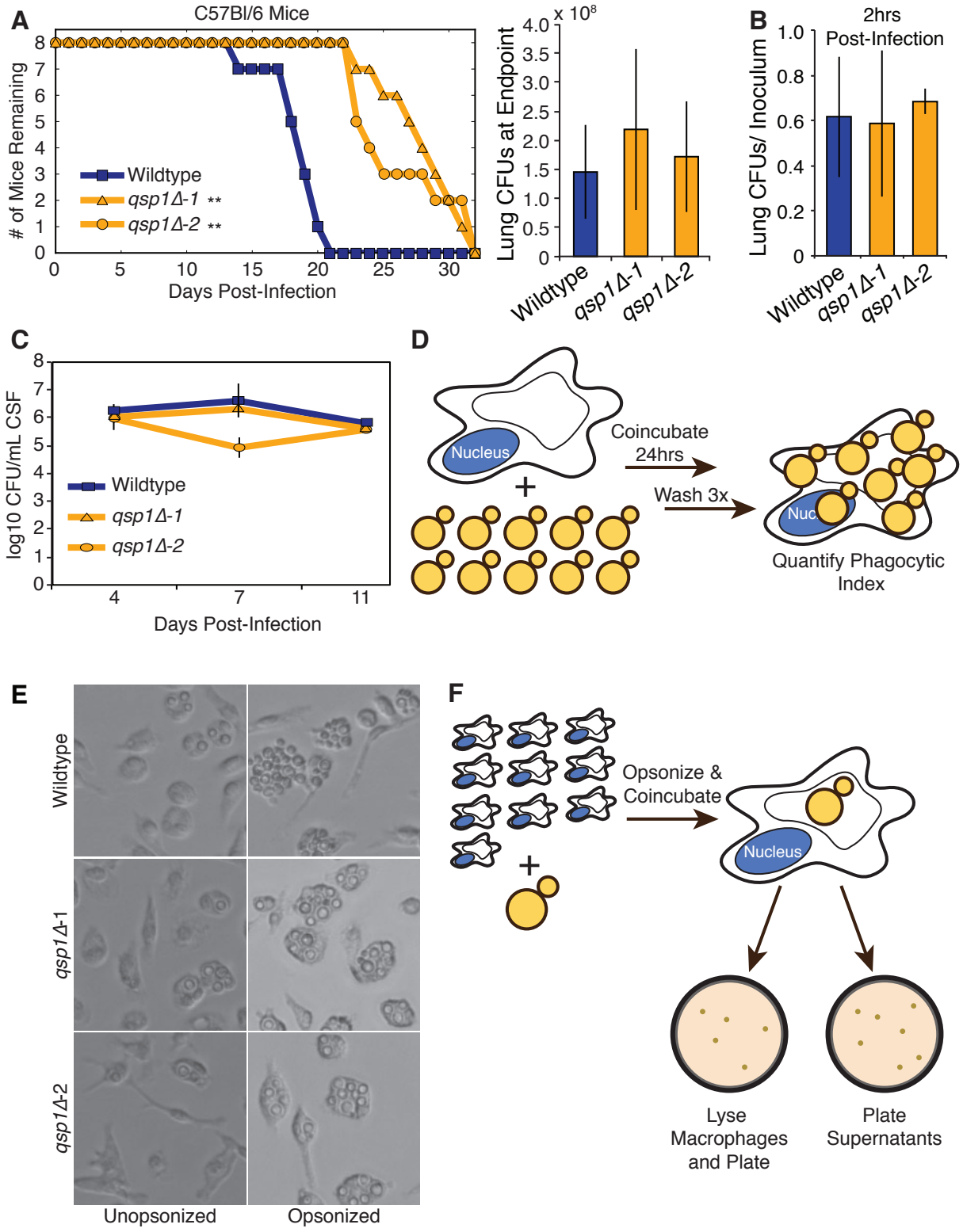

Figure S2

Figure S2: *QSP1* is required for pulmonary virulence but not infection of the central nervous system, Related to Figure 2

a) Lifespan assay. Wild type or *qsp1*Δ mutant *C. neoformans* were used to infect groups of eight C57BL/6 mice. Significance was determined using a log rank test. ** indicates $p < 10^{-4}$. Right: At each mouse's endpoint, lungs were harvested and viable cryptococcal cells were quantified. Error bars are S.D.

b) Infection Control. Groups of three C57BL/6 mice were infected with wild type or *qsp1*Δ mutants. 2 hours post infection, the lungs were harvested and viable cryptococcal cells were quantified. Errors bars are S.D.

c) Neurovirulence assay. Four immunosuppressed New Zealand White rabbits were inoculated intracisternally with wild-type *C. neoformans* or *qsp1*Δ mutants. Cerebrospinal fluid (CSF) was collected on day 4, 7, and 11 post infection and the number of viable cryptococcal cells was assessed. Error bars are S.D.

d) Schematic of phagocytic index determination. IFN-γ stimulated BMDMs were infected with unopsonized or opsonized *C. neoformans* at a modicum of infection (MOI) of 10:1. BMDMs and *C. neoformans* were coincubated for 24 hours and BMDMs were washed three times with sterile PBS to remove nonadhered cryptococcal cells before counting the percentage of BMDMs that have associated cryptococcal cells (phagocytic index).

e) Representative photographs of unopsonized and opsonized BMDM experiments used to calculate phagocytic index.

f) Schematic of intracellular replication experiment. IFN-γ activated BMDMs were infected were infected with opsonized *C. neoformans* at an MOI of 1:10. BMDMs and *C. neoformans* were coincubated for the specified times. The supernatants were plated for CFUs and the BMDMs were lysed and plated for CFUs as well. Each time point represents CFUs of the combined supernatant and lysate.

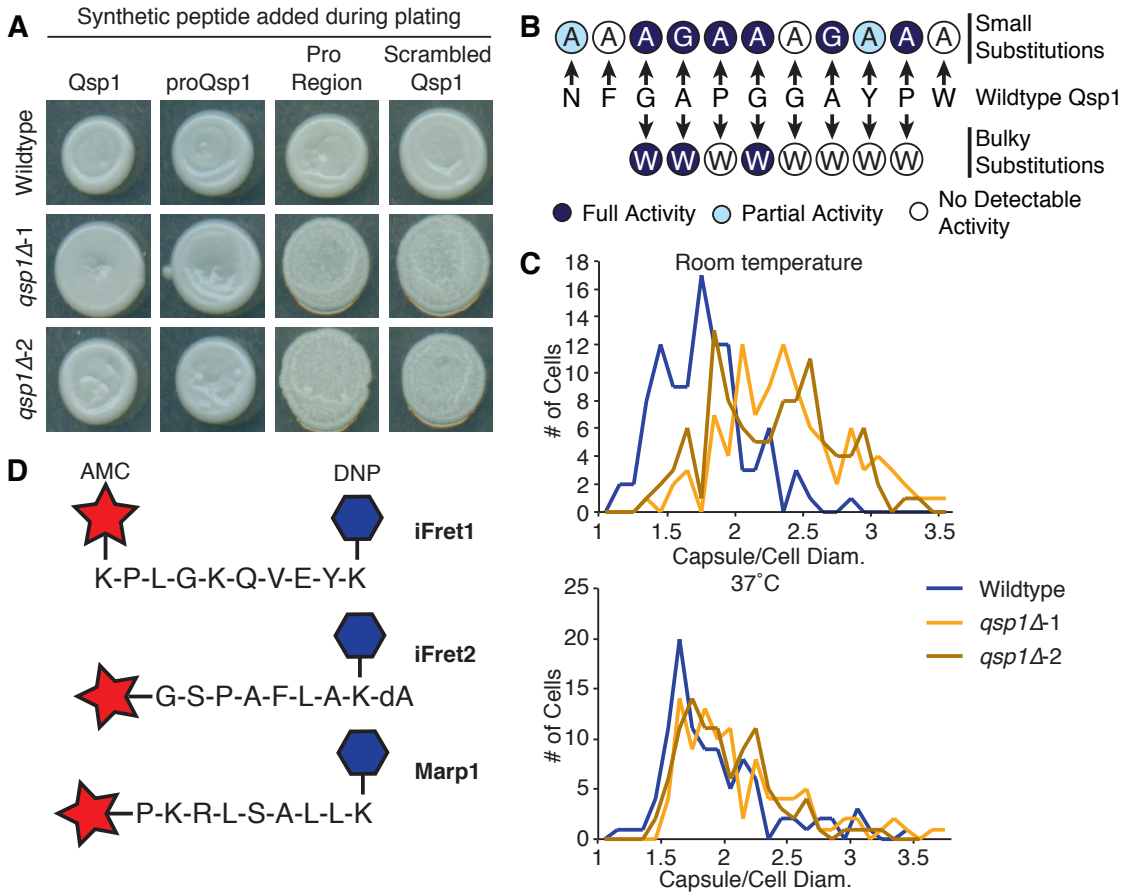

Figure S3

Figure S3: Analysis of Qsp1 activities, Related to Figure 3

a) Spotting Assay. Cultures were spotted with specified synthetic peptide stock and grown at room temperature.

b) The same assay as described in a) was performed with synthetic peptides containing each point mutation as specified. The degree to which it could complement the *qsp1*Δ rough colony morphology is indicated by color.

c) Histograms showing the distribution of capsule sizes at room temperature and 37˚C for wild type and *qsp1*Δ mutants.

d) Schematic of the fluorescent/quencher peptide substrates used in secreted endoprotease activity assays.

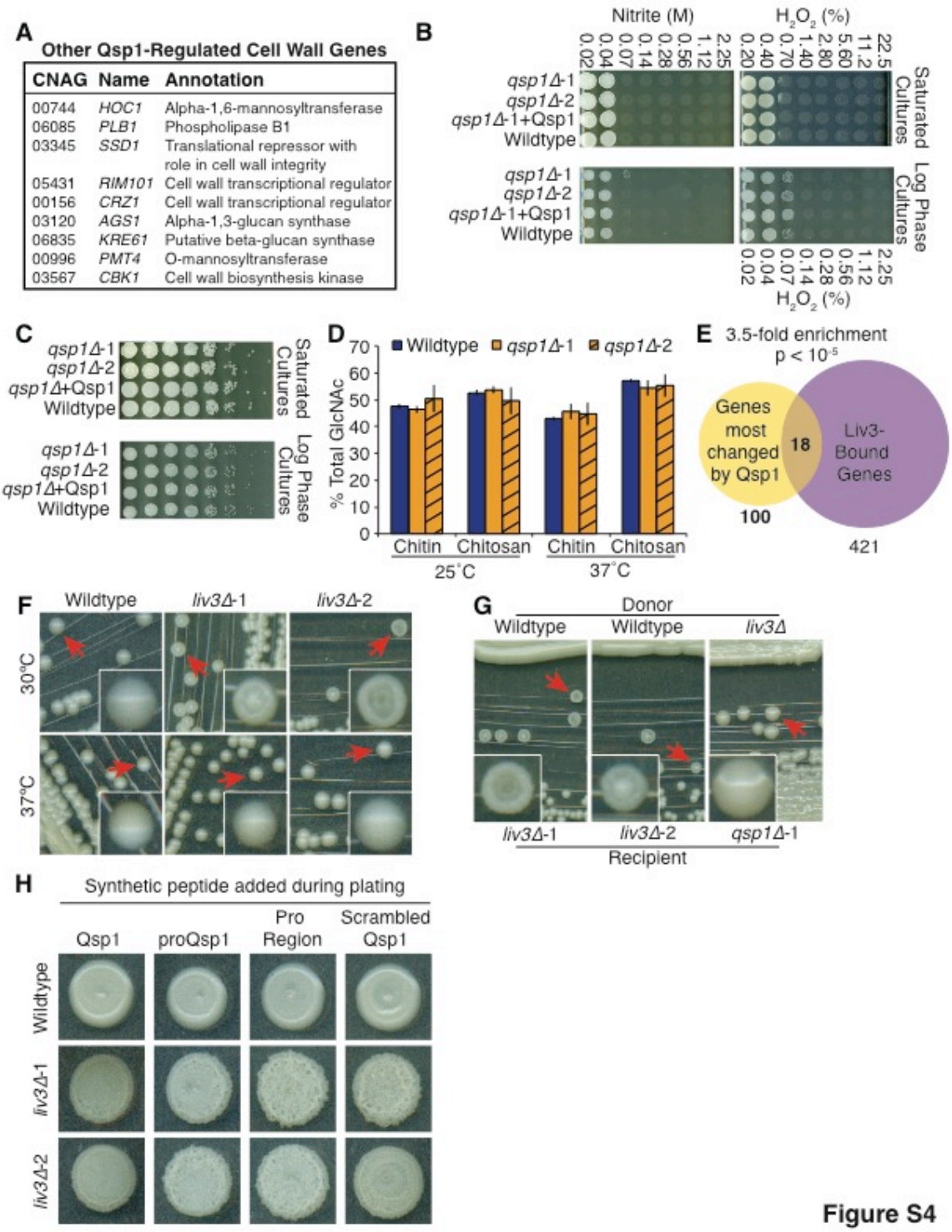

Figure S4: Cell wall assay controls, Related to Figure 4

a) Annotated Cell Wall Genes. *QSP1*-regulated genes that have also been implicated in cell wall function.

b) Stress assays. Saturated and log phase cultures were incubated with indicated levels of stressors and plated for viability.

c) Density-dependent stressor assay controls. Six-fold dilution series of saturated and log-phase cultures were spotted on YPAD plates to confirm amount of cells used in Figure 4A and Figure S4B.

d) Chitin and chitosan measurements from cultures grown in YPD at the indicated temperatures. Chitin and chitosan are measured as percent of total N-acetyl-glucosamine levels. Error bars represent S.D.

e) Liv3-Binding Overlap with Qsp1-Regulated Genes. The top 100 changed genes regulated by Qsp1 in saturated conditions were compared to genes whose promoters were bound by Liv3 in DMEM. Statistical significance was determined using the hypergeometric distribution.

f) Colony morphology of wild-type and *liv3*Δ strains grown at specified temperatures.

g) Complementation assays. Patches of donor cells were grown next to single colonies of recipient cells. When *liv3*Δ was the recipient, the assay was conducted at 30ºC. When *qsp1*Δ was the recipient, the assay was conducted at room temperature.

h) Spotting assay. Cultures were spotted with specified synthetic peptides and grown at 30ºC.

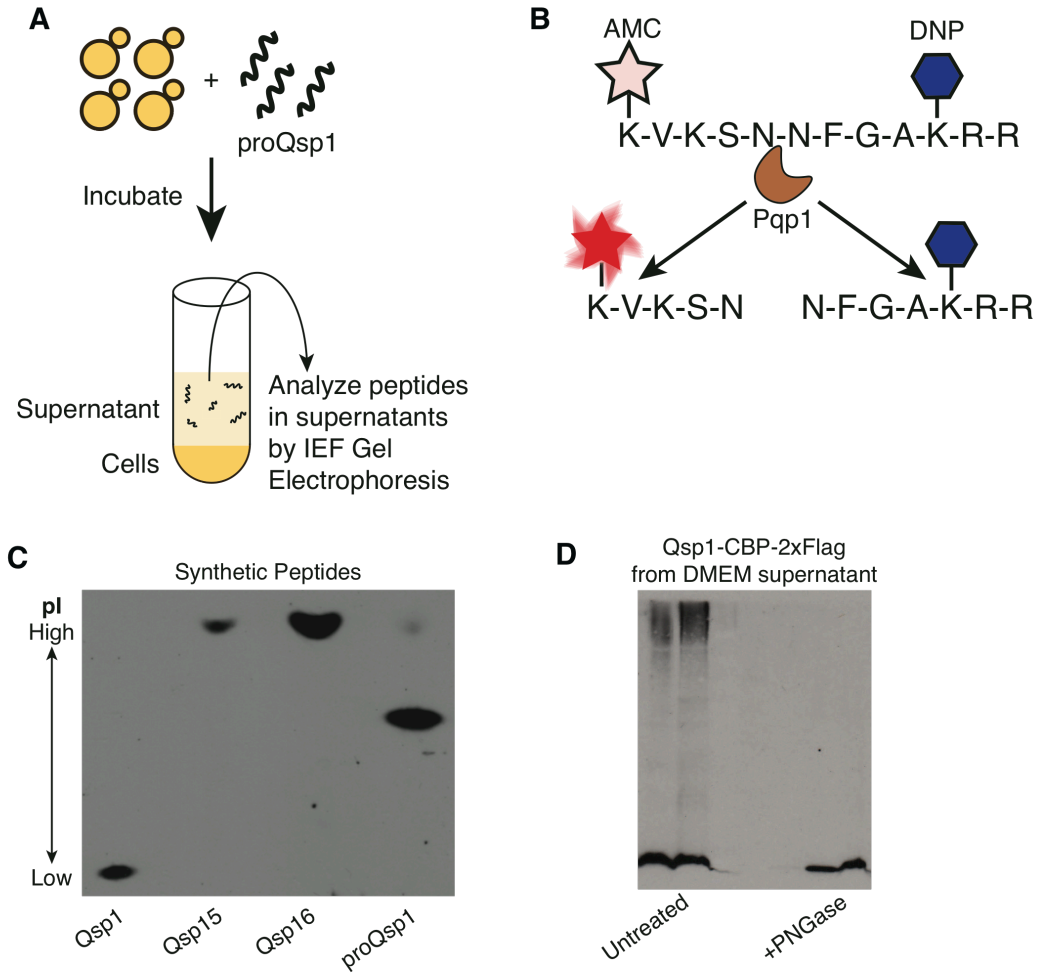

Figure S5

Figure S5: Qsp1 precursor processing assays, Related to Figure 5

a) Schematic of Pqp1-dependent proQsp1 Cleavage Assay. Synthetic Qsp24 was incubated with cultures, allowing the peptide to be cleaved. Supernatants, including peptide species, were isolated and analyzed using isoelectric focusing gel electrophoresis and immunoblotting.

b) Schematic of the fluorescent/quencher Qsp24-like peptide substrate used in Pqp1 activity assays.

c) Qsp1 precursor species. Isoelectric focusing gel electrophoresis and immunoblotting against Qsp1/Qsp15/Qsp16/proQsp1 synthetic peptides.

d) Qsp1 glycosylation. Cultures were grown overnight at 30ºC in YPAD, washed, and then incubated in DMEM at 37ºC, 5% CO_2 for 24 hours. Cells were harvested as described in the methods and analyzed by immunoblotting.

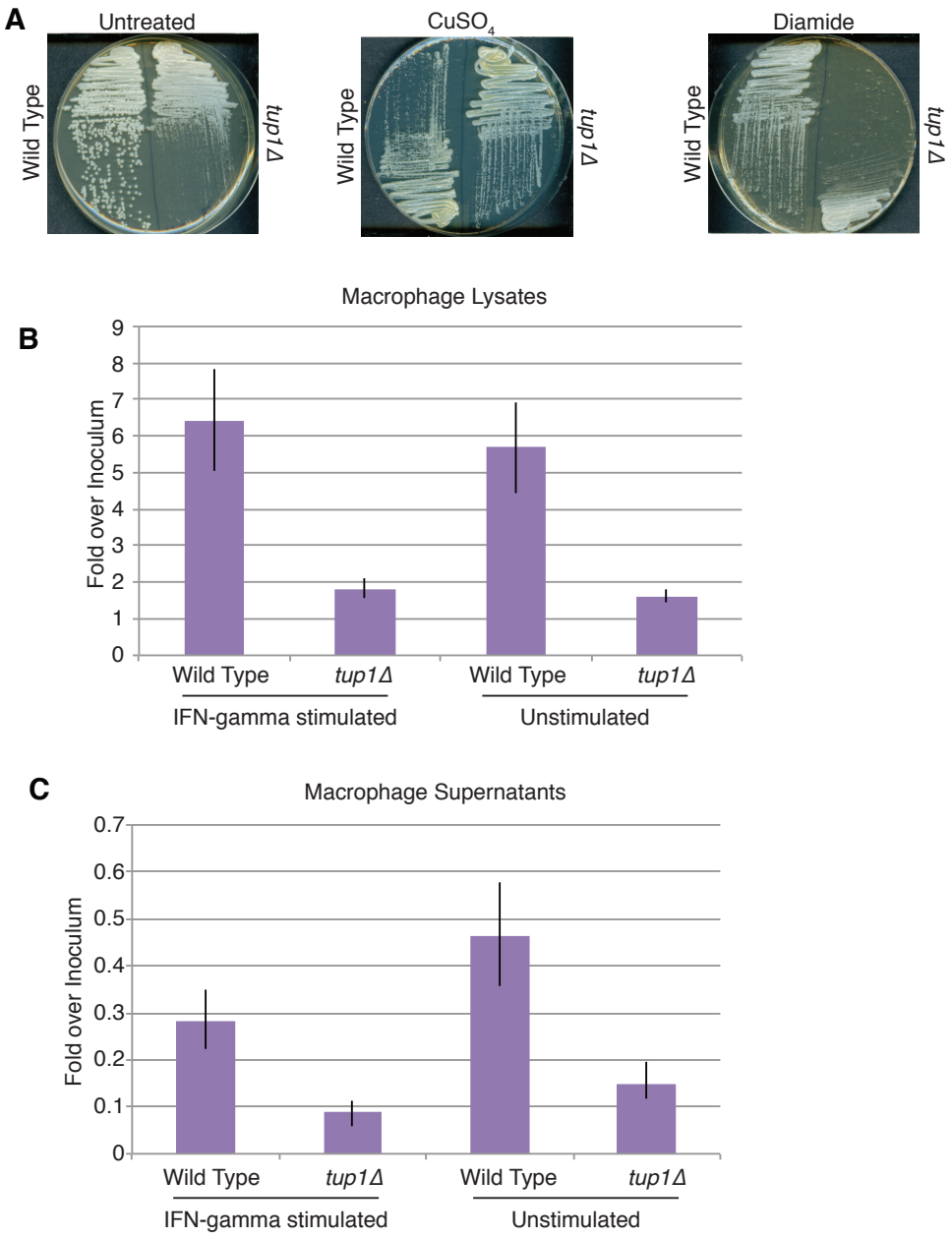

Figure S6

Figure S6: *tup1*Δ mutant displays intracellular proliferation defect when used to infect BMDMs, Related to Figure 6

a) Chemical stressor plating assay. Wild type and *tup1*Δ mutants were streaked on YPAD plates with the specified chemicals added and grown until signal colonies were formed by wild type.

b) Macrophage intracellular accumulation assay from macrophage lysates. CFUs isolated from BMDM cell lysates 24 hours after infection, normalized to starting inoculum. Error bars represent 95% confidence intervals constructed by bootstrapping. Bootstrap analysis was used to test the difference between wild type and mutants. * indicates p value < 0.05.

c) Macrophage intracellular accumulation assay from macrophage supernatants. CFUs isolated from BMDM supernatants 24 hours after infection, normalized to starting inoculum. Error bars represent 95% confidence intervals constructed by bootstrapping. Bootstrap analysis was used to test the difference between wild type and mutants. * indicates p value < 0.05.

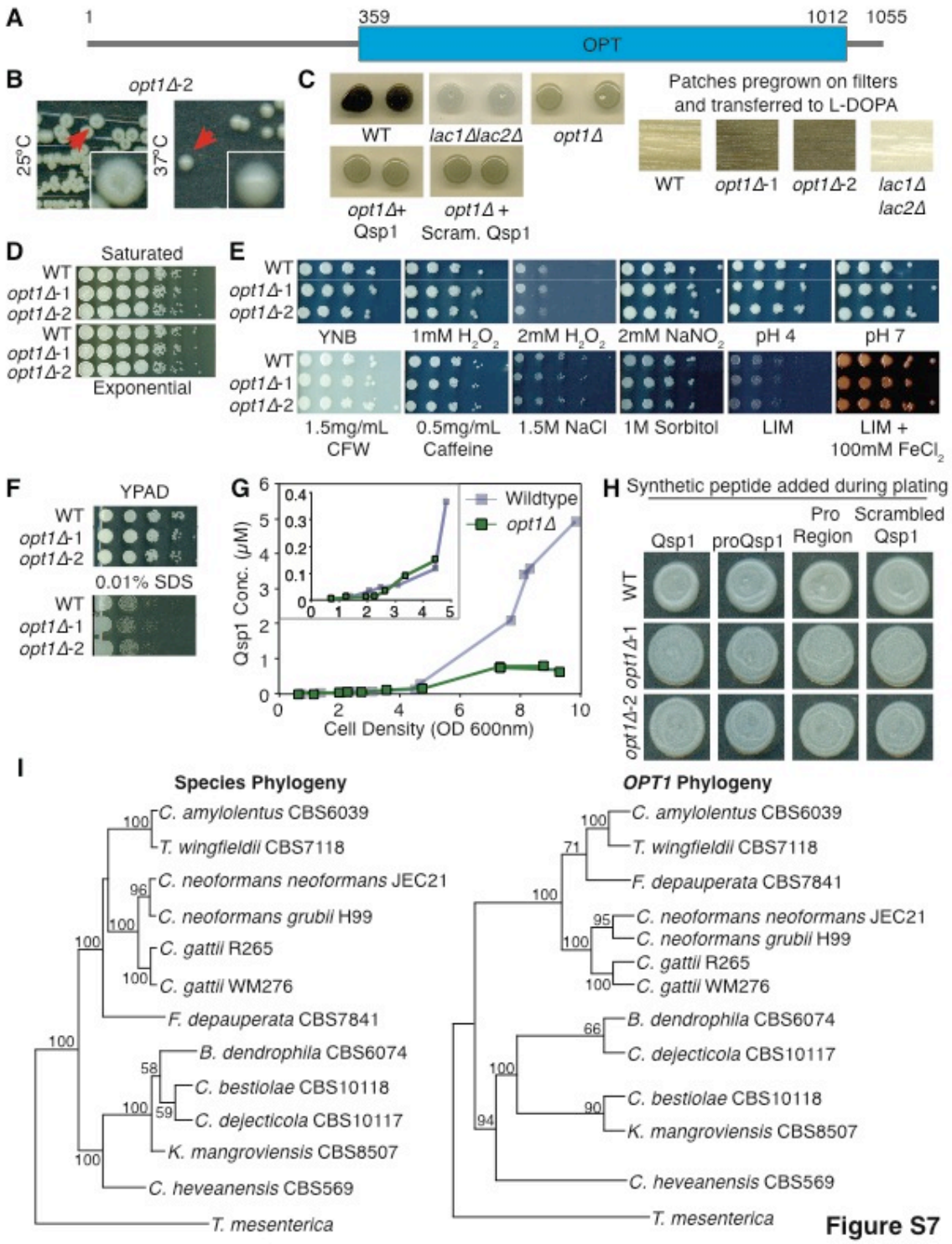

Figure S7: *opt1*Δ mutant displays phenotypes of the *qsp1*Δ mutant but cannot be complemented by synthetic Qsp1, Related to Figure 7

a) The predicted structure of the Opt1 protein.

b) Colony morphology of a second independent *opt1*Δ isolate (*opt1*Δ-2) matches that of *opt1*Δ-1.

c) Melanin assay. All cells were grown at 37˚C on L-DOPA. Left: Cells were grown with or without synthetic peptides before spotting. Right: Patches were grown on sterile membranes before transfer to L-DOPA plates.

d) Assay controls. Six-fold dilution series of saturated and log-phase cultures were spotted on YPAD plates to confirm amount of cells used in Figure 6D.

e) Growth assays. 10-fold dilution series were spotted on YNB plates with specified stressors added.

f) SDS growth assay. 10-fold dilution series were spotted on YPAD plates with and without SDS added.

g) Qsp1 accumulation in *opt1*Δ culture supernatants as measured by ELISA. Wild-type data from Figure 1 included for comparison. Inset: Qsp1 accumulation at lower cell densities.

h) Spotting assay. Cultures were spotted with specified synthetic peptide stock and grown at room temperature.

i) *OPT1* phylogeny. Right: Phylogeny generated from the sequence of the predicted products of *OPT1* genes. Left: Published phylogeny for comparison [94].

Table S1: Qsp1-regulated expression profiling in log-phase and saturated cultures, Related to Figure 4

Fold change (mutant/wildtype, log2 scale) in transcript level was determined by RNA-Seq using replicates for the specified conditions. The average fold change in log2 scale is listed in column B with the p-value in column C.

(Data for Table S1 available on Cell Host & Microbe website due to size.)

Table S2: Dry Mutants Identified in Screen of Deletion Collection, Related to Figures 4, 5, 6, and 7

Table S2: Dry Colony Mutants							
Systematic ID	Name	Annotation	Phenotype at 37ºC	Hyphal /Yeast	Capsule	Melanin at 37ºC	Reference
CNAG_03012	*QSP1*	Qsp1 Secreted Peptide	Smooth	Yeast	Yes	Hypo	Lee et al., 2007
CNAG_03013	*OPT1*	Putative small oligopeptide transporter	Smooth	Yeast	Yes	Hypo	This study
CNAG_05835	*LIV3*	WOR1/PAC2 transcription factor	Smooth*	Yeast	Yes	Normal	Liu et al., 2008
CNAG_04162	*PKA2*	cAMP-dependent protein kinase	Smooth	Yeast	Yes	Hypo	Hicks & Heitman, 2007
CNAG_00788	*NDH1*	Mitochondrial external NADH dehydrogenase	Smooth	Yeast	Yes	Normal	Walton et al., 2006
CNAG_06230	*DRP1*	Putative transporter	Temp. Sensitive	Yeast/ Hyphal	No	Temp. Sensitive	Maeng et al., 2010
CNAG_03567	*CBK1*	RAM signaling network protein kinase	Temp. Sensitive	Hyphal	Yes	Temp. Sensitive **	Walton et al., 2006
CNAG_03622	*TAO3*	RAM signaling network cell polarity protein	Temp. Sensitive	Hyphal	Yes	Temp. Sensitive **	Walton et al., 2006
CNAG_03916	*PGI1*	Glucose-6-phosphate Isomerase	Smooth	Yeast	Yes	Hypo**	This Study
CNAG_07554	*CAP10*	Capsular associated protein	-	-	-	-	Chang & Kwon-Chung, 1999
CNAG_00600	*CAP60*	Capsular associated protein	-	-	-	-	Chang & Kwon-Chung, 1998
CNAG_02885	*CAP64*	Capsular associated protein	-	-	-	-	Chang & Kwon-Chung, 1996
CNAG_01172	*PBX1*	Parallel beta-helix repeat protein	-	-	-	-	Kumar et al., 2014; Liu et al., 2007
CNAG_00150	*PQP1*	Predicted secreted serine protease	-	-	-	-	Eigenheer et al., 2007
CNAG_05445	*SHE4*	UCS domain protein	-	-	-	-	This Study
*Slightly rough at room temperature, most rough at 30ºC **Also hypomelanized at room temperature							

Table S3: Additional Strains Screened for Dry Colony Phenotype, Related to Figures 5 & 6

ID	Strain #	Parent	Annotation	Source
Secreted Proteases				
CNAG_00150		KN99α	Serine protease	1
CNAG_00581		KN99α	Aspartyl protease	1
CNAG_00919		KN99α	Carboxypeptidase	1
CNAG_01040		KN99α	Carboxypeptidase	1
CNAG_02966		KN99α	Carboxypeptidase	1
CNAG_04625		KN99α	Serine protease	1
CNAG_04735		KN99α	Metalloprotease	1
CNAG_05446		KN99α	Serine protease	1
CNAG_05872		KN99α	Aspartyl protease	1
CNAG_05973		KN99α	Carboxypeptidase	1
Two Component Receptors				
CNAG_01850	YSB321	KN99α	Tco1	2
CNAG_05590	YSB412	KN99α	Tco2	2
CNAG_01987	YSB416	KN99α	Tco3	2
CNAG_03355	YSB437	KN99α	Tco4	2
CNAG_00106	YSB419	KN99α	Tco5	2
CNAG_06278	YSB423	KN99α	Tco7	2
G Protein-Coupled Receptors				
CNAG_06020	CDX1	H99α	Gpr1	3
CNAG_01855	CDX3	H99α	Gpr2	3
CNAG_03846	CDX5	H99α	Gpr3	3
CNAG_04730	CDX7	H99α	Gpr4	3
CNAG_04730	CDX9	KN99α	Gpr4	3
CNAG_05586	CDX10	KN99α	Gpr5	3
Not reported	CDX14	KN99α	Gpr6	3
Not reported	CDX16	H99α	Gpr7	3
CNAG_03938	CDX12	H99α	Cpr2	3
1- This Study, 2- [95] 3- [96]				

Table S4: Qsp1 Species in Filobasidiella Species, Related to Figure 6 and Discussion

Qsp1-like peptides identified in other cryptococcal species. The position of the mature Qsp1 peptide is bolded within the larger gene. All species have an Opt1 at the 3' end of the *QSP1*-like gene.

Species	**Gene Sequence with 11mer sequence bolded**	**OPT1 3'?**
C. neoformans H99	MSFTTLFTAALVLIAPALVAAAPAAEPQPSVKSN**NF GAPGGAYPW**	YES
F. depauperata CBS7841	MAHGWRTIGNIWPKFDFSAQKKFDVKQPRKGTRTS LSPRSKLRVVSGTCRRMDVLWQFCVLTPKITSSVAI KGRHFSIFFPLPSPLPIRLIYDFAKPAAMSFTTYLTAV LVLIAPALVAAAPAPVPEHSLKGD**SNNAGGAYPW**	YES
T. wingfieldii CBS7118	MSFTTYVAALLVLVAPAAFAAPAAAAEPTLEGQ**NF GAPGGAGSE**TALIGDTTEDHEREFIERVFPDEELIV KRDGSIVREPQTVLDDDLKPDASFTPDDWYLFQFIK DHNPSHVRHSPGHLRTRFGLSLYFNWNVMTHLSR WIAAKEHWVSDVGSSHWSLGPDETLGSADWLCKR AFGVLRGECEVKQGVMWKRLSRHSFLKTKMSWSS PSGAGNGETHPALPCIPPSNHSFANPFGTLSHLAFEH LQVGTIVKELEMDTTLCQVLTPSGYAPVTLGLWRG FWVNPEDVSYDKNGKARGWLMYVSIQEDMRRGG EWKAVGCWSDVASETREGVVEWLKTVHEMGYTN GDFEPRHLYVAKGGSGWKIIDWGKGRDRSVDEDS LWKEQMGDETYDLRHISYATFSR	YES
C. amylolentus CBS6273	MSFTTYVAALLVLVAPAALAAPAAAAEPSLEGQ**NF GAPGGAFPE**LPPAAQLLSSVFSLLSLHLLSKAYPLF STHPSSQEVHTPHEPSSRIYRPARRLYATGWPLTTRS AFPTISSLNPSIPTLLQTRQG	YES

Table S5: Strains used in this study, Related to Experimental Procedures

Strain #	Name	Species	Genotype	Parent	Source
CM25	WT	*C. neo.*	KN99α (wildtype)	-	1
CK0289	*qsp1*Δ-1	*C. neo.*	*qsp1Δ::NatR*	CM25	3
CM1561	*qsp1*Δ-2	*C. neo.*	*qsp1Δ::NeoR*	CM25	3
CK0326	*opt1*Δ-1	*C. neo.*	*opt1Δ::NatR*	CM25	3
CM1559	*opt1*Δ-2	*C. neo.*	*opt1Δ::NatR*	CM25	3
CK2171	*pqp1*Δ	*C. neo.*	*pqp1Δ::NatR*	CM25	3
CK0080	*liv3*Δ(K)	*C. neo.*	*liv3Δ::NatR*	CM25	3
CK0405	*pka2*Δ	*C. neo.*	*pka2Δ::NatR*	CM25	3
CK1117	*ndh1*Δ	*C. neo.*	*ndh1Δ::NatR*	CM25	3
CK0756	*drp1*Δ	*C. neo.*	*drp1Δ::NatR*	CM25	3
CK2267	*cbk1*Δ	*C. neo.*	*cbk1Δ::NatR*	CM25	3
CK2458	*tao3*Δ	*C. neo.*	*tao3Δ::NatR*	CM25	3
CK2402	*pgi1*Δ	*C. neo.*	*pgi1Δ::NatR*	CM25	3
CM1624	*qsp1*Δ*pqp1*Δ	*C. neo.*	*qsp1Δ::NeoR- pqp1Δ::NatR*	CM25	3
CM146	*lac1*Δ*lac2*Δ	*C. neo.*	*lac1*Δ*::NatR-lac2*Δ*::NeoR*	CM18	2
CM1686	iUbi-Qsp1	*C. neo.*	*pCtr4-Ubi-mQsp1::NatR*	CM25	3
			Sources:		
			1= Gift of J. Heitman		
			2= Liu, Chun [91]		
			3= This study		

Table S6: Qsp1 peptide mutant sequences, Related to Figure S3A and Extended Experimental Procedures

Peptide Name	**Peptide Sequence**
Qsp1	NFGAPGGAYPW
Qsp1 Scrambled	AWAGYFPGPNG
Peptide point variants	
Qsp1N1A	AFGAPGGAYPW
Qsp1F2A	NAGAPGGAYPW
Qsp1G3A	NFAAPGGAYPW
Qsp1A4G	NFGGPGGAYPW
Qsp1P5A	NFGAAGGAYPW
Qsp1G6A	NFGAPAGAYPW
Qsp1G7A	NFGAPGAAYPW
Qsp1A8G	NFGAPGGGYPW
Qsp1Y9A	NFGAPGGAAPW
Qsp1P10A	NFGAPGGAYAW
Qsp1W11A	NFGAPGGAYPA
Qsp1G3W	NFWAPGGAYPW
Qsp1A4W	NFGWPGGAYPW
Qsp1P5W	NFGAWGGAYPW
Qsp1G6W	NFGAPWGAYPW
Qsp1G7W	NFGAPGWAYPW
Qsp1A8W	NFGAPGGWYPW
Qsp1Y9W	NFGAPGGAWPW
Qsp1P10W	NFGAPGGAYWW
Peptide deletion variants	
Qsp1N10	NFGAPGGAYP
Qsp1N9	NFGAPGGAY
Qsp1N8	NFGAPGGA
Qsp1N7	NFGAPGG
Qsp1N6	NFGAPG
Qsp1N5	NFGAP
Qsp1N4	NFGA
Qsp1N3	NFG
Qsp1C10	FGAPGGAYPW
Qsp1C9	GAPGGAYPW
Qsp1C8	APGGAYPW
Qsp1C7	PGGAYPW
Qsp1C6	GGAYPW
Qsp1C5	GAYPW
Qsp1C4	AYPW
Qsp1C3	YPW

Works Cited

1. Denning, D.W. and M.J. Bromley, *Infectious Disease. How to bolster the antifungal pipeline.* Science, 2015. **347**(6229): p. 1414-6.
2. Brown, G.D., et al., *Hidden killers: human fungal infections.* Sci Transl Med, 2012. **4**(165): p. 165rv13.
3. Ostrosky-Zeichner, L., *Invasive mycoses: diagnostic challenges.* Am J Med, 2012. **125**(1 Suppl): p. S14-24.
4. Perfect, J.R., *Cryptococcus neoformans: a sugar-coated killer with designer genes.* FEMS Immunol Med Microbiol, 2005. **45**(3): p. 395-404.
5. Arathoon, E.G., *Clinical efficacy of echinocandin antifungals.* Curr Opin Infect Dis, 2001. **14**(6): p. 685-91.
6. Gauthier, G.M. and N.P. Keller, *Crossover fungal pathogens: the biology and pathogenesis of fungi capable of crossing kingdoms to infect plants and humans.* Fungal Genet Biol, 2013. **61**: p. 146-57.
7. Enoch, D.A., H.A. Ludlam, and N.M. Brown, *Invasive fungal infections: a review of epidemiology and management options.* J Med Microbiol, 2006. **55**(Pt 7): p. 809-18.
8. Armstrong-James, D., G. Meintjes, and G.D. Brown, *A neglected epidemic: fungal infections in HIV/AIDS.* Trends Microbiol, 2014. **22**(3): p. 120-7.
9. Kwon-Chung, K.J., et al., *Cryptococcus neoformans and Cryptococcus gattii, the etiologic agents of cryptococcosis.* Cold Spring Harb Perspect Med, 2014. **4**(7): p. a019760.

10. Steenbergen, J.N. and A. Casadevall, *Prevalence of Cryptococcus neoformans var. neoformans (Serotype D) and Cryptococcus neoformans var. grubii (Serotype A) isolates in New York City.* J Clin Microbiol, 2000. **38**(5): p. 1974-6.

11. Mitchell, T.G. and J.R. Perfect, *Cryptococcosis in the era of AIDS--100 years after the discovery of Cryptococcus neoformans.* Clin Microbiol Rev, 1995. **8**(4): p. 515-48.

12. Nosanchuk, J.D. and A. Casadevall, *Budding of melanized Cryptococcus neoformans in the presence or absence of L-dopa.* Microbiology, 2003. **149**(Pt 7): p. 1945-51.

13. Kraus, P.R., et al., *Identification of Cryptococcus neoformans temperature-regulated genes with a genomic-DNA microarray.* Eukaryot Cell, 2004. **3**(5): p. 1249-60.

14. Doering, T.L., *How sweet it is! Cell wall biogenesis and polysaccharide capsule formation in Cryptococcus neoformans.* Annu Rev Microbiol, 2009. **63**: p. 223-47.

15. Antunes, L.C., et al., *Quorum sensing in bacterial virulence.* Microbiology, 2010. **156**(Pt 8): p. 2271-82.

16. Gerdt, J.P. and H.E. Blackwell, *Competition studies confirm two major barriers that can preclude the spread of resistance to quorum-sensing inhibitors in bacteria.* ACS Chem Biol, 2014. **9**(10): p. 2291-9.

17. Miller, M.B. and B.L. Bassler, *Quorum sensing in bacteria.* Annu Rev Microbiol, 2001. **55**: p. 165-99.

18. Fuqua, C. and E.P. Greenberg, *Listening in on bacteria: acyl-homoserine lactone signalling.* Nat Rev Mol Cell Biol, 2002. **3**(9): p. 685-95.

19. Whitehead, N.A., et al., *Quorum-sensing in Gram-negative bacteria.* FEMS Microbiol Rev, 2001. **25**(4): p. 365-404.

20. Fuqua, C., M.R. Parsek, and E.P. Greenberg, *Regulation of gene expression by cell-to-cell communication: acyl-homoserine lactone quorum sensing.* Annu Rev Genet, 2001. **35**: p. 439-68.

21. Ng, W.L. and B.L. Bassler, *Bacterial quorum-sensing network architectures.* Annu Rev Genet, 2009. **43**: p. 197-222.

22. Albuquerque, P. and A. Casadevall, *Quorum sensing in fungi--a review.* Med Mycol, 2012. **50**(4): p. 337-45.

23. Lee, H., et al., *TUP1 disruption in Cryptococcus neoformans uncovers a peptide-mediated density-dependent growth phenomenon that mimics quorum sensing.* Mol Microbiol, 2007. **64**(3): p. 591-601.

24. Lee, H., et al., *Regulatory diversity of TUP1 in Cryptococcus neoformans.* Eukaryot Cell, 2009. **8**(12): p. 1901-8.

25. Lim, T.S., J.W. Murphy, and L.K. Cauley, *Host-etiological agent interactions in intranasally and intraperitoneally induced Cryptococcosis in mice.* Infect Immun, 1980. **29**(2): p. 633-41.

26. Chun, C.D. and H.D. Madhani, *Applying genetics and molecular biology to the study of the human pathogen Cryptococcus neoformans.* Methods Enzymol, 2010. **470**: p. 797-831.

27. Cinader, B., S. Dubiski, and A.C. Wardlaw, *Distribution, Inheritance, and Properties of an Antigen, Mub1, and Its Relation to Hemolytic Complement.* J Exp Med, 1964. **120**: p. 897-924.

28. Nilsson, U.R. and H.J. Muller-Eberhard, *Deficiency of the fifth component of complement in mice with an inherited complement defect.* J Exp Med, 1967. **125**(1): p. 1-16.

29. Huffnagle, G.B., et al., *IL-5 is required for eosinophil recruitment, crystal deposition, and mononuclear cell recruitment during a pulmonary Cryptococcus neoformans infection in genetically susceptible mice (C57BL/6).* J Immunol, 1998. **160**(5): p. 2393-400.

30. Chun, C.D., J.C. Brown, and H.D. Madhani, *A major role for capsule-independent phagocytosis-inhibitory mechanisms in mammalian infection by Cryptococcus neoformans.* Cell Host Microbe, 2011. **9**(3): p. 243-51.

31. Olszewski, M.A., et al., *Urease expression by Cryptococcus neoformans promotes microvascular sequestration, thereby enhancing central nervous system invasion.* Am J Pathol, 2004. **164**(5): p. 1761-71.

32. Perfect, J.R., S.D. Lang, and D.T. Durack, *Chronic cryptococcal meningitis: a new experimental model in rabbits.* Am J Pathol, 1980. **101**(1): p. 177-94.

33. Petzold, E.W., et al., *Characterization and regulation of the trehalose synthesis pathway and its importance in the pathogenicity of Cryptococcus neoformans.* Infect Immun, 2006. **74**(10): p. 5877-87.

34. Lee, A., et al., *Survival defects of Cryptococcus neoformans mutants exposed to human cerebrospinal fluid result in attenuated virulence in an experimental model of meningitis.* Infect Immun, 2010. **78**(10): p. 4213-25.

35. O'Meara, T.R., et al., *Cryptococcus neoformans Rim101 is associated with cell wall remodeling and evasion of the host immune responses.* MBio, 2013. **4**(1).

36. O'Meara, T.R., et al., *Interaction of Cryptococcus neoformans Rim101 and protein kinase A regulates capsule.* PLoS Pathog, 2010. **6**(2): p. e1000776.

37. Piehler, D., et al., *Eosinophils contribute to IL-4 production and shape the T-helper cytokine profile and inflammatory response in pulmonary cryptococcosis.* Am J Pathol, 2011. **179**(2): p. 733-44.

38. Herring, A.C., et al., *Role and development of TH1/TH2 immune responses in the lungs.* Semin Respir Crit Care Med, 2004. **25**(1): p. 3-10.

39. Zhang, Y., et al., *Robust Th1 and Th17 immunity supports pulmonary clearance but cannot prevent systemic dissemination of highly virulent Cryptococcus neoformans H99.* Am J Pathol, 2009. **175**(6): p. 2489-500.

40. Akuthota, P., et al., *Immunoregulatory roles of eosinophils: a new look at a familiar cell.* Clin Exp Allergy, 2008. **38**(8): p. 1254-63.

41. Qiu, Y., et al., *Scavenger receptor A modulates the immune response to pulmonary Cryptococcus neoformans infection.* J Immunol, 2013. **191**(1): p. 238-48.

42. Zhang, Y., et al., *TLR9 signaling is required for generation of the adaptive immune protection in Cryptococcus neoformans-infected lungs.* Am J Pathol, 2010. **177**(2): p. 754-65.

43. Gordon, S.B. and R.C. Read, *Macrophage defences against respiratory tract infections.* Br Med Bull, 2002. **61**: p. 45-61.

44. Osterholzer, J.J., et al., *Role of dendritic cells and alveolar macrophages in regulating early host defense against pulmonary infection with Cryptococcus neoformans.* Infect Immun, 2009. **77**(9): p. 3749-58.

45. Shao, X., et al., *An innate immune system cell is a major determinant of species-related susceptibility differences to fungal pneumonia.* J Immunol, 2005. **175**(5): p. 3244-51.

46. Coelho, C., A.L. Bocca, and A. Casadevall, *The intracellular life of Cryptococcus neoformans.* Annu Rev Pathol, 2014. **9**: p. 219-38.

47. Charlier, C., et al., *Evidence of a role for monocytes in dissemination and brain invasion by Cryptococcus neoformans.* Infect Immun, 2009. **77**(1): p. 120-7.

48. Nicola, A.M. and A. Casadevall, *In vitro measurement of phagocytosis and killing of Cryptococcus neoformans by macrophages.* Methods Mol Biol, 2012. **844**: p. 189-97.

49. Carnes, E.C., et al., *Confinement-induced quorum sensing of individual Staphylococcus aureus bacteria.* Nat Chem Biol, 2010. **6**(1): p. 41-5.

50. Davis, M.J., et al., *Cryptococcus neoformans-induced macrophage lysosome damage crucially contributes to fungal virulence.* J Immunol, 2015. **194**(5): p. 2219-31.

51. Chang, Y.C. and K.J. Kwon-Chung, *Complementation of a capsule-deficient mutation of Cryptococcus neoformans restores its virulence.* Mol Cell Biol, 1994. **14**(7): p. 4912-9.

52. Chang, Y.C. and K.J. Kwon-Chung, *Isolation of the third capsule-associated gene, CAP60, required for virulence in Cryptococcus neoformans.* Infect Immun, 1998. **66**(5): p. 2230-6.

53. Walton, F.J., J. Heitman, and A. Idnurm, *Conserved elements of the RAM signaling pathway establish cell polarity in the basidiomycete Cryptococcus neoformans in a divergent fashion from other fungi.* Mol Biol Cell, 2006. **17**(9): p. 3768-80.

54. Rivera, J., et al., *Organ-dependent variation of capsule thickness in Cryptococcus neoformans during experimental murine infection.* Infect Immun, 1998. **66**(10): p. 5027-30.

55. Zaragoza, O., B.C. Fries, and A. Casadevall, *Induction of capsule growth in Cryptococcus neoformans by mammalian serum and CO(2).* Infect Immun, 2003. **71**(11): p. 6155-64.

56. Zaragoza, O. and A. Casadevall, *Experimental modulation of capsule size in Cryptococcus neoformans.* Biol Proced Online, 2004. **6**: p. 10-15.

57. Qiu, Y., et al., *Immune modulation mediated by cryptococcal laccase promotes pulmonary growth and brain dissemination of virulent Cryptococcus neoformans in mice.* PLoS One, 2012. **7**(10): p. e47853.

58. Vu, K., et al., *Invasion of the central nervous system by Cryptococcus neoformans requires a secreted fungal metalloprotease.* MBio, 2014. **5**(3): p. e01101-14.

59. Eigenheer, R.A., et al., *Extracellular glycosylphosphatidylinositol-anchored mannoproteins and proteases of Cryptococcus neoformans.* FEMS Yeast Res, 2007. **7**(4): p. 499-510.

60. Siafakas, A.R., et al., *Cell wall-linked cryptococcal phospholipase B1 is a source of secreted enzyme and a determinant of cell wall integrity.* J Biol Chem, 2007. **282**(52): p. 37508-14.

61. Banks, I.R., et al., *A chitin synthase and its regulator protein are critical for chitosan production and growth of the fungal pathogen Cryptococcus neoformans.* Eukaryot Cell, 2005. **4**(11): p. 1902-12.

62. Baker, L.G., et al., *Chitosan, the deacetylated form of chitin, is necessary for cell wall integrity in Cryptococcus neoformans.* Eukaryot Cell, 2007. **6**(5): p. 855-67.

63. Reese, A.J. and T.L. Doering, *Cell wall alpha-1,3-glucan is required to anchor the Cryptococcus neoformans capsule.* Mol Microbiol, 2003. **50**(4): p. 1401-9.

64. Reese, A.J., et al., *Loss of cell wall alpha(1-3) glucan affects Cryptococcus neoformans from ultrastructure to virulence.* Mol Microbiol, 2007. **63**(5): p. 1385-98.

65. Free, S.J., *Fungal cell wall organization and biosynthesis.* Adv Genet, 2013. **81**: p. 33-82.

66. Sakaguchi, N., et al., *Ultrastructural study of Cryptococcus neoformans by quick-freezing and deep-etching method.* Mycopathologia, 1993. **121**(3): p. 133-41.

67. Shepardson, K.M. and R.A. Cramer, *Fungal cell wall dynamics and infection site microenvironments: signal integration and infection outcome.* Curr Opin Microbiol, 2013. **16**(4): p. 385-90.

68. Ding, C., et al., *Cryptococcus neoformans copper detoxification machinery is critical for fungal virulence.* Cell Host Microbe, 2013. **13**(3): p. 265-76.

69. Chang, Y.C. and K.J. Kwon-Chung, *Isolation, characterization, and localization of a capsule-associated gene, CAP10, of Cryptococcus neoformans.* J Bacteriol, 1999. **181**(18): p. 5636-43.

70. Chang, Y.C., L.A. Penoyer, and K.J. Kwon-Chung, *The second capsule gene of cryptococcus neoformans, CAP64, is essential for virulence.* Infect Immun, 1996. **64**(6): p. 1977-83.

71. Liu, O.W., et al., *Parallel beta-helix proteins required for accurate capsule polysaccharide synthesis and virulence in the yeast Cryptococcus neoformans.* Eukaryot Cell, 2007. **6**(4): p. 630-40.

72. Kumar, P., et al., *Pbx proteins in Cryptococcus neoformans cell wall remodeling and capsule assembly.* Eukaryot Cell, 2014. **13**(5): p. 560-71.

73. Lambeth, J.D., *NOX enzymes and the biology of reactive oxygen.* Nat Rev Immunol, 2004. **4**(3): p. 181-9.

74. Marchler-Bauer, A., et al., *CDD: NCBI's conserved domain database.* Nucleic Acids Res, 2015. **43**(Database issue): p. D222-6.

75. Varshavsky, A., *Ubiquitin fusion technique and its descendants.* Methods Enzymol, 2000. **327**: p. 578-93.

76. Ding, C., et al., *The copper regulon of the human fungal pathogen Cryptococcus neoformans H99.* Mol Microbiol, 2011. **81**(6): p. 1560-76.

77. Evans, R.J., et al., *Cryptococcal phospholipase B1 is required for intracellular proliferation and control of titan cell morphology during macrophage infection.* Infect Immun, 2015. **83**(4): p. 1296-304.

78. Ma, H., et al., *The fatal fungal outbreak on Vancouver Island is characterized by enhanced intracellular parasitism driven by mitochondrial regulation.* Proc Natl Acad Sci U S A, 2009. **106**(31): p. 12980-5.

79. Liu, T.B. and C. Xue, *Fbp1-mediated ubiquitin-proteasome pathway controls Cryptococcus neoformans virulence by regulating fungal intracellular growth in macrophages.* Infect Immun, 2014. **82**(2): p. 557-68.

80. Gomolplitinant, K.M. and M.H. Saier, Jr., *Evolution of the oligopeptide transporter family.* J Membr Biol, 2011. **240**(2): p. 89-110.

81. Rutherford, S.T. and B.L. Bassler, *Bacterial quorum sensing: its role in virulence and possibilities for its control.* Cold Spring Harb Perspect Med, 2012. **2**(11).

82. Lazazzera, B.A. and A.D. Grossman, *The ins and outs of peptide signaling.* Trends Microbiol, 1998. **6**(7): p. 288-94.

83. Rocha-Estrada, J., et al., *The RNPP family of quorum-sensing proteins in Gram-positive bacteria.* Appl Microbiol Biotechnol, 2010. **87**(3): p. 913-23.

84. Inglis, D.O., et al., *Literature-based gene curation and proposed genetic nomenclature for cryptococcus.* Eukaryot Cell, 2014. **13**(7): p. 878-83.

85. Janbon, G., et al., *Analysis of the genome and transcriptome of Cryptococcus neoformans var. grubii reveals complex RNA expression and microevolution leading to virulence attenuation.* PLoS Genet, 2014. **10**(4): p. e1004261.

86. Dumesic, P.A., et al., *Product binding enforces the genomic specificity of a yeast polycomb repressive complex.* Cell, 2015. **160**(1-2): p. 204-18.

87. Zhang, Z., et al., *Strand-specific libraries for high throughput RNA sequencing (RNA-Seq) prepared without poly(A) selection.* Silence, 2012. **3**(1): p. 9.

88. Trapnell, C., et al., *Differential gene and transcript expression analysis of RNA-seq experiments with TopHat and Cufflinks.* Nat Protoc, 2012. **7**(3): p. 562-78.

89. Anders, S. and W. Huber, *Differential expression analysis for sequence count data.* Genome Biol, 2010. **11**(10): p. R106.

90. Jambunathan, K., et al., *Proteolytic fingerprinting of complex biological samples using combinatorial libraries of fluorogenic probes.* Curr Protoc Protein Sci, 2012. **Chapter 21**: p. Unit21 22.

91. Liu, O.W., et al., *Systematic genetic analysis of virulence in the human fungal pathogen Cryptococcus neoformans.* Cell, 2008. **135**(1): p. 174-88.

92. Zhang, J., et al., *Isolation of lymphocytes and their innate immune characterizations from liver, intestine, lung and uterus.* Cell Mol Immunol, 2005. **2**(4): p. 271-80.

93. Petersen, T.N., et al., *SignalP 4.0: discriminating signal peptides from transmembrane regions.* Nat Methods, 2011. **8**(10): p. 785-6.

94. Findley, K., et al., *Phylogeny and phenotypic characterization of pathogenic Cryptococcus species and closely related saprobic taxa in the Tremellales.* Eukaryot Cell, 2009. **8**(3): p. 353-61.

95. Bahn, Y.S., et al., *A unique fungal two-component system regulates stress responses, drug sensitivity, sexual development, and virulence of Cryptococcus neoformans.* Mol Biol Cell, 2006. **17**(7): p. 3122-35.

96. Xue, C., et al., *G protein-coupled receptor Gpr4 senses amino acids and activates the cAMP-PKA pathway in Cryptococcus neoformans.* Mol Biol Cell, 2006. **17**(2): p. 667-79.

Chapter 4

An expanded family of Barwin-like proteins in *Cryptococcus neoformans*

Summary

Cryptococcus neoformans is an opportunistic yeast pathogen responsible for over 1 million infections and 600,000 deaths annually. In a published study, we identified a transcriptional regulator Gat201 that inhibits phagocytosis independently of the polysaccharide capsule. Previously, the major component of the polysaccharide capsule, glucoronoxylomannan (GXM), was believed to be the only mechanism by which the fungus could evade phagocytosis by macrophages. Our laboratory performed studies using custom microarrays to define which genes were controlled by Gat201 and screened each Gat201-regulated gene for its effect on phagocytosis. We determined that Blp1, a protein regulated by Gat201, inhibited *C. neoformans* phagocytosis by macrophages. I performed subsequent chromatin immunoprecipitation and sequencing (ChIP- Seq) experiments and discovered that two other proteins in the same family as Blp1 (Blp2 and Blp4) are targets of Gat201. Here, I determined that Blp2 functions redundantly with Blp1 to inhibit phagocytosis. Additionally, Blp4 has a unique role among the Blp family members tested in promoted proliferation within macrophages. These findings open the possibility that additional Blp protein family members have unique roles in mediating *C. neoformans*' interactions with macrophages. And, finally, these findings raise the possibility that Blp proteins could be excellent treatment targets since they mediate the crucial interaction of *C. neoformans* with first-line immune cells during infection.

Introduction

Double-ψ β-barrel (DPBB) domain-containing proteins are important in plant-pathogen interactions [1]. These proteins are extremely stable over wide pH and temperature ranges [2]. They are found both in plants, where they affect wound response, in plant pathogens, where they affect virulence, and in biocontrol fungi, where they protect host plants from attack [3]. Understanding the function of this protein family has been difficult since they are important in both pathogenic and non-pathogenic contexts [4, 5].

Cerato platanin (CP) is the flagship member of this protein family and is secreted by the pathogen *Ceratocystis platani,* which causes epidemic canker stain of plane trees [6]. Prior work showed that CP binds a fragment of chitin but lacks endoglucanase and chitinase activity found in related proteins [2]. Chitin is a component of the fungal cell wall, composed of monomers of N-acetylglucosamine (GlcNAc) and CP was found to bind a tetramer of GlcNAc (GlcNAc-4) [2]. CP localizes to fungal cell walls and is hypothesized to be involved in cell wall remodeling during *C. platani's* growth [7]. One theory is that CP aggregates form a scaffold for cell wall remodeling [8].

Cryptococcus neoformans, the pathogenic fungus our laboratory studies, has a family of eight Barwin-like proteins (Blps) which all contain the same double-psi beta-barrel domain as CP. Each family member has a signal sequence. As published previously, out laboratory has identified a transcription factor that mediates a novel mechanism for evading phagocytosis, independent of the polysaccharide capsule[9]. Part of this capsule-independent phagocytosis evasion occurred through the Blp1 protein [10]. As described in Chapter 2, I characterized the targets of Gat201 further by ChIP-Seq and found a remarkable overlap with two other transcription factors, Gat204 and Liv3, comprising a regulatory network. Gat201, Gat204, and

Liv3 all bound the promoters of three Blp protein family members: Blp1, Blp2, and Blp4.

Blp1 is a small 15 kiloDalton protein whose entire sequence is composed solely of a 17 amino-acid signal sequence and a double-psi beta-barrel (DPBB) structural domain. Since this structural domain dominates Blp1's amino acid content, it is almost certainly involved in Blp1's function to inhibit phagocytosis. A bioinformatic investigation of this domain in other fungi shows that most have only two or three proteins with the DPBB domain. Only two fungi have greater than four proteins with this structural motif; one is *C. neoformans* while the other is *Fusarium oxysporum*, a fungal pathogen that infects a number of plants and animals [11, 12], and is emerging as a macrophage-resistant human pathogen found in immunocompromised patients [13]. Given the expansion of this protein family in two macrophage-resistant pathogenic fungi and data that three cryptococcal family members are regulated by the same virulence-implicated transcription factor network, it is reasonable that they play a role in capsule-independent phagocytosis inhibition.

Based on their structural similarity and evidence suggesting that certain Blp proteins are co-regulated, we hypothesized that the co-regulated Blp1, Blp2, and Blp4 proteins functioned redundantly to mediate the capsule-independent antiphagocytic phenotype by changing how macrophages recognize *C. neoformans*. As described below, we characterized the Blp protein family in *C. neoformans* and examined the role of the Gat201-regulated Blp1, Blp2, and Blp4 proteins in regulating phagocytosis. Additionally, we examined the role of Blp1, Blp2, and Blp4 in Cryptococcus intracellular proliferation inside of macrophages.

Results

C. neoformans has eight proteins that are considered members of the Blp family, defined

by containing a signal sequence and a barwin-like domain. Despite sharing the same Barwin structural motif, the double-psi beta-barrel domain, the Blp family of proteins in *C. neoformans* show considerable structural variation (Table 1). Blp1 and Blp2 are the shortest members of the family. Their sequence is almost entirely comprised of a signal sequence and the Barwin domain. Blp8 is not much longer than Blp1 and Blp2. On the other hand, Blp4, Blp5, Blp6, and Blp7 all have approximately 150-200 amino acids that are not in the barwin domain. Finally, Blp3 is the outlier in the Blp family of proteins—Blp3 is both much longer than Blp1 and Blp2, with more than 400 amino acids that are not within the Barwin domain. Additionally, the Blp protein family has considerable variation in the percentage of each family member that is predicted to be disordered, from 6.45% of Blp2 to Blp3 which is predicted to have more than half of its length be disordered. Interestingly, seven of the eight Blp protein family members are predicted to have a pI of approximately 4. Blp3 is the only outlier in this regard: it is predicted to have a pI of 7.

Using the protein sequences of each of the Blp protein family members, I constructed a phylogeny (Figure 1A). By sequence homology, Blp1 and Blp2 are the most related to each other. They are also located in flanking loci on chromosome 13 in the genome (Figure S1A). Blp3 is closely related to Blp1 and Blp2 by sequence homology. Interestingly, Blp4's sequence is less related to Blp1 and Blp2 but it is also regulated by the three virulence-related transcription factors described in Chapter 2 (Figure S1B). The remaining Blp protein family members are much more distantly related than Blp1-4 (Figure 1A).

For the remainder of this project, I focused on Blp1, Blp2, and Blp4, since they are the closely-related members of the protein family that are regulated by virulence-related transcription factors. Following work done previously in the lab [14], I purified recombinant Blp1 protein (Figure 1B). Using recombinant Blp1, I tested whether this member of the Blp

protein family could bind glucose, chitin, and purified cryptococcal polysaccharide capsule using the PAHBAH reagent to detect the amount of reducing sugars in solution with and without recombinant Blp1 [15, 16]. In this assay, only glucose seemed to be a substrate for Blp1 binding, although the effect size was weak (Figure 1C). Additionally, I tested whether recombinant Blp1 had any pectinase, glycosylase hydrolase, or chitinase activity using the same PAHBAH assay. However, this preparation of recombinant Blp1 did show any activity under the conditions tested (Figured 1D and data not shown). Finally, using purified recombinant protein, I tested the ability of Blp1 to bind a variety of substrates using a glycan array with 610 substrates (Table S1). We detected no Blp1 binding to any of the substrates studied (Figure 1E).

Although we were not able to detect significant binding or enzymatic activity for Blp1, our best hypothesis remained that Blp protein family members interact with the exterior surface of *C. neoformans* cells due to Blp1's previously-published antiphagocytic effects [17]. Therefore, we investigated the role of other Blp family members in *C. neoformans'* interactions with macrophages. As described in Chapter 3, I infected bone marrow-derived macrophages with different cryptococcal strains at an MOI of 10. After 24 hours, I washed non-adhered cryptococcal cells off and determined the phagocytic index (PI) (the percentage of macrophages that had associated cryptococcal cells either attached or internalized). In conditions where the macrophages were not activated with interferon gamma, I observed the slight increase in PI previously seen when infecting macrophage-like cell lines and BMDMs with *blp1*Δ (Figure 2A). Additionally, I observed a similar slight increase in PI for infections with *blp2*Δ, although the effect was not quite statistically significant, and an even greater increase in PI for a *blp1*Δ*blp2*Δ double mutant (Figure 2A). I observed an insignificant increase in PI when infecting BMDMs with *blp4*Δ mutants, although the effect size was not as large as I observed for *blp1*Δ and *blp2*Δ

(Figure 2A). When macrophages were activated, the increases in PI became less apparent with none of them statistically significant (Figure 2B). Finally, when infecting with strains that were opsonized with monoclonal anti-capsular antibodies, all mutants showed a similar PI (Figure 2C).

Once cryptococcal cells are internalized, the fungal cells survive and replicate within the hostile environment of macrophage phagolysosomes [18]. Using the model of intracellular infection described in Chapter 3, I tested the ability of *blp1*Δ, *blp2*Δ, *blp4*Δ, and *blp1*Δ*blp2*Δ to survive within macrophages. I found that *blp4*Δ had an intracellular replication, with significantly fewer fungal cells found in macrophage supernatants and lysates across all experiments (Figure 3A, B, and C). Notably, the magnitude of *blp4*Δ's intracellular replication defect is similar to *qsp1*Δ's intracellular replication defect. *blp4*Δ is also a direct transcriptional target of Qsp1. In log-phase cultures, *BLP4* is upregulated more than 2-fold in *qsp1*Δ cells (Figure S2A). However, in saturated cultures, *BLP4* is downregulated by approximately 5-fold in *qsp1*Δ cells (Figure S2B). *BLP4* is also induced almost 2-fold by increasing cell density in wild type cells (Figure S3B), raising the possibility that *BLP4* transcription is regulated by Qsp1 and by cell culture density.

Discussion

Thus far, our laboratory has found a unique, previously-uncharacterized capsule-independent antiphagocytic mechanism. This mechanism is mediated, in part, by the protein Blp1 [10]. Blp1 is one member of a family of eight candidate effectors, the Blp proteins. Here, I characterized the Blp protein family further and found that Blp1, Blp2, and Blp4 are closely-related members of the protein family that are co-regulated by three transcription factors

discussed in Chapter 2, Gat201, Gat204, and Liv3.

Although Blp1 does not seem to have any enzymatic activity, I did determine that it binds glucose with low affinity. Given that Blp1-like proteins in other fungal pathogens have carbohydrate-binding roles [2], this could indicate a role for Blp1 in binding an unknown carbohydrate species on the outer surface of *C. neoformans* cells. Since the carbohydrate-binding array used to test Blp1 binding affinity was not specific for fungal carbohydrates, it is possible that I have not detected robust carbohydrate binding for Blp1 because I have not tested the correct binding substrate. In particular, the hypothesis that Blp1 and other Blp proteins bind the polysaccharide capsule or cell wall of *C. neoformans* seems possible given the polysaccharide-binding capabilities of the double-psi beta-barrel domain [2], the previously characterized role of Blp1 in inhibiting phagocytosis by macrophages [10], and the fact that Blp4 has been previously detected in cryptococcal cell wall preparations [19].

With this hypothesis in mind, I tested the ability of other members of the Blp protein family to inhibit phagocytosis by macrophages. I found that Blp1 and Blp2 may function redundantly to inhibit phagocytosis. In particular, the *blp1*Δ*blp2*Δ double mutant shows a larger increase in PI than either mutant alone, indicating syngergy or redundancy between the two genes. While there may also be a slight increase in PI for the *blp4*Δ mutant, the most notable phenotype for *blp4*Δ is that it has an intracellular proliferation defect after 24 hours co-culture with macrophages. *blp1*Δ and *blp2*Δ may have a slight intracellular proliferation defect but do not have as strong of a phenotype, if any at all. This raises the possibility of specializations within the Blp protein family. Perhaps, Blp1 and Blp2 are redundant and function to alter the fungal cell surface to prevent macrophage recognition and uptake. Then, Blp4 appears to function after phagocytosis to promote fungal survival inside the phagolysosome.

Based on the findings of this research, there are many potentially interesting areas for further study. The remaining Blp protein members (Blp3, Blp5, Blp6, Blp7, and Blp8) will need to be tested for roles in phagocytosis inhibition and intracellular survival. The mechanism by which Blp1 and Blp2 inhibit phagocytosis could broadly be either of two non-mutually-exclusive models: (1) Blp proteins mask a pathogen-associated molecular pattern (PAMP) on *C. neoformans'* surface, preventing macrophages from recognizing and phagocytosing the fungus. (2) Blp proteins engage an inhibitory receptor on macrophages to prevent phagocytosis. These models can be tested by infecting mutant macrophages with Blp mutants. Macrophages lacking the Syk protein cannot respond to PAMPs and macrophages lacking SHP-1 cannot respond to inhibitory molecules. If Blp proteins mask PAMPs, they should exhibit equal PI in mutant macrophages lacking the Syk protein. On the other hand, if Blp proteins engage inhibitory receptors on macrophages, their PI should be equal to wild type when they infect mutant macrophages lacking SHP-1. I anticipate that these experiments will provide insight into the role of this protein family in *C. neoformans'* ability to elude the human immune system through a capsule-independent virulence mechanism. Such a finding would not be without precedent, as *C. neoformans* is thought to survive and perhaps more successfully spread from within macrophages [20-22].

Additionally, we should determine whether the in vitro phenotypes of *blp1*Δ, *blp2*Δ, and *blp4*Δ relate to in vivo success by infecting mice with wildtype *C. neoformans* and any mutants that demonstrate increased phagocytosis. I propose infection through two routes, using the murine inhalation model and the murine tail vein injection model of cryptococcal infection [23]. In the inhalation model, the infection will assess relative competencies of the mutant and wild type fungus in the specific pulmonary environment, where *C. neoformans* infection is

established. The tail vein injection model assesses the relative abilities of mutant and wild type strains to survive in the bloodstream and establish a disseminated infection throughout the host.

After their initial characterization, identification of Blp binding partners or binding substrates will allow us to design small molecule inhibitors, and ultimately drugs, to disrupt these interactions, thereby disabling the phagocytosis inhibition and intracellular proliferation advantage they impart. Since our laboratory has shown that loss of the Gat201-mediated antiphagocytic mechanism leaves strains essentially avirulent, treatments which inhibit this mechanism will undoubtedly be an important avenue for therapy in patients infected with *C. neoformans*.

Experimental Procedures

Materials

Strains (Table S1) were grown in YPAD (1% yeast extract, 2% Bacto-peptone, 2% glucose, 0.015% L-tryptophan, 0.004% adenine), YNB, or DMEM at temperatures specified in the text.

Phylogeny

The phylogeny for Blp1-8 was generated using the protein sequences available from the Broad H99 genome sequence. Sequences were aligned and a bootstrapped N-J tree was generated using Clustal2 [24]. The phylogeny was visualized using NJplot [25].

Purification of Recombinant Blp1

20 mL 2x LB media with kanamycin were inoculated with BHM1643 freezer stock and grown overnight at 37ºC. Diluted overnight cultures 1:100 into 1L 2x LB media with kanamycin and

grew at 37ºC until cells were at OD 0.5-0.6. Then, cells were induced for 3 hours at 37ºC with 0.5mM IPTG. Cells were harvested by spinning at 3500 rpm for 10 minutes at 4ºC, washed 1x in ice cold water, and flash frozen in liquid nitrogen. Pellets could be stored at -80ºC if desired. When needed, pellets were thawed in ice cold water and resuspended in 20 mL ice-cold lysis buffer (50 mM NaH_2PO_4, 300 mM NaCl, 10 mM imidazole, pH 8.0) with 1 mg/mL lysozyme and one Complete Mini EDTA-free Protease inhibitor cocktail tablet (Roche). The pellet was incubated in this buffer at 4ºC for 20 minutes. Cells were lysed further with a microtip sonicator for 15 pulses, six times (50% duty cycle, power 4). Samples were maintained in an ice water bath between sonication cycles.

DNA was removed from the lysate with DNase1 treatment at 50U/mL for 30 minutes at 4ºC. Lysate was clarified by centrifugation at 16k rpm for 25 minutes at 4ºC before adding Ni-NTA beads (prepared by washing beads 3x in 10 mL lysis buffer and resuspending in 5 mL lysis buffer with protease inhibitors and lysozyme as described above). Lysate was incubated with beads on nutator for 1.5 hours at 4ºC before addition to a polyprep chromatography column (Bio-Rad). After lysate flowed through column slowly, beads were washed with 15 bed volumes of wash buffer (50 mM NaH_2PO_4, 300 mM NaCl, 20 mM imidazole, pH 8.0) and eluted in 5-6 bed volumes of elution buffer (50 mM NaH_2PO_4, 300 mM NaCl, 250 mM imidazole, pH 8.0). Eluate was concentrated in an Amicon ultra 10 kDa spin filter (Millipore) and buffer exchanged on the spin filter with 5mL 2X storage buffer (20 mM Tris pH 7.4, 200mM NaCl), repeating three times total. Recombinant protein was stored at 4ºC until use.

Polysaccharide Binding and Glycosidase Assays

Recombinant Blp1, prepared as described above, was sent to Emory's Functional Glycomics Core and screened using their standard protocols on their mammalian glycan array. Using either 0.5, 1, or 2 µg/mL recombinant Blp1, reactions were set up at 37ºC to test glycosidase activity using the substrates laminarin (5 mg/mL), polygalacturonic acid (10 mg/mL), carboxymethylcellulose (20 mg/mL), and chitin azure (5 mg/mL). Reactions proceeded for 3.5 hours at 37ºC. After stopping the reaction by boiling for 5 minutes, glycosidase activity was determined for laminarin, polygalacturonic acid, and carboxymethylcellulose were measured by adding 125 µL of PAHBAH reagent to 25 µL of the reaction, incubating plate at 100ºC for 6 minutes, incubating plate on ice for 5 minutes, and then bringing plate to room temperature before reading absorbance at 410 nm on a Tecan M1000 plate reader. Chitinase activity was measured using the chitin azure substrate and measuring absorbance at 560 nm on a Tecan M1000 plate reader. Binding to the same substrates listed above in addition to glucose were determined by mixing Blp1 with the substrate and immediately performing the PAHBAH assay quantification as described above.

Macrophage Uptake (Opsonized and Unopsonized)

Macrophage uptake and intracellular proliferation assays were performed as previously described [26] with minor changes described below. Bone-marrow derived macrophages (BMDMs) were isolated from the bone marrow of C57BL/6 mice and cultured for 7 days in BMDM growth media containing DMEM H-21, 20% v/v FBS, 2mM glutamine, 0.11 mg/mL sodium pyruvate, and 10% MCSF derived from A549 cell supernatants in the presence of penicillin/streptomycin. 10,000 BMDMs were seeded per well in a 96-well plate (Costar) and stimulated with 100 ng/mL

Interferon-γ (Roche) for 24 hours before infection and maintained under stimulation throughout infection. Overnight cultures of *C. neoformans*, grown in YPAD, were washed once in DMEM and then resuspended in BMDM growth media. For opsonized experiments, cells were opsonized with mAb1255 (10μg/mL) at 37ºC for 1 hour prior to infection. Uptake experiments were done at an MOI of 10 (plated serial dilutions of inoculum to confirm MOI) and uptake was assessed after 24hrs co-culture at 37ºC, 5% CO_2 and 3 washes with PBS to remove non-adherent *C. neoformans* cells. >200 BMDMs quantified per well, with 6 wells per genotype.

Macrophage Killing Assay

BMDMs were prepared as described above and 100,000 cells were seeded per well in a 24-well plates (Corning 353047). BMDMs were stimulated with Interferon-γ as described above and then infected with opsonized *C. neoformans* (see above) at an MOI of 0.1 (plated serial dilutions of inoculum to confirm MOI). After 24 hours co-cultures at 37ºC, 5% CO_2, supernatants were removed and serial dilutions were plated for CFUs. Macrophages were lysed in 500 μL sterile water, sitting at 37ºC for 15 minutes. Wells were washed with an additional 500 μL sterile water and combined with lysate, yielding 1mL lysate. Serial dilutions of this lysate were plated for CFUs. The ratio of CFUs over input was quantified and this value was analyzed by bootstrapping, generating 95% confidence intervals. Non-overlapping 95% confidence intervals were considered significantly different; $p < 0.05$.

RNA-Seq Library Preparation

Total RNA was isolated and libraries prepared as described previously [27]. Cell pellets were lyophilized overnight and then RNA was isolated using TRIzol (Invitrogen). To obtain mRNA,

50-200 μg of total RNA (isolated as described above) was purified using the Oligotex mRNA mini kit (Qiagen). For each RNA sample, two successive rounds of purification were performed. Input RNA quality and mRNA purity were verified by Bioanalyzer Pico RNA chips (Agilent). The purified RNA (120 ng) was treated by on-column DNase digestion as described previously [28], then used to prepare sequencing libraries using the NEBNext Ultra Directional RNA Library Prep Kit (New England Biolabs). Libraries were analyzed for quality and average size on Bioanalyzer High Sensitivity DNA chips (Agilent) and quantified by qPCR with KAPA Library Quant Standards. Libraries were sequenced on the HiSeq 2500 platform (Illumina).

RNA-Seq Analysis

RNA-seq data, which included two biological replicates per genotype, were aligned using Tophat [29]. Expression analysis for each transcription factor mutant was performed as follows: First, the number of reads aligning to an entire mRNA was counted. For each genotype examined, any region with <20 reads in the mutant or wild-type sample was excluded from analysis. Next, counts were compared between datasets after normalizing the datasets using the TMM algorithm [30]. Gene expression profiles for each transcription factor mutant are contained in Table S2. Fold changes averaged between the two replicates and genes were considered significantly changed if they were >1.5-fold or <0.67-fold changed between datasets.

Acknowledgements

I thank members of the Madhani lab for helpful discussions and Nguyen Nguyen for media preparation. This work was supported by a grant from the National Institute of Allergy and Infectious Disease (R01AI096869) and a fellowship from the National Heart, Lung, and Blood Institute (F30HL120496-01A1). CMH and HDM designed the study. CMH performed the experiments and HDM supervised the work.

Figures and Tables

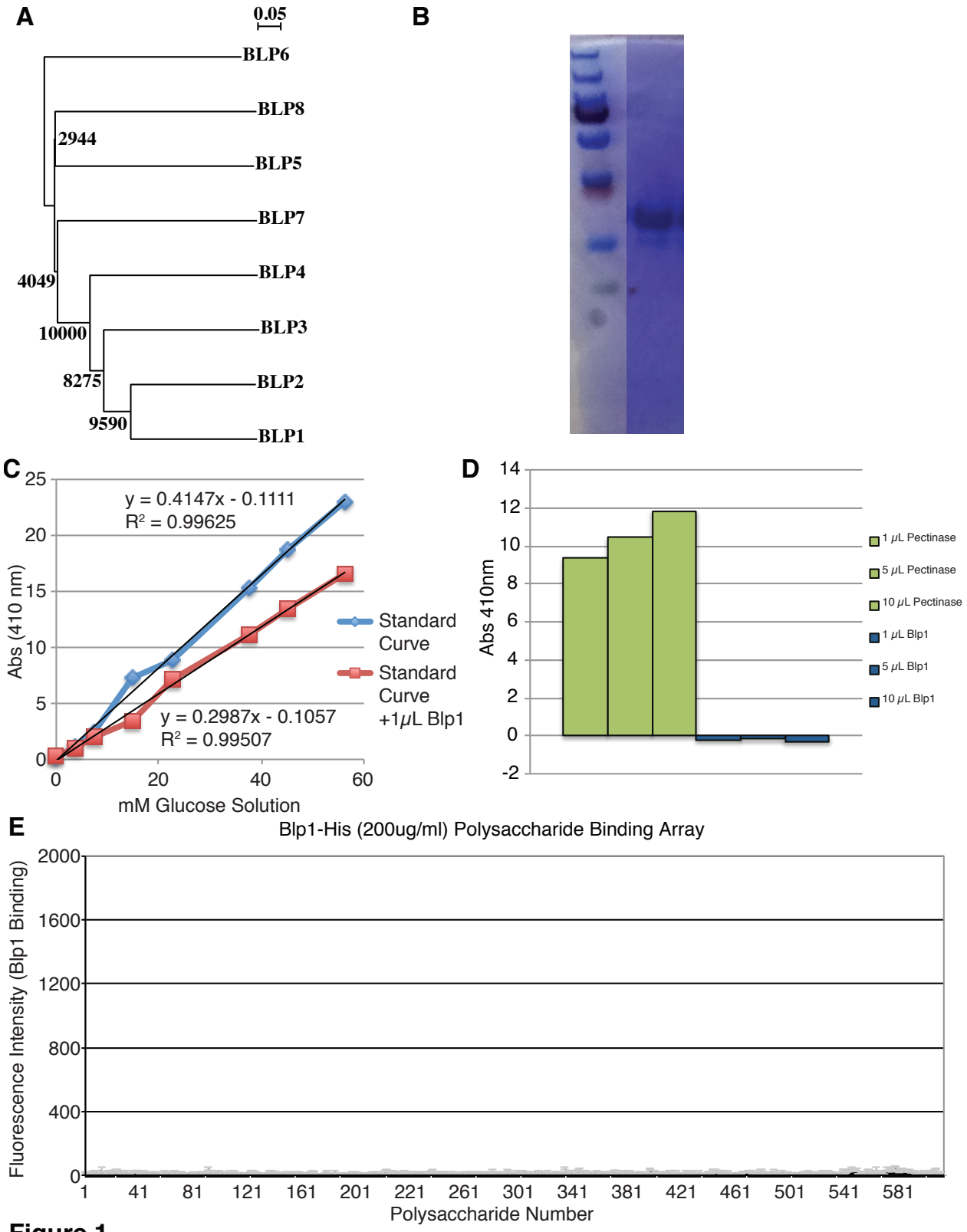

Figure 1

Figure 1: Proteins of the Blp family in *C. neoformans* are predicted to bind polysaccharides

a) Blp phylogeny. Phylogeny was determined using protein sequence for each of the *BLP* genes in *C. neoformans*.

b) Blp1 recombinant protein. Coomassie-blue stained polyacrylamide gel showing the final purified Blp1 recombinant protein.

c) Blp1 glucose binding. Adding Blp1 to a glucose solution causes a change in the amount of free reducing ends as measured by the PAHBAH reagent.

d) Pectinase assay. Pectinase activity was measured against the substrate polygalacturonic acid. Pectinase was used as a positive control but Blp1 exhibited no activity under these conditions as measured by the PAHBAH reagent.

e) Glycan binding array. No binding was detected for recombinant Blp1 by fluorescent anti-6xHis antibody binding.

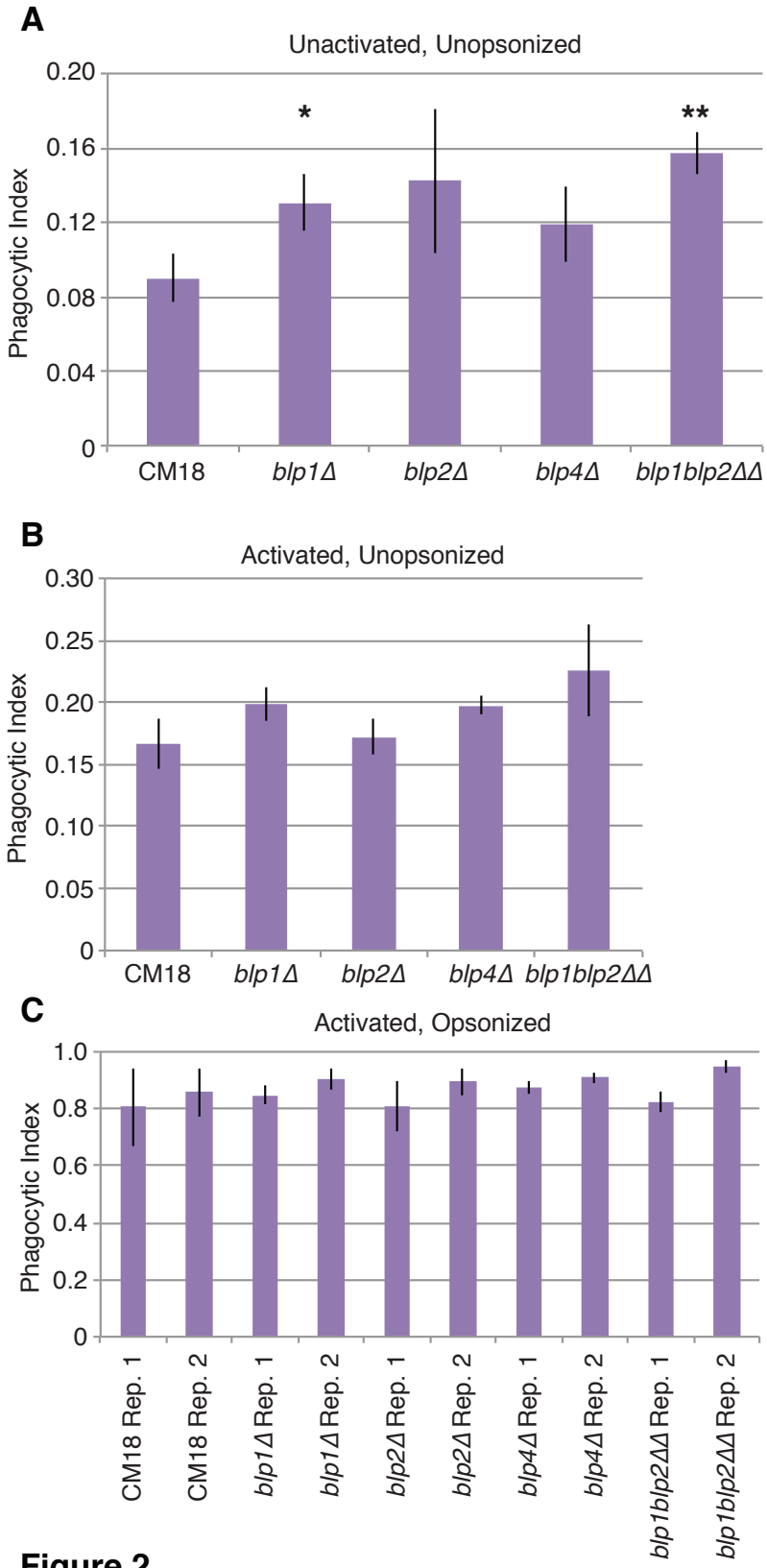
A
Unactivated, Unopsonized
Phagocytic Index
0.20
0.16
0.12
0.08
0.04
0
*
**
CM18
blp1Δ
blp2Δ
blp4Δ
blp1blp2ΔΔ
B
Activated, Unopsonized
Phagocytic Index
0.30
0.25
0.20
0.15
0.10
0.05
0
CM18
blp1Δ
blp2Δ
blp4Δ
blp1blp2ΔΔ
C
Activated, Opsonized
Phagocytic Index
1.0
0.8
0.6
0.4
0.2
0
CM18 Rep. 1
CM18 Rep. 2
blp1Δ Rep. 1
blp1Δ Rep. 2
blp2Δ Rep. 1
blp2Δ Rep. 2
blp4Δ Rep. 1
blp4Δ Rep. 2
blp1blp2ΔΔ Rep. 1
blp1blp2ΔΔ Rep. 2

Figure 2

Figure 2: *BLP1* and *BLP2* influence phagocytosis by BMDMs

a) Phagocytic index of unopsonized, unstimulated, b) unopsonized and IFN-gamma stimulated, and c) opsonized and IFN-gamma stimulated *C. neoformans*. >600 BMDMs quantified per genotype. Error bars are S.D. Student t test was used to determine significance and $p < 0.05$ is indicated by *.

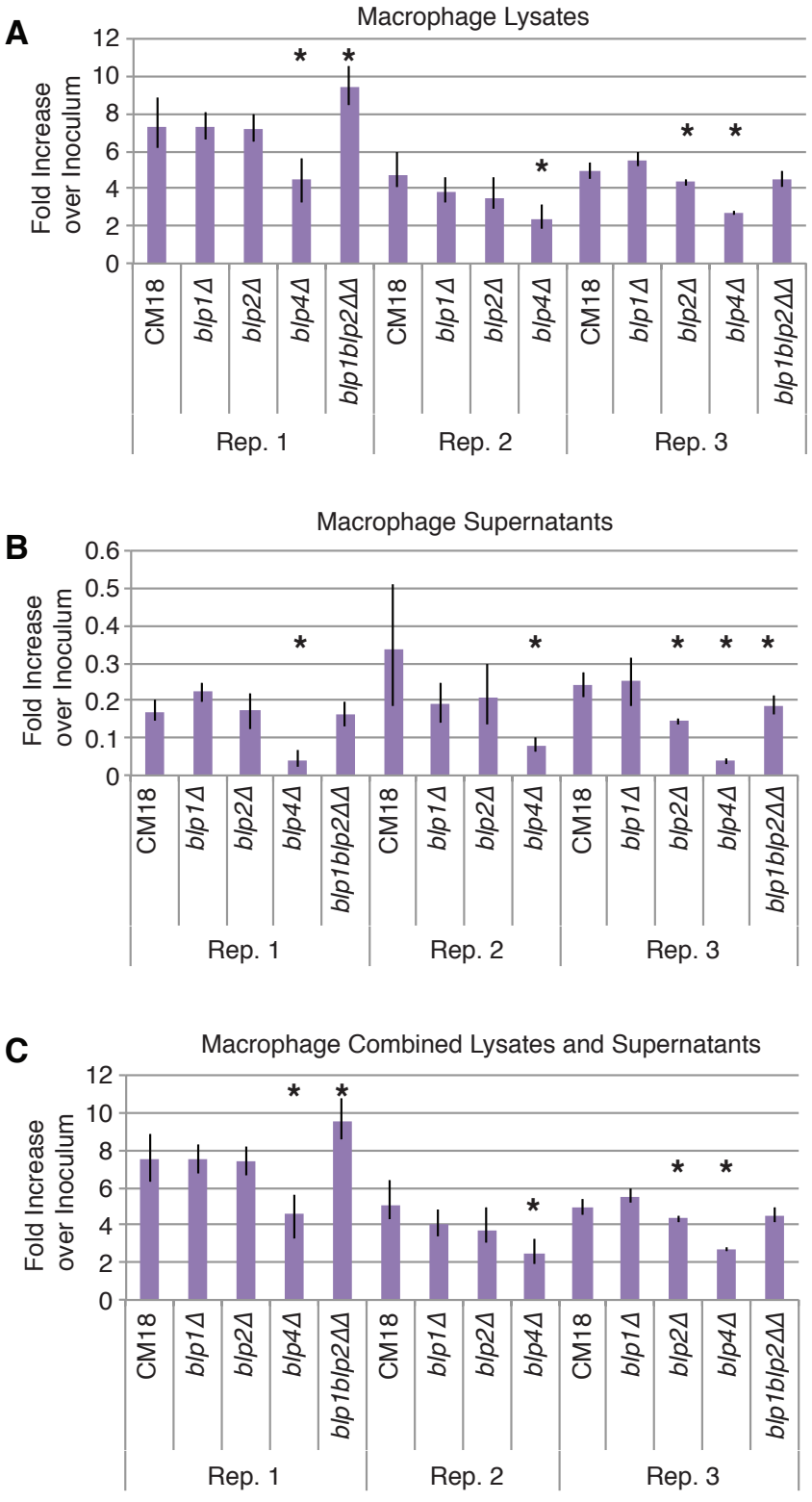
A
Macrophage Lysates
Fold Increase over Inoculum
12
10
8
6
4
2
0
CM18
blp1Δ
blp2Δ
blp4Δ
blp1blp2ΔΔ
Rep. 1
Rep. 2
Rep. 3
B
Macrophage Supernatants
0.6
0.5
0.4
0.3
0.2
0.1
C
Macrophage Combined Lysates and Supernatants

Figure 3

Figure 3: *BLP4* is required for intracellular proliferation during BMDM infection

a) Macrophage intracellular accumulation assay. CFUs isolated from BMDM lysates, b) supernatants, or c) lysate and supernatants combined 24 hours after infection, normalized to starting inoculum. Error bars represent 95% confidence intervals constructed by bootstrapping. Bootstrap analysis was used to test the difference between wild type and mutants. * indicates p value < 0.05.

Table 1: Physical characteristics of the *C. neoformans* Blp protein family

Name	Signal Sequence	Barwin Domain (A.A. into protein)	Protein Length (A.A.)	% Disordered Predicted	% Homology to Barwin Domain	pI	MW (kiloDaltons)
Blp1	1-17	39-102	138	21.01	100	4.32	14.8
Blp2	1-18	24-121	124	6.45	99.9	4.07	13.1
Blp3	1-15	406-484	499	56.71	99.9	7.04	50.7
Blp4	1-18	108-299	299	43.48	99.9	4.05	30.8
Blp5	1-17	102-171	354	52.26	99.9	4.54	37.6
Blp6	1-22	76-141	305	54.75	100	4.33	32.1
Blp7	1-21	39-176	347	30.84	94.8	3.88	35.6
Blp8	1-16	54-192	175	37.72	76.6	4.1	35.8

Supplemental Figures and Tables

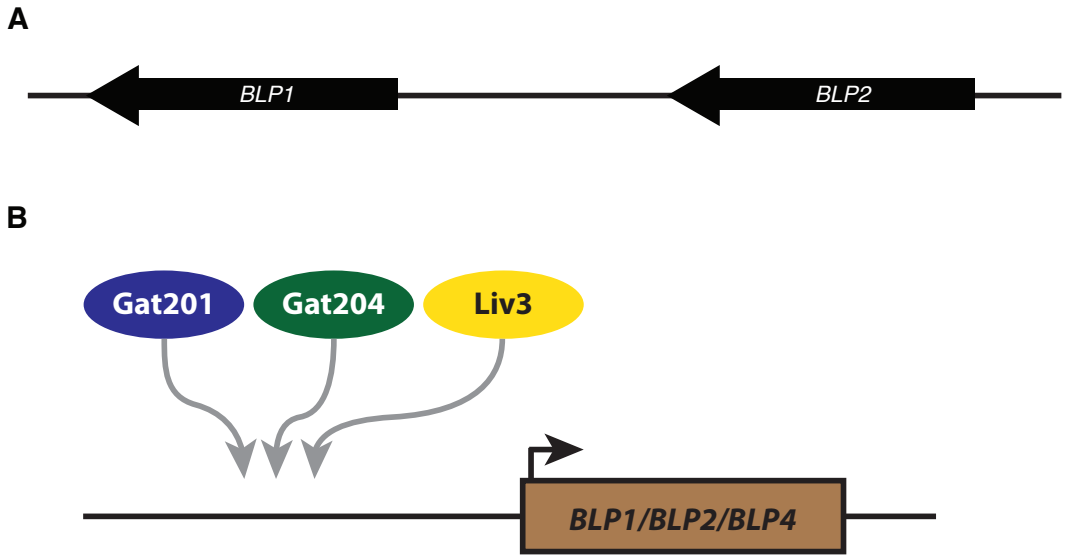

Figure S1

Figure S1: Blp promoter binding and gene organization, Related to Figure 1

f) Schematic of *BLP1* and *BLP2* gene orientation. Both genes are in tandem on chromosome 13 of the *C. neoformans* genome.

g) Gat201, Gat204, and Liv3 bind the promoters of *BLP1*, *BLP2*, and *BLP4* by ChIP-Seq.

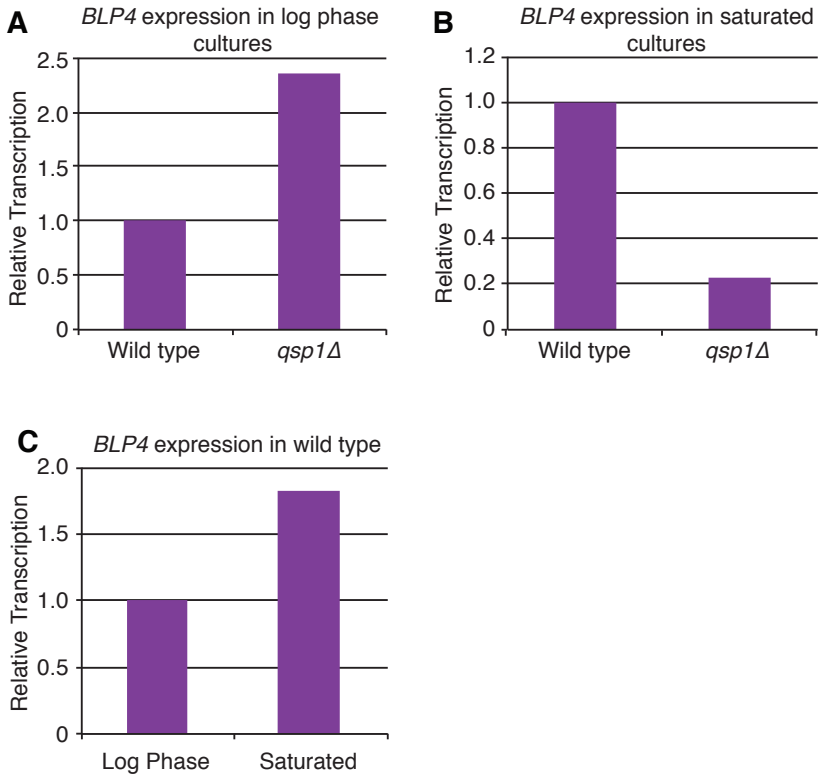

Figure S2

Figure S2: *BLP4* is regulated by cell density and QSP1, Related to Figure 3

b) *BLP4* expression in log phase cultures. *BLP4* has increased transcript amount in the *qsp1*Δ mutant compared to wild type.

c) *BLP4* expression in saturated cultures. *BLP4* has decreased transcript amount in the *qsp1*Δ mutant compared to wild type.

d) *BLP4* expression as a function of cell density. *BLP4* transcript is induced by increasing cell density in wild type.

Table S1. Strains used in this study, Related to Experimental Procedures

Strain #	Name	Species	Genotype	Parent	Source
CM18	WT	*C. neo.*	H99 (wild type)	-	1
D1863	*blp1*Δ	*C. neo.*	*blp1Δ::NatR*	CM18	2
D1895	*blp2*Δ	*C. neo.*	*blp2Δ::NeoR*	CM18	2
D1894	*blp4*Δ	*C. neo.*	*blp4Δ::NeoR*	CM18	2
D1896	*blp1*Δ *blp2*Δ	*C. neo.*	*blp1Δ::NatR-blp2*Δ*::NeoR*	CM18	2
BHM1643	p6xHisBlp1	*E. coli*	BL21 pET28b-*6xHis-Blp1::KanR*	BL21	3
			Sources:		
			1= Gift of J. Heitman		
			2= Chun et al, [10]		
			3= Chun. [14]		

Works Cited

1. Edreva, A., *Pathogenesis-related proteins: research progress in the last 15 years.* General and Applied Plant Physiology, 2005. **31**(1-2): p. 105-124.
2. de Oliveira, A.L., et al., *The structure of the elicitor Cerato-platanin (CP), the first member of the CP fungal protein family, reveals a double psibeta-barrel fold and carbohydrate binding.* J Biol Chem, 2011. **286**(20): p. 17560-8.
3. Seidl, V., et al., *Epl1, the major secreted protein of Hypocrea atroviridis on glucose, is a member of a strongly conserved protein family comprising plant defense response elicitors.* FEBS J, 2006. **273**(18): p. 4346-59.
4. Bouzarelou, D., et al., *EglD, a putative endoglucanase, with an expansin like domain is localized in the conidial cell wall of Aspergillus nidulans.* Fungal Genet Biol, 2008. **45**(6): p. 839-50.
5. Lang, S.K., W. Hort, and P. Mayser, *Differentially expressed genes associated with tryptophan-dependent pigment synthesis in Malassezia furfur--a comparison with the recently published genome of Malassezia globosa.* Mycoses, 2011. **54**(4): p. e69-83.
6. Roberto G. Ocasio-Morales, P.T., and Thomas C. Harrington, *Origin of Ceratocystis platani on Native Platanus orientalis in Greece*

and Its Impact on Natural Forests Plant Disease, 2007: p. 901-904.

7. Baccelli, I., et al., *The expression of the cerato-platanin gene is related to hyphal growth and chlamydospores formation in Ceratocystis platani.* FEMS Microbiol Lett, 2012. **327**(2): p. 155-63.

8. Frischmann, A., et al., *Self-assembly at air/water interfaces and carbohydrate binding properties of the small secreted protein EPL1 from the fungus Trichoderma atroviride.* J Biol Chem, 2013. **288**(6): p. 4278-87.

9. Liu, O.W., et al., *Systematic genetic analysis of virulence in the human fungal pathogen Cryptococcus neoformans.* Cell, 2008. **135**(1): p. 174-88.

10. Chun, C.D., J.C. Brown, and H.D. Madhani, *A major role for capsule-independent phagocytosis-inhibitory mechanisms in mammalian infection by Cryptococcus neoformans.* Cell Host Microbe, 2011. **9**(3): p. 243-51.

11. Nelson PE, D.M., Anaissie EJ., *Taxonomy, biology, and clinical aspects of Fusarium species.* Clin Microbiol Review, 1994. **7**: p. 479-504.

12. Teetor-Barsch, G.H. and D.W. Roberts, *Entomogenous Fusarium species.* Mycopathologia, 1983. **84**(1): p. 3-16.

13. Winn, R.M., et al., *Interactions of human phagocytes with moulds Fusarium spp. and Verticillium nigrescens possessing different pathogenicity.* Med Mycol, 2003. **41**(6): p. 503-9.

14. Chun, C.D., *The pathogenic fungus Cryptococcus neoformans and its adaptation to the host environment [dissertation]*. 2010, University of California, San Francisco: Ann Arbor.

15. Lever, M., *Colorimetric and fluorometric carbohydrate determination with p-hydroxybenzoic acid hydrazide.* Biochem Med, 1973. **7**(2): p. 274-81.

16. Lever, M., *A new reaction for colorimetric determination of carbohydrates.* Anal Biochem, 1972. **47**(1): p. 273-9.

17. Cheryl D. Chun, J.C.S.B., and Hiten D. Madhani, *A Major Role for Capsule-Independent Phagocytosis-Inhibitory Mechanisms in Mammalian Infection by Cryptococcus neoformans.* Cell Host & Microbe, 2011. **9**: p. 243-251.

18. Coelho, C., A.L. Bocca, and A. Casadevall, *The intracellular life of Cryptococcus neoformans.* Annu Rev Pathol, 2014. **9**: p. 219-38.

19. Eigenheer, R.A., et al., *Extracellular glycosylphosphatidylinositol-anchored mannoproteins and proteases of Cryptococcus neoformans.* FEMS Yeast Res, 2007. **7**(4): p. 499-510.

20. Del Poeta, M., *Role of phagocytosis in the virulence of Cryptococcus neoformans.* Eukaryot Cell, 2004. **3**(5): p. 1067-75.

21. Sarantis, H. and S. Grinstein, *Subversion of phagocytosis for pathogen survival.* Cell Host Microbe, 2012. **12**(4): p. 419-31.

22. Steenbergen, J.N., H.A. Shuman, and A. Casadevall, *Cryptococcus neoformans interactions with amoebae suggest an explanation for its virulence and intracellular pathogenic strategy in macrophages.* Proc Natl Acad Sci U S A, 2001. **98**(26): p. 15245-50.

23. Chun, C.D. and H.D. Madhani, *Applying genetics and molecular biology to the study of the human pathogen Cryptococcus neoformans.* Methods Enzymol, 2010. **470**: p. 797-831.

24. Larkin, M.A., et al., *Clustal W and Clustal X version 2.0.* Bioinformatics, 2007. **23**(21): p. 2947-8.

25. Perriere, G. and M. Gouy, *WWW-query: an on-line retrieval system for biological sequence banks.* Biochimie, 1996. **78**(5): p. 364-9.

26. Nicola, A.M. and A. Casadevall, *In vitro measurement of phagocytosis and killing of Cryptococcus neoformans by macrophages.* Methods Mol Biol, 2012. **844**: p. 189-97.

27. Dumesic, P.A., et al., *Product binding enforces the genomic specificity of a yeast polycomb repressive complex.* Cell, 2015. **160**(1-2): p. 204-18.

28. Zhang, Z., et al., *Strand-specific libraries for high throughput RNA sequencing (RNA-Seq) prepared without poly(A) selection.* Silence, 2012. **3**(1): p. 9.

29. Trapnell, C., et al., *Differential gene and transcript expression analysis of RNA-seq experiments with TopHat and Cufflinks.* Nat Protoc, 2012. **7**(3): p. 562-78.

30. Oshlack, A., M.D. Robinson, and M.D. Young, *From RNA-seq reads to differential expression results.* Genome Biol, 2010. **11**(12): p. 220.

Publishing Agreement

It is the policy of the University to encourage the distribution of all theses, dissertations, and manuscripts. Copies of all UCSF theses, dissertations, and manuscripts will be routed to the library via the Graduate Division. The library will make all theses, dissertations, and manuscripts accessible to the public and will preserve these to the best of their abilities, in perpetuity.

Please sign the following statement:

I hereby grant permission to the Graduate Division of the University of California, San Francisco to release copies of my thesis, dissertation, or manuscript to the Campus Library to provide access and preservation, in whole or in part, in perpetuity.

Author Signature

03/26/16

Date